CHARACTERIZATION OF WET AND DRY DEPOSITION TO THE NITROGEN SENSITIVE ALPINE ECOSYSTEMS IN THE COLORADO ROCKY MOUNTAINS

by

KALEY MICHELLE OLDANI

B.S., California State Polytechnic University, Pomona, 2010

A THESIS

submitted in partial fulfillment of the requirements for the degree

MASTER OF SCIENCE

Department of Civil Engineering
College of Engineering

KANSAS STATE UNIVERSITY
Manhattan, Kansas

2014

Approved by:

Major Professor
Dr. Natalie Mladenov

Abstract

The Colorado Front Range of the Rocky Mountains contains undeveloped, barren soils, yet in this environment there is strong evidence for a microbial role in increased nitrogen (N) export. Barren soils in alpine environments are severely carbon-limited, and organic carbon (OC) is the main energy source for heterotrophic microbial activity and sustenance of life. Atmospheric deposition can contain high amounts of OC. Atmospheric pollutants, dust events, and biological aerosols, such as bacteria, may be important contributors to the atmospheric OC load. In this stage of the research we evaluated seasonal trends and annual loadings in the chemical composition and optical spectroscopic (fluorescence and UV-vis absorbance) signatures of wet deposition and dry deposition in an alpine environment, at Niwot Ridge in the Rocky Mountains of Colorado to better understand the sources and chemical characteristics of atmospheric deposition. Dry deposition was found to be an important source of OC to the alpine. Wet deposition contributed substantially greater amounts of dissolved ammonium, nitrate, and sulfate. There were also positive relationships between dissolved organic carbon (DOC) concentrations and ammonium, nitrate and sulfate concentrations in wet deposition, which may be derived from such sources as dust and urban air pollution. We also observed the presence of seasonally-variable fluorescent components in atmospheric samples that are different from aquatic dissolved organic matter (DOM). Finally, the quality of atmospheric organic compounds reflects photodegradation during transport through the atmosphere. These results are relevant because atmospheric inputs of carbon and other nutrients may influence nitrification in barren, alpine soils and, ultimately, the export of nitrate from alpine watersheds.

Table of Contents

List of Figures

List of Tables

Acknowledgements

Dedication

I would like to dedicate this thesis to my family and friends. Thank you for believing in me. Your support and encouragement through these last two years helped me get through the tough times.

Chapter 1 - Dry and Wet Deposition Inputs to Alpine Environments as Important Contributions to the Nitrification of Alpine Streams in the Colorado Rocky Mountains

1. Introduction

Extensive research has been conducted in alpine catchments for decades showing that biogeochemical and hydrologic processes in seasonally snow-covered catchments are changing, which is directly affecting water quality (Williams et al., 1996, 2011; Brooks and Williams, 1999). In alpine environments the soil is generally snow covered for greater than 9 months of the year, therefore access to carbon (C) and other nutrients by microorganisms is limited to the short snow-free period (Ley et al., 2004). As glacier and snow melt accelerates, more barren soils are being exposed to physical and biological weathering processes while simultaneously producing new hydrologic pathways and connections. In many alpine and high elevation catchments, a trend of increasing nitrate export in surface waters has been observed, such as those in the Colorado Rocky Mountains, USA (Williams et al., 1996, 2011; Baron et al., 2009). Increased nitrate export from alpine streams in the Colorado Rocky Mountains is an indication that high alpine catchments are currently in transition from nitrogen (N) limitation to N saturation (Williams and Tonnessen 2000; Elser et al. 2009). This transition to an N-saturated system is partly attributed to short growing seasons, sparse vegetation, shallow soils, and harsh climate that make high-elevation catchments particularly vulnerable to environmental change (Williams and Tonnessen 2000). The increase in nitrate concentrations in surface waters draining the Green Lake (GL4) catchment, part of the Niwot Ridge Long Term Ecological Research site (NWT

1

LTER), located in the Front Range of Colorado illustrates the transition to N-saturation of an alpine catchment. Since the mid 1980's, annual volume weighted-mean nitrate concentrations at the outlet of GL4 have increased at a rate of 0.27 μmol N year^{-1} (Barnes et al., 2013). This trend of increasing nitrate export in surface waters in high elevation catchments has been detected in several alpine catchments worldwide (Baron et al. 2009; Rogora, 2007; de Wit et al., 2007). As full nitrogen saturation occurs in alpine environments, these alpine basins become a source of nitrate in the headwaters of the primary drinking water source for many urban populated areas. High nitrate concentrations in water can cause eutrophication in rivers, lakes, and streams and, if consumed in drinking water, can cause Blue Baby Syndrome. Despite the severely carbon-limited, undeveloped, barren soils of the Colorado Rocky Mountains, high microbial activity is occurring, providing strong evidence that microorganisms are playing an important role in increased nitrogen (N) export from high elevation catchments (Williams et al., 1997, 2007).

Atmospheric constituents, such as ice, snow, rain, dust, biological organisms and fragments, and aerosols from the atmosphere that often deposit to the Earth's surface are called atmospheric deposition. Studies have shown that alpine environments, usually located in remote, high-elevation regions, are exceptionally sensitive to atmospheric deposition (Psenner, 1999; Mladenov et al., 2011). The transfer of atmospheric constituents into alpine areas may also provide significant sources of carbon and other nutrients to these remote, high-elevation catchments. Dust emission may contribute substantial amounts of nutrients, such as iron (Fe), phosphorous (P), nitrogen (N), and organic C to alpine areas (Neff et at., 2008; Lawrence and Neff et al., 2009; Reche et al., 2009; Mladenov et al., 2009, 2010). Studies have shown that organic C makes up 10 to 20% of Aeolian deposition that is deposited into alpine environments (Liator, 1987; Ley et al., 2004; Mladenov et al., 2009, 2010).

The atmosphere is composed mainly of a few abundant gases, but also includes trace gases and aerosols. The simplest group of organic compounds is hydrocarbons, where molecules are built up by carbon and hydrogen atoms only. Volatile organic compounds (VOCs) that are emitted from trees, such as terpenes, have been termed biogenic VOCs (BVOCs). Biogenic and anthropogenic VOCs are essential components of secondary organic aerosol (SOA) formation. Often secondary aerosol formation occurs due to reactions between gases that are in the atmosphere. Once these SOA particles form, they tend to stabilize by nucleating and condensing with other SOA particles. As the SOA particle continues to react with other atmospheric gases and particles, its mass increases and can form ice nuclei (IN), cloud condensation nuclei (CCN), or remain as an aerosol particle. The SOA particle can undergo a series of physical or chemical transformations between the gas and particle phase and the particle growth and fragmentation stage. Chemical transformation may occur quickly via bulk adsorption and reactions within liquid particles or occur rather slowly via surface adsorption and reaction onto solid particles.

Organic matter has now been recognized as an important atmospheric component that contributes significantly to climate, air quality, and ecosystem health. Precipitation is an efficient scavenger of organic matter from the atmospheric reservoir. Studies have shown that DOC is an abundant component in rainwater and can be higher in concentration than the well-studied inorganic species, such as nitric and sulfuric acids (Willey at al., 2000). Moreover, organic acids contribute 14 to 36% to the total DOC in rainwater and <10% of other known compounds, such as aldehydes and amino acids (Avery et al., 2006). Studies have shown that DOC is a major component of marine and continental rainwater, yet approximately 50% of rainwater DOC is uncharacterized (Wiley et al., 2000) creating a difficult challenge to determine the role of rainwater DOM in regional and global C budgets (Raymond, 2005). Because organic aerosol

sources are indeterminate, likely this material signifies a wide range of compounds of diverse origin and not a single compound with a single source (Neff et al., 2002).

All atmospheric aerosols and particulates can be removed from the atmosphere in two ways: wet deposition or dry deposition. Wet deposition is a process that involves the dissolution of gases and particles into droplets either in below-cloud scavenging as falling rain or snow particles colliding with aerosols or in-cloud scavenging where aerosol particles work as CCN or IN. Dry deposition is a process that transfers atmospheric species to the Earth's surface without precipitation. Instead it involves gravitational sedimentation of particles, interception of particles and collision with an obstacle, impaction of particles and collision with an obstacle, turbulence in eddies in the air which transfer particles which can collide, or diffusion or Brownian motion, which is defined as random collisions with gas molecules. Both wet deposition and dry deposition involve the transfer of atmospheric organic matter, which is a mixture of organic compounds, to the biosphere, either onto the land or into the water.

In this study we compiled data collected during two consecutive years (January 2012 – December 2013) on chemistry and fluorescence and absorbance properties from atmospheric wet deposition as well as the water soluble (<0.7 µm) compounds found in atmospheric dry deposition. The main goals of this thesis were to 1) quantify the nutrient loadings in deposition to alpine environments, especially the less-studied dry inputs, 2) assess the spectral properties of fluorescent atmospheric organic matter for general characterization and evaluation of the similarity to signatures of aquatic DOM, and 3) look for significant differences, relationships, and trends in these datasets that may provide additional information about the sources and chemical quality of atmospheric deposition to the alpine. The quantification of carbon and nutrient inputs to the alpine, especially dry deposition, has not been previously done and directly

analyzed over the course of several years and therefore represents a missing link to nutrient cycles within alpine catchments. Also, organic matter has been extensively characterized in aquatic environments, and rapid techniques, such as absorbance and fluorescence spectroscopy, have been used to indicate the quality and potential source of organic matter. However, there is still much to be learned about the chemical and spectroscopic signatures of atmospheric deposition. I sought to develop a better understanding of atmospheric inputs of nutrients and DOM for a remote, high-elevation watershed in the Colorado Rocky Mountains, USA by examining the optical spectroscopic properties to provide additional information on the quality and sources of DOM in atmospheric deposition.

2. Hypotheses

My hypotheses were 1) dry deposition is just as significant as wet deposition as a source of C and other nutrients to alpine environments in the Rocky Mountains, 2) atmospheric pollutants, NO_x and SO_x, and organic C from Front Range sources contribute substantially to the high summer atmospheric load in the remote alpine environment of the Rocky Mountains, 3) dust particles, especially during the spring season, are being transported in the atmosphere long distances and are largely responsible for nutrient and DOC deposition in the alpine, and 4) the quality of atmospheric organic compounds reflects photodegradation during transport through the atmosphere.

Chapter 2 - Seasonality and Chemical Characteristics of Atmospheric Wet and Dry Deposition to Alpine Environments in the Colorado Rocky Mountains

1. Introduction

Alpine ecosystems contain a variety of unique plant and animal species that have lived in these extreme environments for hundreds of thousands to millions of years, yet these alpine species are considered to be highly endangered because of climatic changes that are altering biogeochemical and hydrologic processes in seasonally snow-covered catchments (Parry, 2007; Theurillat and Guisan, 2001; Williams et al., 1996, 2011; Brooks and Williams, 1999). Alpine environments are often characterized as remote, "pristine" areas that have undeveloped, barren soil. The barren, high altitude alpine soils are severely carbon (C) limited and highly deficient in most nutrients (Williams et al., 1997; Ley et al., 2001). Atmospheric wet and dry deposition may be important sources of C and other nutrients to remote alpine environments. Alpine soils are generally snow covered for the majority of the year with approximately 3 months of snow-free period. Therefore, availability of C and other nutrients for soil microorganisms is limited to the short snow-free period (Ley et al., 2004).

As alpine deglaciation and snow melt accelerate with increasing temperatures, physical and biological weathering processes are increasing in the exposed barren alpine soils. Additionally, the increased melting of alpine glaciers and ice are producing new hydrologic pathways and biogeochemical interactions. An increasing trend in nitrate export from streams in alpine and high elevation catchments has been observed in several locations in the Rocky Mountains, USA (Williams et al., 1996, 2011; Baron et al., 2009). This trend of increasing

nitrate export from alpine streams is a sign of high alpine catchments currently transitioning from nitrogen (N) limitation to N saturation (Williams and Tonnessen, 2000; Elser et al., 2009). Alpine ecosystems are typically very small N sinks compared to more densely vegetated forests (Sievering, 1992). This relatively rapid shift to an N-saturated system is primarily in response to high atmospheric N-deposition, however, the short growing seasons, sparse vegetation, shallow soils, and harsh climate are additional factors that make high-elevation catchments particularly vulnerable to environmental changes (Williams and Tonnessen, 2000). At Niwot Ridge Long Term Ecological Research station (NWT LTER) in the Front Range of Colorado, elevated nitrate concentrations in surface waters draining the Green Lake (GL4) catchment illustrate the transition to N-saturation of an alpine catchment. From 1985 to 2009, annual volume weighted-mean nitrate concentrations at the outlet of GL4 have increased at a rate of 0.27 µmol N year^{-1} (Barnes et al., 2013). This trend of increasing nitrate export in surface waters in high elevation catchments has been detected in several alpine catchments worldwide; in Rocky Mountain National Park in Colorado (Baron et al., 2009), the Alps of northern Italy (Rogora, 2007), and southern Norway (de Wit et al., 2007). With increasing temperature, there has also been a trend of increasing concentrations of base cations in the outflow of GL4 (Caine, 2011.

Studies have shown that remote, high-elevation catchments are exceptionally sensitive to atmospheric deposition (Psenner, 1999; Mladenov et al., 2011). Atmospheric deposition is the process in which precipitation (rain, snow, fog), particles (dust, fungi, bacteria), aerosols, vapors, and gases move from the atmosphere to the earth's surface. The Colorado Front Range of the Rocky Mountains contains undeveloped, barren soils that are severely carbon-limited, which is the main energy source for microbial activity and sustenance of life. Nevertheless, high microbial activity has been observed in these barren alpine soils providing strong evidence for a

microbial role in increased nitrogen (N) export from high elevation catchments (Williams et al. 1997, 2007). The transfer of atmospheric aerosols into alpine areas may be a significant source of carbon and other nutrients for these remote, high-elevation catchments. Dust emission may contribute substantial amounts of nutrients in the form of iron (Fe), phosphorous (P), and nitrogen (N) to alpine areas, for instance in arid regions of the western US (Neff et at., 2008; Lawrence and Neff et al., 2009) and southern Europe (Reche et al., 2009). Wet deposition to alpine environments is known to contain about 10% to 20% organic C in studies of the Colorado Rocky Mountains (Liator, 1987; Ley et al., 2004) and the Sierra Nevada of Spain (Mladenov et al., 2009, 2010). Mladenov et al. (2009, 2010) revealed that dry deposition to the Sierra Nevada of Spain originating from the Sahara comprised about 10 to 20% organic C.

Additionally, the atmosphere contains several hundred trace gases, such as VOCs. VOCs derived from vegetation, including terpenes, Pinene, and limonene ($C_{10}H_{16}$) from pine trees, are referred to as biogenic volatile organic compounds (BVOCs). VOCs emitted from vegetation are aromatic essences that consist of hydrogen and carbon bonds also called biogenic hydrocarbons. BVOCs are emitted by vegetation as a byproduct of photosynthesis and respiration. Humans also contribute an extensive variety of trace gases to the atmosphere due to transportation and other industrial practices, including solvents and VOC byproducts from the combustion of fossil fuels. Most trace gases have short mean residence times because they are highly reactive and concentrations widely vary in space and time. VOCs, biogenic or anthropogenic, are essential in the formation of secondary particles. Atmospheric measurement studies estimate that 10,000 to 100,000 unique organic compounds exist in the atmosphere (Goldstein and Galbally, 2007). The formation of secondary particles in the atmosphere occurs by gas-particle conversion processes such as nucleation, condensation and heterogeneous multiphase chemical reactions. The

mechanisms by which inorganic gases such as sulfur dioxide (SO_2), nitrogen dioxide (NO_2) and ammonia (NH_3) convert into particulate phase sulfate (SO_4^{2-}), nitrate (NO_3^-) and ammonium (NH_4^+) are now fairly well understood. However, there is considerable uncertainty over the mechanisms of formation of secondary organic aerosols (SOA) from VOCs. The structure of the VOC compound along with the concentrations and behaviors of other oxidizers in the atmosphere dictates the direction in which reaction will likely occur. Although the kinetics of the gas-phase partitioning of BVOCs are well understood, the products and reaction mechanisms of certain environmental conditions are still not well known (Atkinson and Arey, 2003).

Once secondary aerosol formation occurs, the SOA may continue to evolve by a variety of process and physical phase states, such as growth of homogeneously solid and liquid nucleated particles, heterogeneous oxidation mechanisms, condensation, and evaporation. Depending on phase state and diffusivity, the chemical and physical transformation, and atmospheric oxidations reactions with other trace compounds may proceed differently, such as if the SOA particles are solid or semi-solid, compounds that are of low-volatility and viscous oligomerized SOA material, including isoprene, may accumulate on the particle surface layer upon evaporation and limit the loss of the other more volatile compounds (Roldin et al., 2014). Chemical transformations may be relatively slow via surface adsorption and reaction on solid particles, such as with dry deposition constituents, or relatively fast via bulk absorption and reaction in liquid particles, like wet deposition. Upon cloud formation, solid aerosol particles are more likely to be activated as ice nuclei (IN), forming ice crystals, whereas liquid aerosol particles are more likely to be activated as cloud condensation nuclei (CNN), forming water droplets.

The average lifetime of a molecular species in the atmosphere is called the residence time of that species. Aerosols can persist in the atmosphere from around less than a minute to greater than eight years. The mean residence time for aerosol nitrate, organics, sulfate, and ammonium is about 3–7 days, and the lifetime of the total aerosol number density was estimated at 9.8 days (Millet et al., 2004). Therefore, these aerosol particles may be traveling from far distances before reaching these remote alpine environments. In addition, local SOA formation from BVOCs may also play an important role to the deposition of other atmospheric constituents.

In the US, the National Atmospheric Deposition Program (NADP, http://nadp.sws.uiuc.edu/) has long-term precipitation chemistry data of mainly the inorganic fraction of atmospheric deposition. Few quantitative studies exist on organic C content of atmospheric deposition, and often the dry form of atmospheric deposition is not tracked. Dissolved organic carbon (DOC) is common in rainwater and can be higher in concentration than inorganic species such as nitric acid and sulfuric acid (Willey et al., 2000). Organic acids have been the main focus of studies because they contribute considerably to acidity in urban areas (Pena et al., 2002) and primarily account for acidity (80-90%) in remote areas of the world (Andreae et al., 1988). However, the contribution of the organic acids, specifically mono- and di-carboxylic acids, accounts for only 14-36% to the total amount of DOC in rainwater (Avery et al. 2006). Therefore a large fraction of DOC in atmospheric deposition remains to be better characterized.

In this study we compiled data for two consecutive years (January 3, 2012 – December 17. 2013) of chemistry from atmospheric wet deposition and the water soluble (<0.7 µm) compounds found in atmospheric dry deposition. Our goals were to quantify the C and nutrient loadings in deposition to alpine environments, especially dry inputs. The quantification of

nutrients deposited to the alpine, especially in dryfall, is important because currently there is no direct tracking of nutrients to alpine environments and therefore it is a missing link for the nutrient cycles in these environments. We seek to develop a better understanding of atmospheric inputs of C and nutrients for a remote, high-elevation watershed in the Colorado Rocky Mountains.

2. Site Description

Niwot Ridge Long Term Ecological Research Station (NWT-LTER) located in the Colorado Front Range of the Rocky Mountains, manages three official NADP sites, at which long-term wet deposition is collected (Figure 1). These sites are along an elevation gradient: CO94 at 2,524 m, CO91 at 3,287 m, and CO02 at 3,520 m, and a fourth, unofficial site at Soddie (3,345 m elevation), located on the leeward side of the Rocky Mountains near the Continental Divide in the Colorado Front Range (40°03' N, 105°35' W). NWT-LTER is located at approximately 25 km west of Boulder, Colorado, which lies within the City of Boulder Watershed. The City of Boulder also operates the Boulder Creek Critical Zone Observatory at this research location because this site contains the headwaters of the North Boulder Creek. The meteorology of this site has been described extensively (Brazel and Brazel, 1983; Parish et al., 1990; Williams et al., 1996; Turnipseed et al., 2002). In summer months, NWT-LTER commonly exhibits a typical valley-mountain flow: typical wind patterns are generally westerly at night (downslope drainage) bringing relatively clean air from the continental divide, whereas daytime heating creates easterly flow causing upslope wind conditions and bringing air from the Denver-Boulder metro area (Brazel and Brazel, 1983).
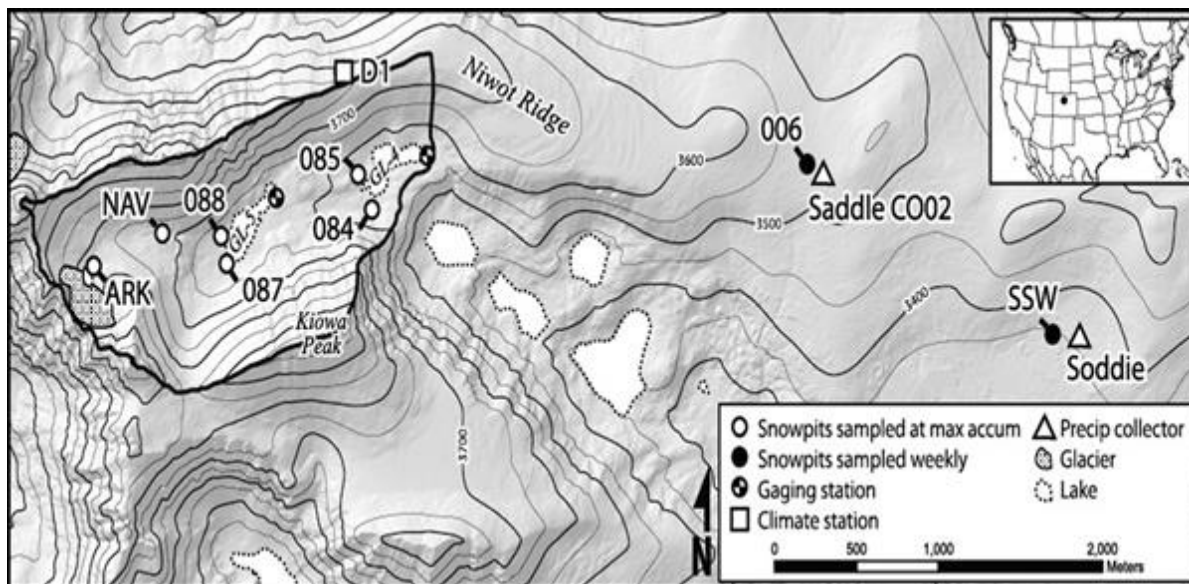
Figure 1. Map of Niwot Ridge and the Green Lake 4 (GL4) catchment (outlined), showing Green Lake 4 (GL-4), Green Lake 5 (GL-5), the gauging station at GL-4, the D1 climate station, and sites of deposition collectors (Saddle site NADP collector CO02 and Soddie site collector). Inset shows the location of the Niwot Ridge LTER, Colorado, USA. Art credit: Parrish, E.

3. Methods

3.1 Sample Collection

Physical and chemical properties of wet deposition and dry deposition as well as amounts of wet deposition collected in NADP style precipitation collectors at the Soddie site on Niwot Ridge are measured as part of the NWT LTER program (Figure 2). Soddie contains the same instrumentation as official NADP sites, including an Aerometrics Wet and Dry Chemistry system consisting of bucket containers collecting wet and dry deposition. Both wet deposition samples and dry deposition samples are analyzed for DOC, pH, and other cations and anions at the NWT LTER Kiowa Environmental Chemistry Laboratory. Trends in DOC concentration measurements at Soddie and the 3 official NADP sites in the surrounding area (CO02, CO94, and CO91) were determined to be statistically similar (Mladenov et al., 2012).Wet deposition is

collected on a weekly basis following NADP protocols and dry deposition is collected on a biweekly basis. Dry deposition collectors are composed of approximately 800 g (~150) marbles that are placed into a plastic colander, which in turn rests inside a sealable Sterilite® container, as described in Goss et al. (2013). This device sits on a platform that is 3.2 cm below the top of the 5-gallon dry deposition collection bucket and is exposed to dryfall for 14 days. To test whether marble inserts improved the retention of dry deposition, a second dry deposition collection study was conducted using a 5-gallon bucket without the marble insert during 7 consecutive collection events during summer and fall in 2012 and 8 events during spring and summer 2013 for comparison. After the collection period, the marble inserts were sealed with a leak-resistant Sterilite®lid, placed into a closed, transparent bag, and stored in a refrigerator at 4°C. Dry deposition (excluding visible insects) was collected by rinsing the bucket with 1000 mL of Milli-Q®, agitating for a minute, and then allowing the solution to rest for 20 minutes. The aqueous solution was filtered through combusted, pre-weighed and pre-rinsed (with 100 mL ultrapure water) 47 mm Whatman glass fiber (GFF) filters with an effective pore size of 0.7 μm. After filtration, the GFF filters were dried at 60°C for 24 hours. Once removed from the oven, the GFF filters were exposed to ambient air conditions for an hour before total particulate matter (PM) mass was recorded. To determine the particulate organic carbon (POC) fraction, GFF filters were combusted in a muffle furnace at 450°C for four hours to burn off all organic particulate mass. The GFF filters were exposed to ambient air conditions for one hour, and the mass was recorded. Particulate organic carbon, or water insoluble organic carbon (WISOC), was determined as the difference between the mass of the filter before and after combustion.
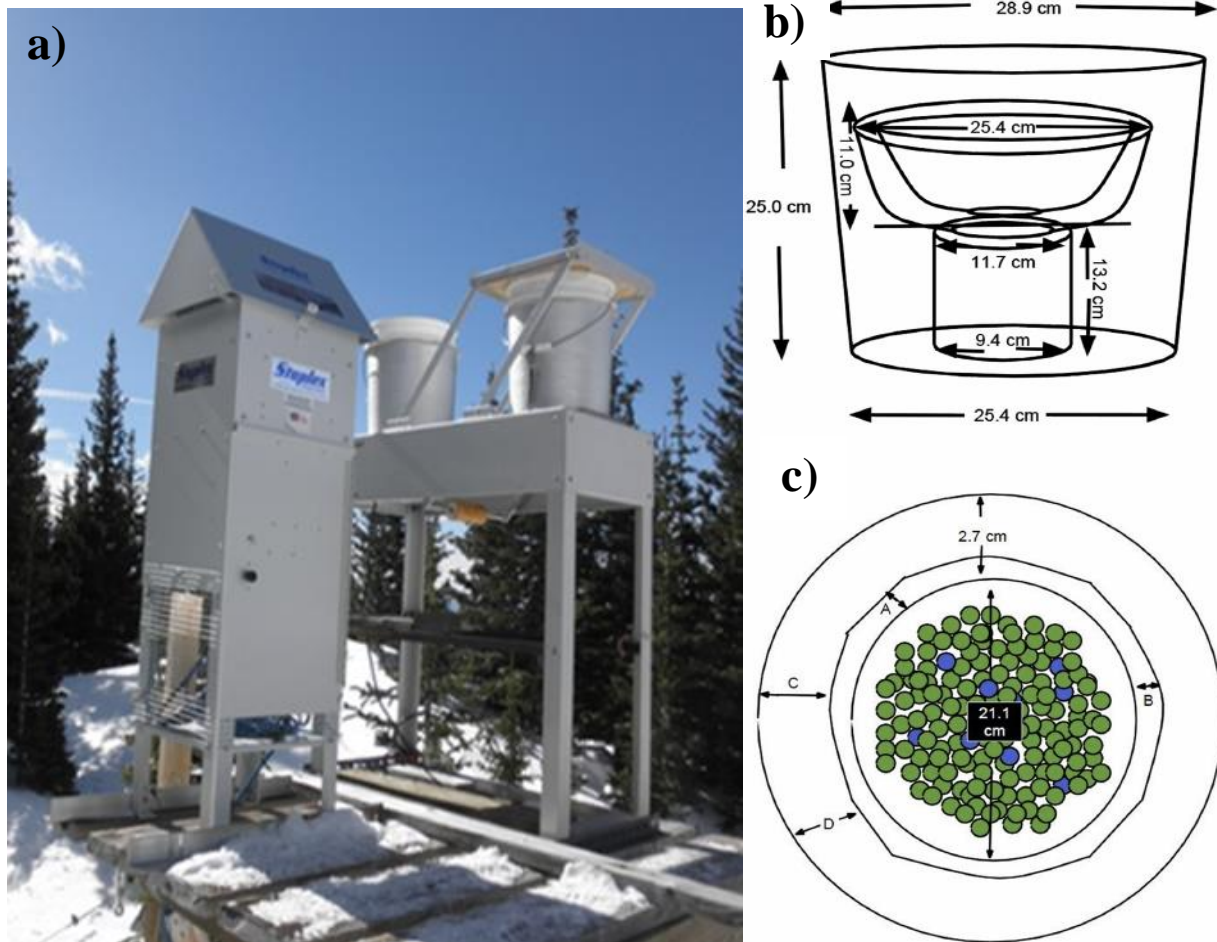
Figure 2. NADP Style Collector at the Soddie site at Niwot Ridge with Marble Insert.
a) NADP style collector at the Soddie site at Niwot Ridge, b) and c) Marble insert. A standard 5-gallon NADP deposition bucket holds the insert on a platform. The insert consists of a sealable Sterilite© container that holds a Chefmate © colander. Nominal widths were A = 0.6 cm, B = 0.9 cm, C = 0.8 cm, and D= 1.8 cm. The colander contains approximately three layers of marbles. For space reasons, the lid of the container is placed between the insert and the platform when deployed in the field. Diagram not to scale.

3.2 Water Chemistry Analysis

Both wet and dry deposition samples were analyzed for several specific chemical constituents such as pH, conductance, ammonium (NH_4^+), calcium (Ca^{2+}), magnesium (Mg^{2+}), nitrate (NO_3^-), sulfate (SO_4^{2-}), phosphate (PO_4^{3-}), DOC, total nitrogen (TN), total dissolved nitrogen (TDN),

total phosphorus (TP), and total dissolved phosphorus (TDP) at the Institute for Artic and Alpine

Research (INSTAAR) Kiowa Environmental Chemistry Laboratory in Boulder, CO. The dry

deposition filtered samples were stored in the dark at 4°C until analysis. Dissolved species of

interest (DOC, TDN, and TDP) are referred to as "water soluble" compounds. Specific

conductance and pH were measured using the Gran titration technique. Subsamples were

immediately filtered through pre-combusted and pre-rinsed (300 ml) 47-mm Whatman or

Gelman A/E glass fiber filters with an effective pore size of 0.7 μm. Filtered samples were stored

in the dark at 4 C for subsequent analyses within 1 to 12 weeks. NH_4^+ was determined by using

the BioTek Synergy 2 analyzer. Ca^{2+}, Mg^{2+}, potassium (K^+), and sodium (Na+) concentrations

were determined using the Perkin Elmer Atomic Absorption Analyzer. Chloride (Cl^-), NO_3^-, and

SO_4^{2-} were determined using the Metrohm 761 Compact ion chromatograph (IC). TDP, PO_4^{3-},

and silica (Si) was determined by digestion using the Lachat Quik Chem 8500 FIA series of

instruments. TDN was determined by potassium persulfate digestion to oxidize all dissolved

forms of N into NO_3^--N. DON was calculated by subtracting measured inorganic N (NO_3^-- N–

NH_4^+-N) from the TN value of the filtered sample. DOC concentrations were measured by high

temperature catalytic oxidation with a Shimadzu TOC-550A total organic carbon analyzer. Total

organic carbon (TOC) in the dry deposition was calculated as the sum of purgeable organic

carbon, DOC, and nonpurgeable organic carbon, which was estimated to be 60% of the mass lost

by combustion.

3.3 Wet Deposition Loadings

Wet deposition is reported as an aerial loading (kg ha^{-1} yr^{-1}). Mean daily loadings of solutes

were calculated by multiplying the precipitation solute concentration (μEQ L^{-1}) by the total

gauge precipitation amount in grams for the summary period and dividing by the valence charge

of the ion and by 1000 (g L^{-1}), the area of the collection bucket (m^2), and the number of days for

the collection period. Annual loadings of solutes in wet deposition were calculated by the sum of the weekly loadings. Values below detection limits were treated as half the detection limit (Williams et al., 2006).

Equations used to determine deposition loadings

$Loading \ (\mu moles \ m^{-2} day^{-1})$

$$= \frac{Concentration \ (\mu Equvialents \ l^{-1}) * rain \ sample \ weight \ (g) * 10{,}000 \ (cm^2 \ m^{-2})}{1{,}000 \ (g \ l^{-1}) * Area \ of \ collection \ bucket \ (cm^2) * number \ of \ days}$$

$Loading \ (kg \ \text{ha})$

$$= \frac{Loading \ (\mu moles \ m^{-2} day^{-1}) * days * 10{,}000 \ (m^2 \ ha^{-1}) * molecular \ weight \ (\mu g \ \mu mole^{-1})}{1{,}000{,}000{,}000 \ (\mu g \ kg^{-1})}$$

3.4 Dry Deposition Loadings

Dry deposition is reported as an aerial loading (kg ha^{-1} yr^{-1}). Mean daily loadings of solutes were calculated by multiplying the solute concentration ($\mu EQ \ L^{-1}$) by the total amount of ultrapure water used to extract the solutes (L) and dividing by the valence charge of the ion, the area of the collection bucket (m^2), and the number of days for the collection period. Annual loadings of solutes in dry deposition were calculated as the sum of bi-weekly loadings. Values below detection limits were treated as half the detection limit (Williams et al., 2006) Total organic carbon (TOC) was calculated as the sum of DOC and 60 percent (Appendix A-1) of the weight of organic matter on the glass fiber filter which was lost during combustion at 450° C.

The following equations were used to determine atmospheric deposition loadings:

$Loading \ (\mu moles \ m^{-2} day^{-1})$

$$= \frac{Concentration \ (\mu Equvialents \ l^{-1}) * water \ used \ to \ extract \ sample \ (ml) * 10{,}000 \ (cm^2 \ m^{-2})}{1{,}000 \ (ml \ l^{-1}) * Area \ of \ collection \ bucket \ (cm^2) * number \ of \ days}$$

$Loading \ (kg \ /\text{ha})$

$$= \frac{Loading \ (\mu moles \ m^{-2} day^{-1}) * days * 10{,}000 \ (m^2 \ ha^{-1}) * molecular \ weight \ (\mu g \ \mu mole^{-1})}{1{,}000{,}000{,}000 \ (\mu g \ kg^{-1})}$$

3.5 Chemistry Correlations

Correlations between the various chemical constituents were analyzed to better understand patterns hidden the data. Atmospheric deposition average daily loadings reported as µmoles m^{-2} day^{-1} were used to determine correlations between chemical constituents. Various chemical constituents were plotted against each other to determine the degree of a linear relationship by coefficient of determination (R^2). The R^2 value indicates how well data fit a statistical model and the p value indicates the significance of the correlation.

3.6 CASTNET Comparison

The Clean Air Status and Trends Network (CASTNET) is a national air quality monitoring network designed to provide data to assess trends in air quality, atmospheric deposition, and ecological effects due to changes in air pollutant emissions and is directed by the United States Environmental Protection Agency (US EPA). CASTNET measurements primarily assess long-term, regional trends in sulfur and nitrogen pollutants. CASTNET tracks atmospheric wet and dry deposition. Atmospheric wet deposition is obtained through the NADP program that is directed by the EPA. Atmospheric dry deposition flux is calculated from the estimated deposition velocity and the measured pollutant concentration. Dry deposition velocity estimates are from the Multi-Layer Model (MLM), a dry deposition model. Missing deposition velocities, according to the EPA website, have been replaced with historical averages for the interpolated dry deposition loadings. Pollutant concentration data are collected at each site with open-faced, 3-stage filter packs, containing a teflon filter for collection of particulate species, a nylon filter for nitric acid and a base-impregnated cellulose (Whatman) filter for sulfur dioxide.

At Rocky Mountain National Park (40° 16' N, 105° 32' W; 2743 m elevation) filter packs are exposed for 1-week intervals (i.e., Tuesday to Tuesday) at a flow rate of 3.0 liters per

minute and sent to the Harding ESE, Gainesville, FL laboratory for chemical analysis. Similarly, dry deposition at NWT-LTER was primarily also collected on Tuesday on a bi-weekly basis. Since dry deposition in this study was collected every two weeks, for this comparison, the weekly measurements from CASTNET had to be added to the week that was also represented during that same time period that our study was collecting dry deposition (bi-weekly collection) for each sample. The CASTNET site that was used to compare dry deposition from our study was less than 20 miles away in Rocky Mountain National Park.

3.7 Backwards Trajectories

For representative wet and dry deposition samples, we examined the source of air masses over Niwot Ridge in the Colorado Rocky Mountains (40.05 N, 105.58 W) by computing backward trajectories (http://www.arl.noaa.gov/ready.html) over the collection dates. For wet deposition, the date of heaviest rainfall events were determined using the Community Collaborative Hail, Rain, and Snow Network (CoCoRaHS) in conjunction with Weather Underground archived radar images to determine the time of the rain fall event. Using the date and time of the rain fall event, seven consecutive backward trajectories with 72 h run times were computed at 4 h intervals using the HYSPLIT model (Draxler and Rolph, 2003) and archived data from the Global Data Assimilation System (GDAS) meteorological dataset. Trajectories were only obtained for the three highest loadings of DOC, NH_4+, Ca^{2+}, Mg^{2+}, NO_3^-, SO_4^{2-}, and PO_4^{3-} during the two year study. Some wet deposition samples had several trajectory images. For dry deposition, the time of collection or noon was used as the starting point and seven consecutive backward trajectories with 72 h run times were computed at 24 h intervals using the HYSPLIT model (Draxler and Rolph, 2003) and archived data from the Global Data Assimilation System (GDAS)

18

meteorological dataset. Each dry deposition sample had about two images displaying roughly 7 trajectories for analysis of each week of deposition.

3.8 Imputations of Missing Data

We consider the issue of summarizing deposition loadings seasonally and annually over the two year study period when some samples are missing information. The fact that some or, sometimes, all constituent analyses for a specific deposition sample were not recorded during this period, unfortunately, causes seasonal or annual loadings to become biased. The cause for missing data points could be from an insufficient quantity of the sample to run the analysis, contamination of the sample rendering the sample unusable, or misplacement of the sample. Linear interpolation was used for the missing data points by examining the strong correlations between two constituents and using the linear equation to determine the rough value of the missing nutrient loading, for example one sample in spring 2012 the missing DOC loading was determined by NH_4^+ using the linear function that was determined by the best fit line (Appendix A-3). If the linear function returned a negative number, the sample was first analyzed to see if concentrations of other constituents were low, then half the detection limit was used. For samples that were missing all the nutrient concentrations, those samples were excluded from the analysis which will consequently reduce the total annual loadings and some of the seasonal loadings. The missing dates are: 21 – 28 February 2012, 11 – 18 June 2013, and 8 – 15 October 2013 which equals at total of 21 days in the wet deposition and 30 October – 13 November 2012, 27 November – 27 December 2012, 8 – 22 October 2013, and 19 November – 3 December 2013 which equals a total of 72 days. All the missing dates for the dry deposition happened during the fall season, therefore the dry deposition annual and seasonal loadings in the fall seasons would likely be greater than the determined value.

3.9 Statistical Analysis

Statistical analysis was conducted on the wet and dry deposition. Correlations and p values were determined with the use of Statistica software. Two-sided t-tests with unequal variances were conducted on the data to determine if there was a statistical significance between the annual and seasonal average loadings of each constituent in wet and dry deposition using Microsoft Excel. Seasonal loadings and standard deviations were obtained using Microsoft Excel. One-sided, two sample paired t-test was used to determine if there was a significant difference between the amounts of dry deposition collected using the marble insert method and the standard NADP style collection method. Analytical precision for all solutes was assessed with spikes, blanks, and replicates. Detection limits can be found on the Kiowa Environmental Chemistry Laboratory website (http://snobear.colorado.edu Seiboldc/kiowa.html).

4. Results

4.1 Nutrient Loadings in Wet Deposition

Wet deposition nutrient loadings collected during the roughly two-year period, 3 January 2012 - 20 December 2012 and 21 December 2013 – 17 December 2013, can be found in Appendix A, Table A.1 and are summarized in Table 1 below. The annual VWM DOC concentration in wet deposition at Soddie was 1.10 mg C l^{-1} in 2012 and 0.84 mg C l^{-1} in 2013. Weekly DOC concentrations ranged from as low as 0.016 mg C l^{-1} in the winter 2013 to a maximum value of 3.41 mg C l^{-1} on 7 - 21 August 2012. The annual DOC loading in wet deposition was 6.38 kg C ha^{-1} yr^{-1} in 2012 and 6.36 kg C ha^{-1} yr^{-1} in 2013. DOC loadings peaked in the summer during the 3 - 10 July 2012 collection period with 1.69 kg C ha^{-1} deposited during that week. The mean weekly DOC loading was 0.17 ± 0.23 kg C ha^{-1} (Table 1).

Annual NH_4^+ loadings during this period were 2.07 kg NH_4^+ ha^{-1} yr^{-1} in 2012 and 2.0 kg NH_4^+ ha^{-1} yr^{-1} in 2013. The mean weekly NH_4^+ loading was 0.055 ± 0.089 kg NH_4^+ ha^{-1} (Table 1). Annual Ca^{2+} loadings during this period were 1.27 kg Ca^+ ha^{-1} yr^{-1} in 2012 and 2.64 kg Ca^+ ha^{-1} yr^{-1} in 2013. The mean weekly Ca^{2+} loading was 0.053 ± 0.125 kg Ca^+ ha^{-1}. Annual Mg^{2+} loadings during this period were 0.15 kg Mg^{2+} ha^{-1} yr^{-1} in 2012 and 0.24 kg Mg^{2+} ha^{-1} yr^{-1} in 2013. The mean weekly Mg^{2+} loading was 0.0052 ± 0.0082 Mg^{2+} ha^{-1}. Annual NO_3^- loadings during this period were 5.74 kg NO_3^- ha^{-1} yr^{-1} in 2013 and 5.82 kg NO_3^- ha^{-1} yr^{-1} in 2013. The mean NO_3^- loading was 0.156 ± 0.197 NO_3^- ha^{-1}. Annual SO_4^{2-} loadings during this period were 5.89 kg SO_4^{2-} ha^{-1} yr^{-1} in 2012 and 3.40 kg SO_4^{2-} ha^{-1} yr^{-1} in 2013. The mean weekly SO_4^{2-} loading was 0.126 ± 0.155 kg SO_4^{2-} ha^{-1}. Annual PO_4^{3-} loadings were 0.073 PO_4^{3-} ha^{-1} yr^{-1} in 2012 and 0.151 kg PO_4^{3-} ha^{-1} yr^{-1} in 2013. The mean weekly PO_4^{3-} loading was 0.003 ± 0.0049 kg PO_4^{3-} ha^{-1}. NH_4^+, NO_3^-, and SO_4^{2-} loadings peaked in the summer on during the 3-10 July 2012 collection period, depositing 0.68 kg NH_4^+ ha^{-1}, 1.40 kg NO_3^- ha^{-1}, and 1.04 kg SO_4^{2-} ha^{-1}. Ca^{2+} and Mg^{2+} loadings peaked in the spring on $16 - 23$ April 2013, depositing 1.02 kg Ca^{2+} ha^{-1} and 0.06 kg Mg^{2+} ha^{-1}, and PO_4^{3-} loading peaked two weeks later from 30 April - 7 May 2013, depositing 0.025 kg PO_4^{3-} ha^{-1}.

Table 1. Summary of Weekly Wet Deposition Loadings and Annual Loadings.

	Minimum	Maximum	Mean	Std. Dev.	Total 2012	Total 2013
DOC (mg l^{-1})	0.0155	3.4	1.02	0.75	-	-
DOC (kg ha^{-1})	0.0003	1.69	0.172	0.234	6.38	6.36
NH_4^+	$6.36E^{-5}$	0.68	0.055	0.089	2.07	2.0
Ca^{2+}	$8.079E^{-5}$	1.02	0.053	0.125	1.27	2.64
Mg^{2+}	$1.553E^{-5}$	0.057	0.0052	0.0082	0.15	0.24
NO_3^-	0.005	1.4	0.156	0.197	5.74	5.82
SO_4^{2-}	0.0015	1.05	0.126	0.155	5.89	3.4
PO_4^{3-}	$3.84E^{-5}$	0.025	0.003	0.0049	0.073	0.151

4.2 Nutrient Loadings in Dry Deposition

Dry deposition nutrient loadings during 3 January 2012 - 17 December 2013 collected bi-weekly can be found in Appendix A, Table A.2 and are summarized in Table 2 below. During this two-year period, DOC concentrations in dry deposition ranged from 0.23 mg C l^{-1} and reached a maximum of 4.59 mg C l^{-1} on 18 June – 2 July 2013. The annual DOC loading in dry deposition each year during the two-year period was 4.09 kg C ha^{-1} yr^{-1} in 2012 and 4.41 kg C ha^{-1} yr^{-1} in 2013. DOC loadings peaked in the summer during 18 June - 2 July 2013 with 0.90 kg C ha^{-1} yr^{-1} deposited during those two weeks week. The mean DOC loading was 0.14 ± 0.043 kg C ha^{-1} (Table 2). The annual TOC loading in 2013 was 19.7 kg C ha^{-1} yr^{-1}. The mean TOC bi-weekly loading was 0.855 kg C ha^{-1}. Winter dry deposition loadings C, both as TOC and as DOC, were significantly greater than wet deposition loadings of DOC (p value ≤ 0.001).

Annual NH_4^+ loadings during this period were 0.15 kg NH_4^+ ha^{-1} yr^{-1} in 2012 and 0.16 kg NH_4^+ ha^{-1} yr^{-1} in 2013. The mean weekly NH_4^+ loading 0.007 ± 0.013 kg NH_4^+ ha^{-1} (Table 2). Annual Ca^{2+} loadings during this period were 1.31 kg Ca^+ ha^{-1} yr^{-1} in 2012 and 0.91 kg Ca^+ ha^{-1} yr^{-1} in 2013. The mean weekly Ca^{2+} loading was 0.049 ± 0.048 kg Ca^{2+} ha^{-1}. Annual Mg^{2+} loadings during this period were 0.13 kg Mg^{2+} ha^{-1} yr^{-1} in 2012 and 0.095 kg Mg^{2+} ha^{-1} yr^{-1} in 2013. The mean bi-weekly Mg^{2+} loading was 0.005 ± 0.0044 kg Mg^{2+} ha^{-1}. Annual NO_3^- loadings during this period were 2.41 kg NO_3^- ha^{-1} yr^{-1} in 2012 and 1.56 kg NO_3^- ha^{-1} yr^{-1} in 2013. The mean bi-weekly NO_3^- loading was 0.088 ± 0.052 kg NO_3^- ha^{-1}. Annual SO_4^{2-} loadings during this period were 1.18 kg SO_4^{2-} ha^{-1} yr^{-1} in 2012 and 1.22 kg SO_4^{2-} ha^{-1} yr^{-1} in 2013. The mean bi-weekly SO_4^{2-} loading was 0.053 ± 0.026 kg SO_4^{2-} ha^{-1}. Annual PO_4^{3-} loadings during this period were 0.11 kg PO_4^{3-} ha^{-1} yr^{-1} in 2012 and 0.34 kg PO_4^{3-} ha^{-1} yr^{-1} in 2013. The mean bi-weekly PO_4^{3-} loading week was 0.010 ± 0.021 kg PO_4^{3-} ha^{-1}. NH_4^+, SO_4^{2-}, and PO_4^{3-} loadings

peaked in the summer on 18 June – 2 July 2013, depositing 0.017 kg NH_4^+ ha^{-1}, 0.062 kg SO_4^{2-} ha^{-1}, and 0.13 kg PO_4^{3-} ha^{-1}. NO_3^- loadings peaked in the summer on 12 – 17 July 2012 depositing 0.096 kg NO_3^- ha^{-1} and PO_4^{3-} loading peaked in the summer on 18 June – 7 May 2013. Ca^{2+} and Mg^{2+} loadings peaked in the spring on 9 – 23 April 2013.

Table 2. Summary of Weekly Dry Deposition Loadings and Annual Loadings.

	Minimum	Maximum	Mean	Std. Dev.	Total 2012	Total 2013
DOC (mg l^{-1})	0.23	4.59	0.96	0.76	-	-
DOC (kg ha^{-1})	0.045	0.9	0.14	0.043	4.09	4.41
TOC (kg ha^{-1})	0.125	7.94	0.855	1.62	-	19.7
NH_4^+	6.39E-4	0.087	0.0069	0.013	0.15	0.16
Ca^{2+}	7.12E-4	0.27	0.049	0.048	1.31	0.91
Mg^{2+}	9.6E-5	0.025	0.005	0.0044	0.13	0.095
NO_3^-	0.02	0.26	0.088	0.052	2.41	1.56
SO_4^{2-}	0.01	0.12	0.053	0.026	1.18	1.22
PO_4^{3-}	5.9E-4	0.13	0.010	0.021	0.11	0.34

4.3 Seasonal Dynamics for Wet Deposition

DOC concentrations in wet deposition showed a seasonal cycle of the lowest concentrations in the winter and maximum concentration in the summer. Wet deposition DOC loadings followed the same trend as the concentrations and were substantially higher in the summer, especially in July, than in other seasons (Figure 3). Wet deposition loadings of DOC in the summer were significantly greater than wet deposition loadings of DOC in the spring (p value < 0.001). Peaks in NH_4^+, NO_3^- , and SO_4^{2-} loadings in wet deposition occurred during the summer with minima in the winter (Figures 4, 7, and 8). Ca^{2+}, Mg^{2+}, PO_4^{3-} wet deposition loadings showed a seasonal cycle of minima in the winter, but the maxima shifted from being maximum in the summer in 2012 and then spring in 2013 (Figures 5, 6, and 9).

Wet deposition loadings in the summer months were significantly greater than summer dry deposition loadings of NH_4^+, Ca^{2+}, Mg^{2+}, NO_3^-, SO_4^{2-}, and DOC (p value < 0.003). Wet

deposition loadings for NH_4^+ and SO_4^{2-} were significantly greater than dry deposition loadings for each season (p value ≤ 0.045). Wet deposition loadings of NO_3^- were significantly greater than dry deposition loadings of NO_3^- during the summer and spring seasons (p value < 0.001).

4.4 Seasonal Dynamics for Dry Deposition

DOC concentrations in dry deposition showed a seasonal cycle of lowest concentrations in the winter and maximum concentrations in the spring and summer (Figure 3). Dry deposition DOC loadings were substantially higher in the summer, especially in July, than during other seasons. TOC loadings in dry deposition, which are the sum of DOC and particulate OC, had maxima during the summer and minima in the winter (Figure 10). Dry deposition loadings of DOC were not significantly different between each season. The loadings of only dissolved forms of Ca^{2+}, Mg^{2+}, and SO_4^{2-} , PO_4^{3-}, NO_3^-, etc. are presented here because concentrations of those species were only measured in the water soluble fraction of dry deposition and not in the particulates. Ca^{2+}, Mg^{2+}, and SO_4^{2-} loadings in dry deposition occurred during the spring with minima in the winter (Figures 5, 6, and 8). PO_4^{3-} dry deposition loadings showed a seasonal cycle of minima in the winter and maxima in the summer (Figure 9). Peaks in N loadings as NH_4^+ showed minima in winter and a maximum in the summer of 2012 and the spring 2013, yet NO_3^- showed minima in winter and maximum in the spring of 2012 and the summer of 2013 (Figures 4 and 7).
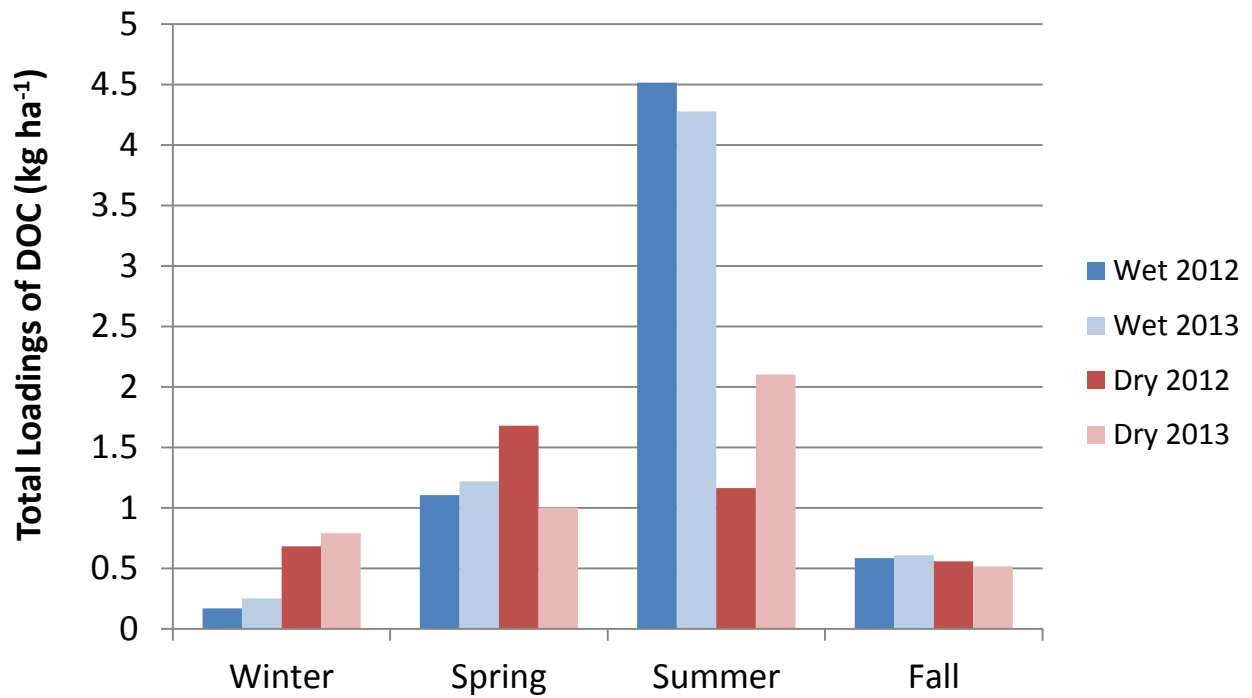
Figure 3. Total Seasonal Loadings of DOC in Wet and Dry Deposition.
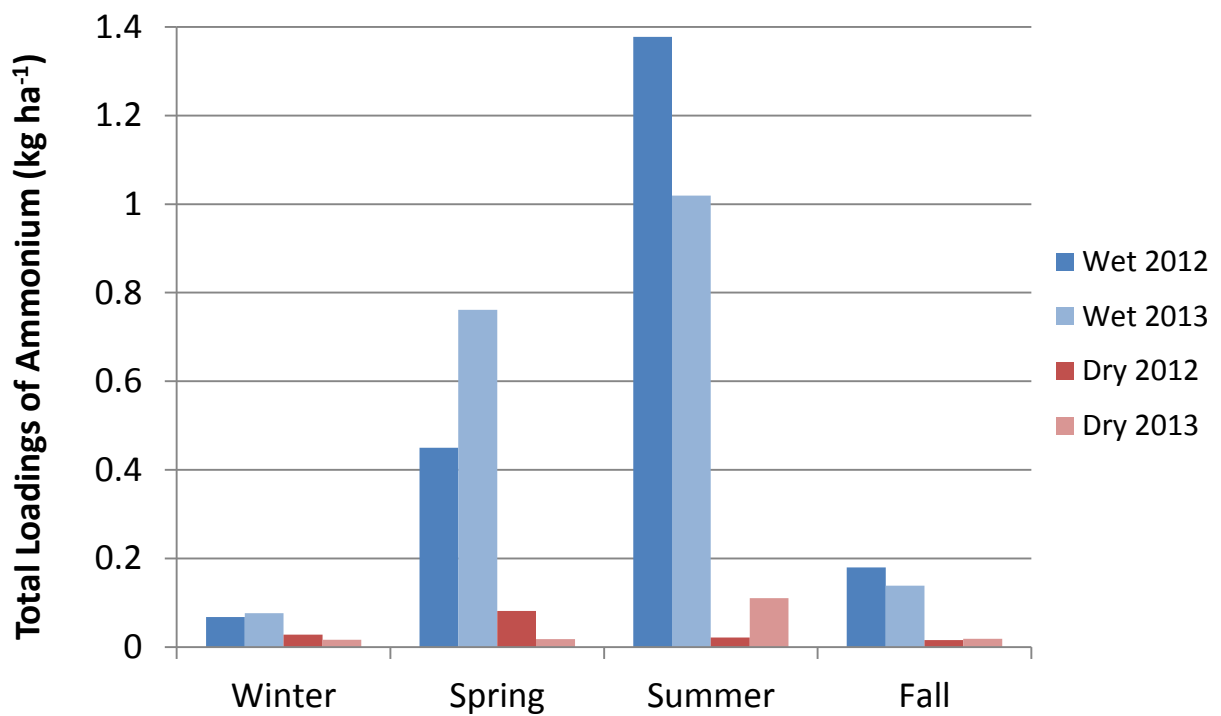
Figure 4. Total Seasonal Loadings of Dissolved Ammonium in Wet and Dry Deposition.
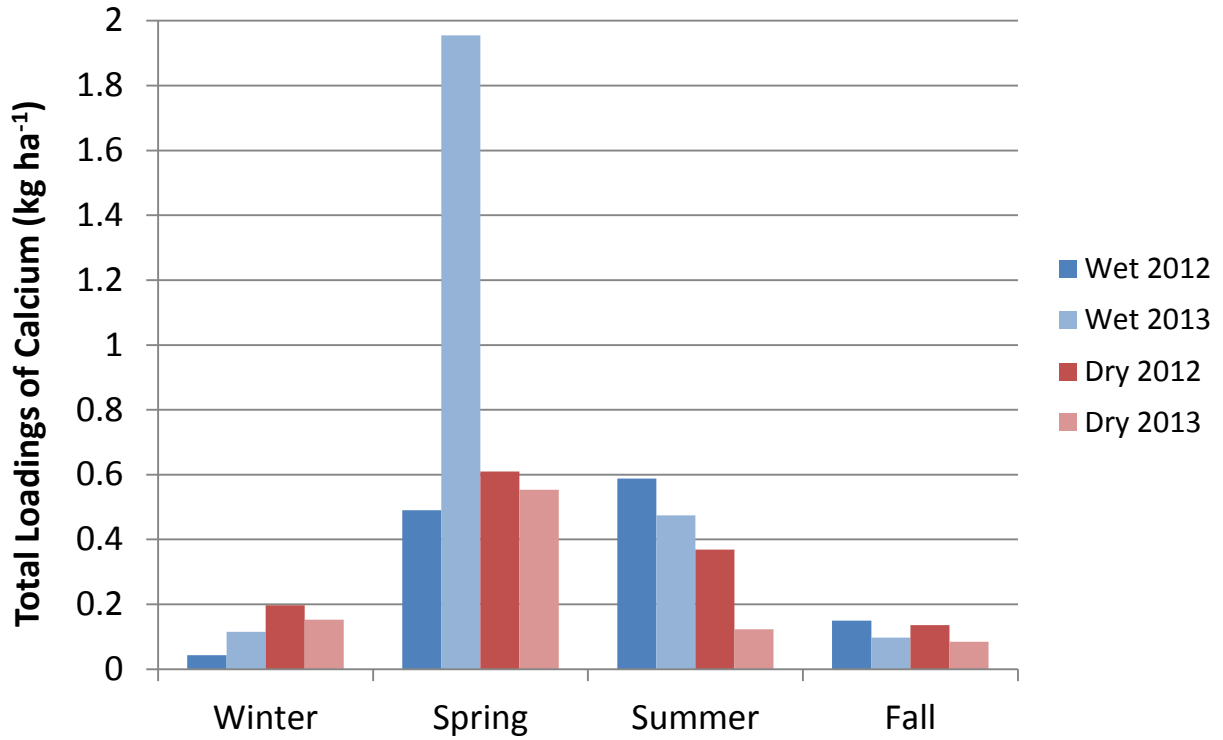
Figure 5. Total Seasonal Loadings of Dissolved Calcium in Wet and Dry Deposition.
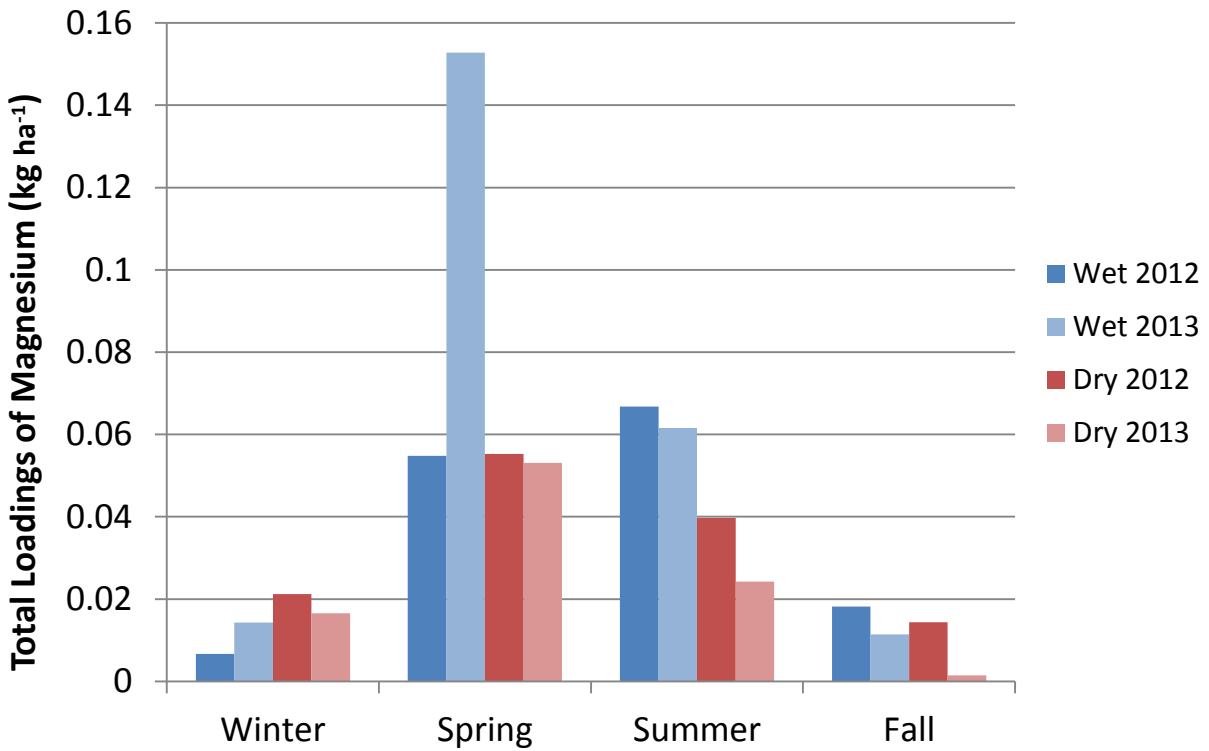
Figure 6. Total Seasonal Loadings of Dissolved Magnesium in Wet and Dry Deposition.
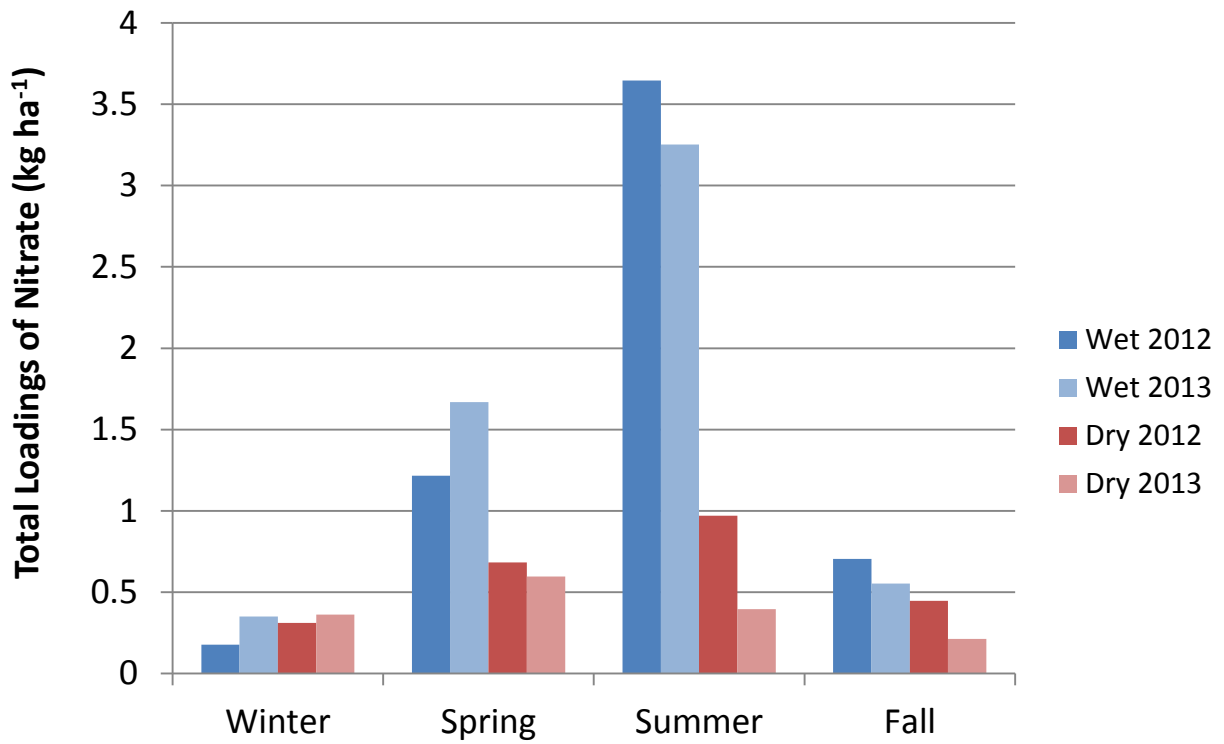
Figure 7. Total Seasonal Loadings of Dissolved Nitrate in Wet and Dry Deposition.
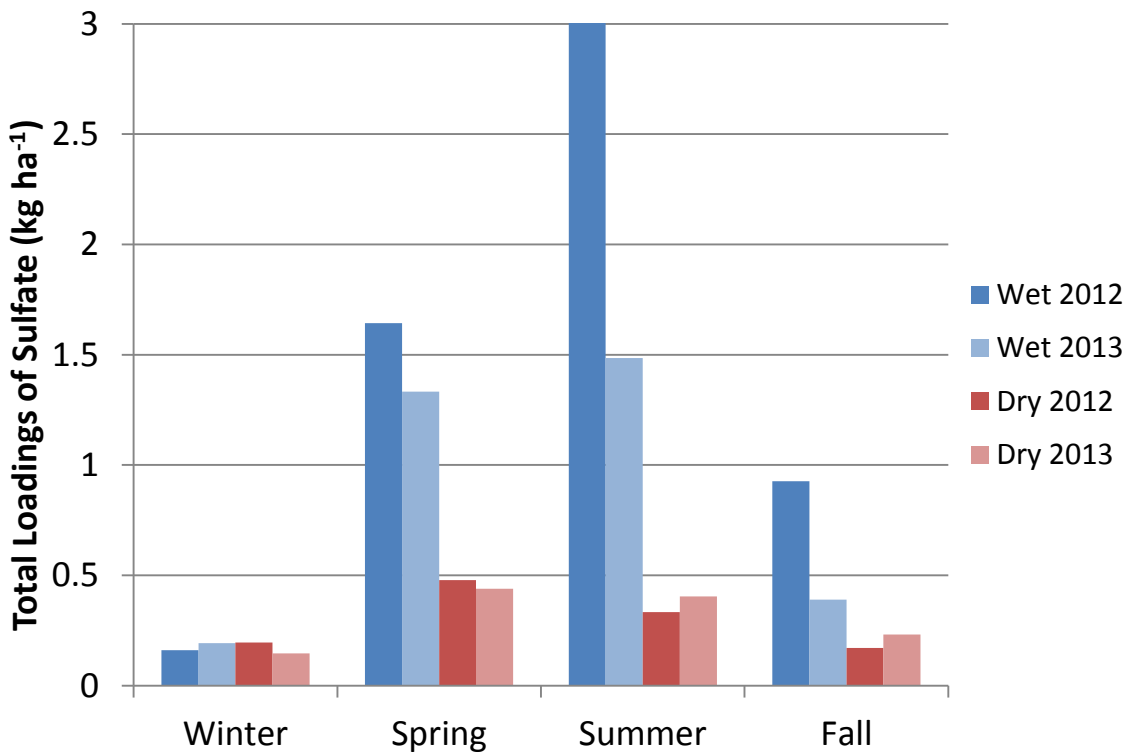
Figure 8. Total Seasonal Loadings of Dissolved Sulfate in Wet and Dry Deposition.
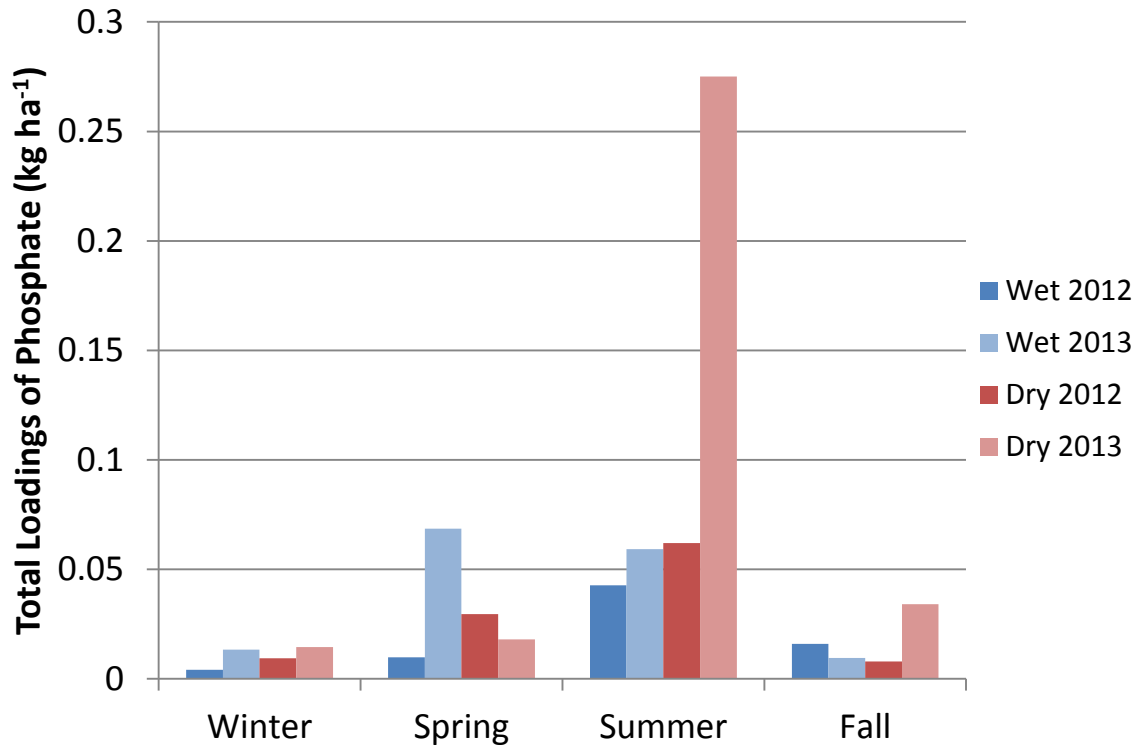
Figure 9. Total Seasonal Loadings of Dissolved Phosphate in Wet and Dry Deposition.
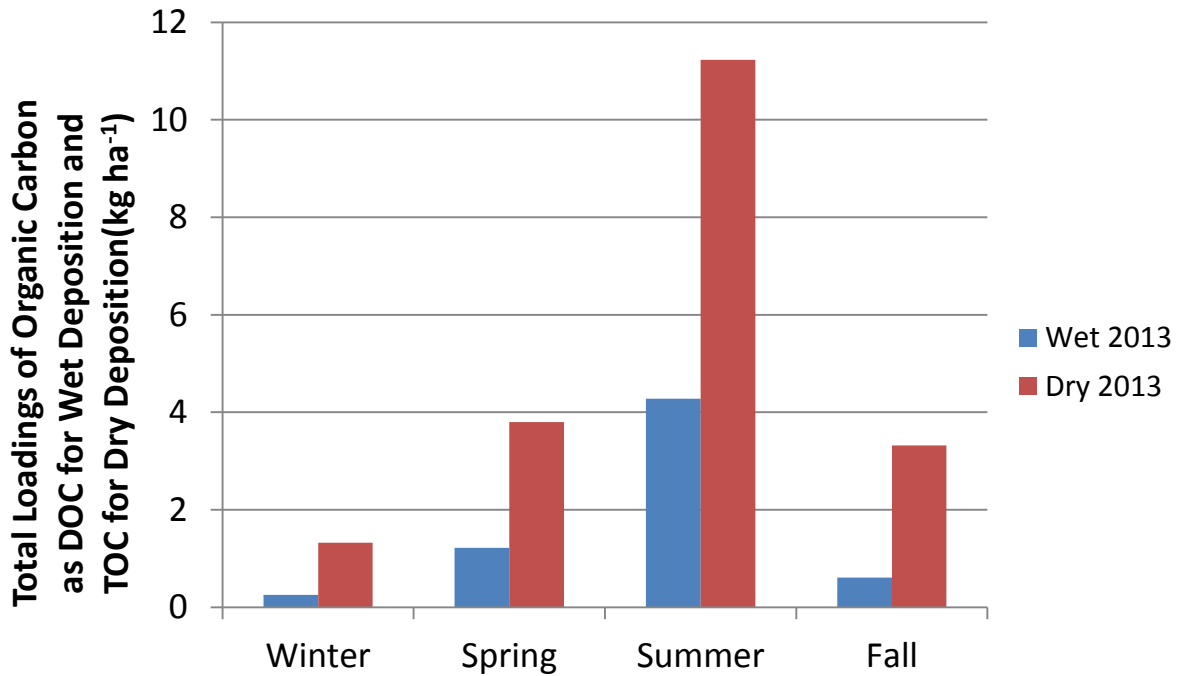
Figure 10. Loadings as DOC for Wet Deposition and TOC (particulate and dissolved) for Dry Deposition.

4.5 Chemistry Correlations

The two year data set showed that DOC loadings were strongly correlated with NH_4^+ ($R^2 = 0.826$; p value < 0.01), NO_3^- ($R^2 = 0.8997$; p value < 0.01), and SO_4^{2-} ($R^2 = 0.6900$; p value < 0.01) in the wet deposition. DOC loadings in the dry deposition were significantly correlated with NH_4^+ ($R^2 = 0.6943$; p value < 0.001) and PO_4^{3-} ($R^2 = 0.6765$; p value < 0.001), yet TOC loadings in the dry deposition were even more strongly correlated with NH_4^+ ($R^2 = 0.9116$; p value < 0.001) and PO_4^{3-} ($R^2 = 0.8781$; p value < 0.001) (Appendix A-3). Correlations were strongest in the summer for both wet and dry deposition constituents, for example the summer wet deposition of DOC and NH_4^+ correlation explains 93% of the data during that season ($R^2 = 0.9324$; p value < 0.001) and summer dry deposition of DOC and NH_4^+ correlation explains 82% of the data ($R^2 = 0.8256$; p value < 0.001) and the TOC and NH_4^+ correlation explains greater than 99% of the data ($R^2 = 0.9962$; p value < 0.001). The summer season also introduces other relationships, such as NH_4^+ and SO_4^{2-} correlations were .strongest in wet deposition ($R^2 = 0.8383$; p value < 0.001) and had a significant relationship in dry deposition, but the data is not as well fit ($R^2 = 0.3913$; p value < 0.001). Ca^{2+} and Mg^{2+} were strongly correlated in both wet deposition ($R^2 = 0.9166$; p value < 0.001) and dry deposition ($R^2 = 0.8129$; p value < 0.001), and were the most strongly correlated for both spring wet deposition ($R^2 = 0.9216$; p value < 0.001) and dry deposition ($R^2 = 0.8567$; p value < 0.001). Additionally, TOC in the spring dry deposition is strongly correlated with PO_4^{3-} ($R^2 = 0.8696$; p value $= 0.007$).

4.6 CASTNET Comparison

During the two year study, the CASTNET data and our Niwot Ridge data followed a similar trend with peaks and minima occurring roughly during the same. Correlations between the two datasets were significant for Ca^{2+} (p value $= 0.001$; $R^2 = 0.19$), Mg^{2+} (p value < 0.0001; $R^2 =$

0.26), and SO_4^{2-} (p value < 0.0001; $R^2 = 0.42$). The Niwot Ridge data for dry deposition loadings were an order of magnitude greater than the CASTNET data for Ca^{2+}, Mg^{2+}, NO_3^-, and SO_4^{2-} (Figures 11-15). NH_4^+ concentrations and loadings in the CASTNET data were not significantly different from the Niwot Ridge data.
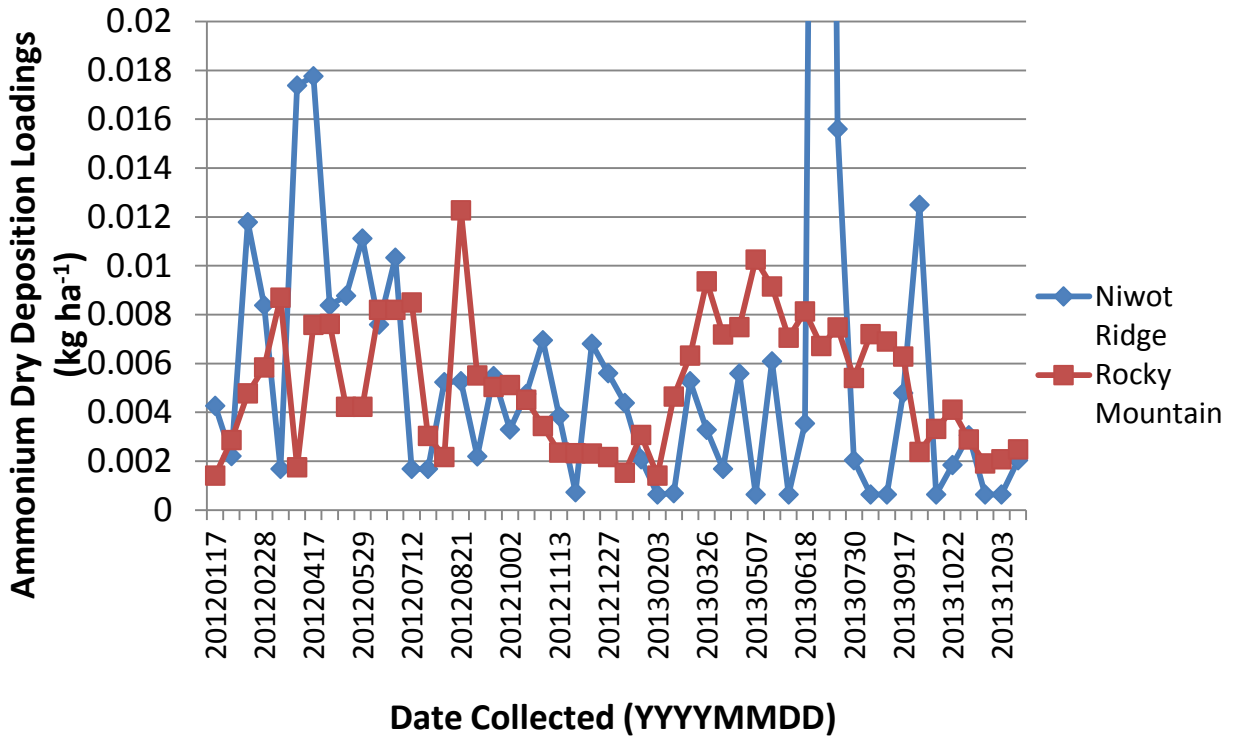
Figure 11. Ammonium Loadings in Dry Deposition for CASTNET at Rocky Mountain vs LTER Niwot Ridge. Outlier removed from July 2013 (0.087 kg ha^{-1}).
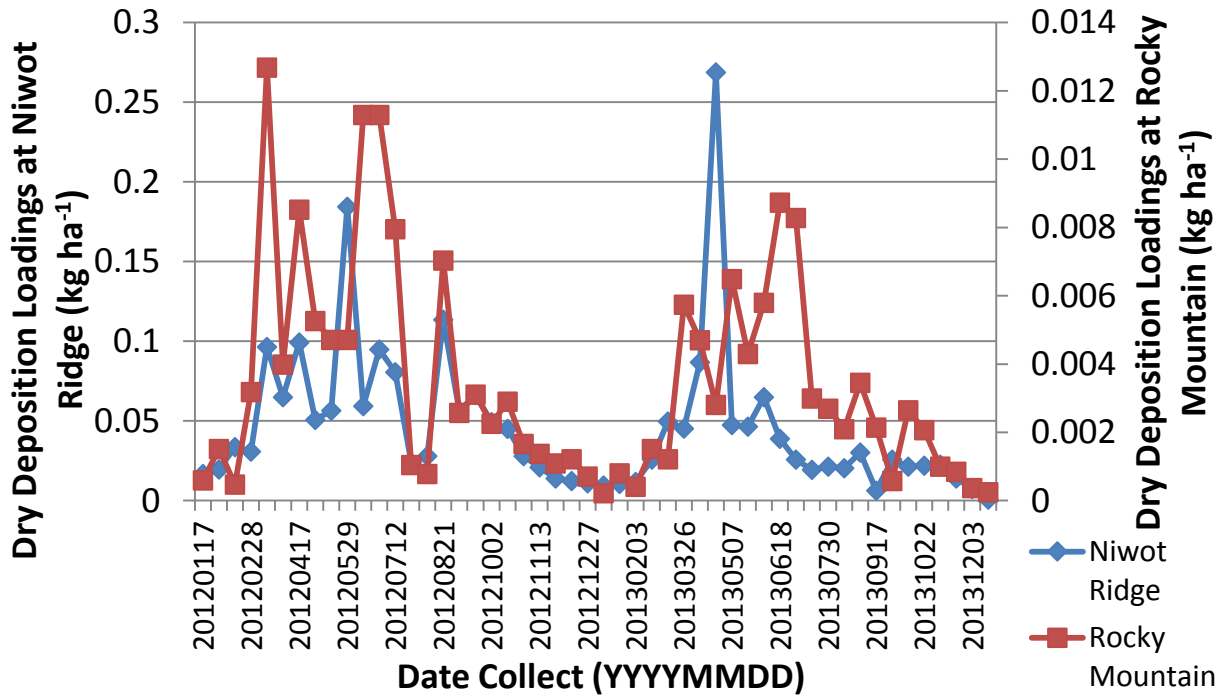
Figure 12. Calcium Loadings in Dry Deposition of CASTNET at Rocky Mountain vs LTER Niwot Ridge.
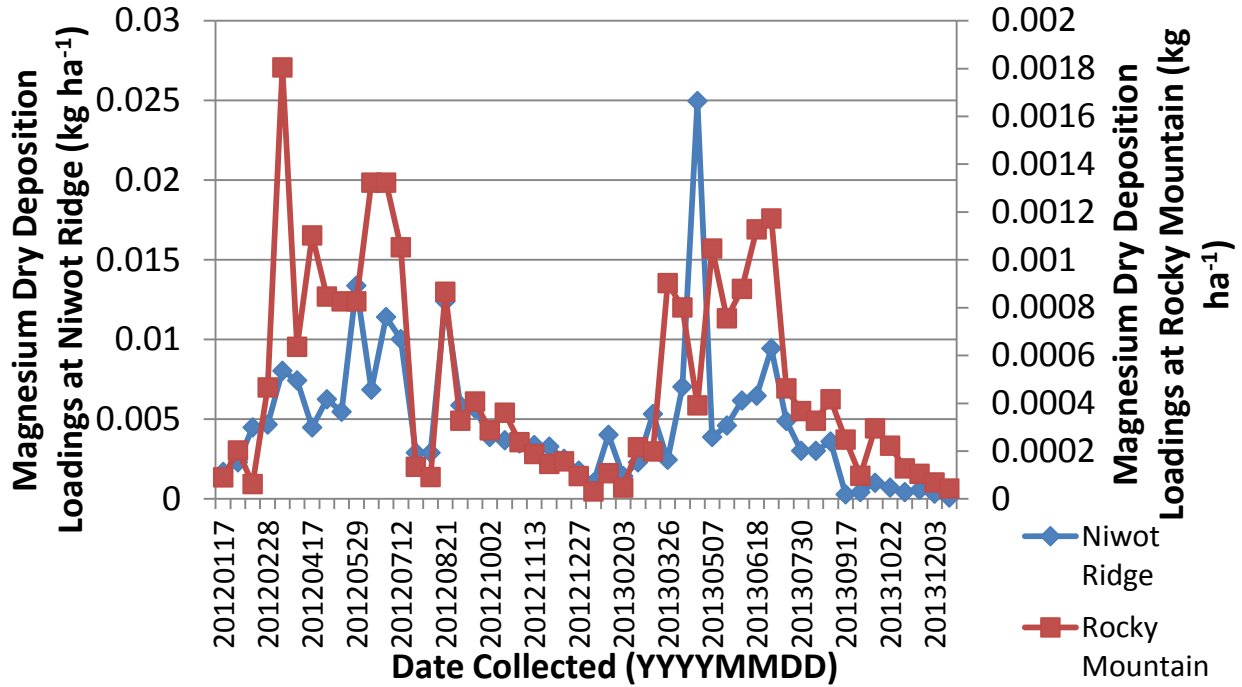
Figure 13. Magnesium Loadings in Dry Deposition for CASTNET at Rocky Mountain vs LTER Niwot Ridge.
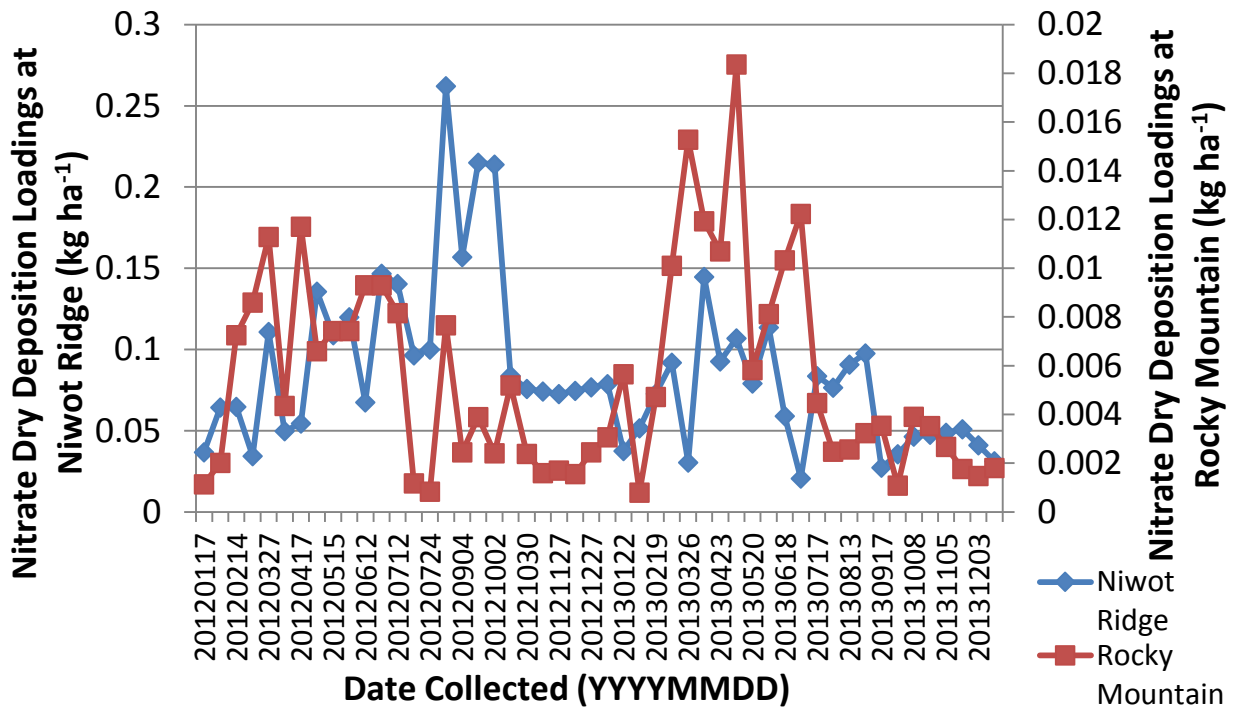
Figure 14. Nitrate Loadings in Dry Deposition for CASTNET at Rocky Mountain vs LTER Niwot Ridge.
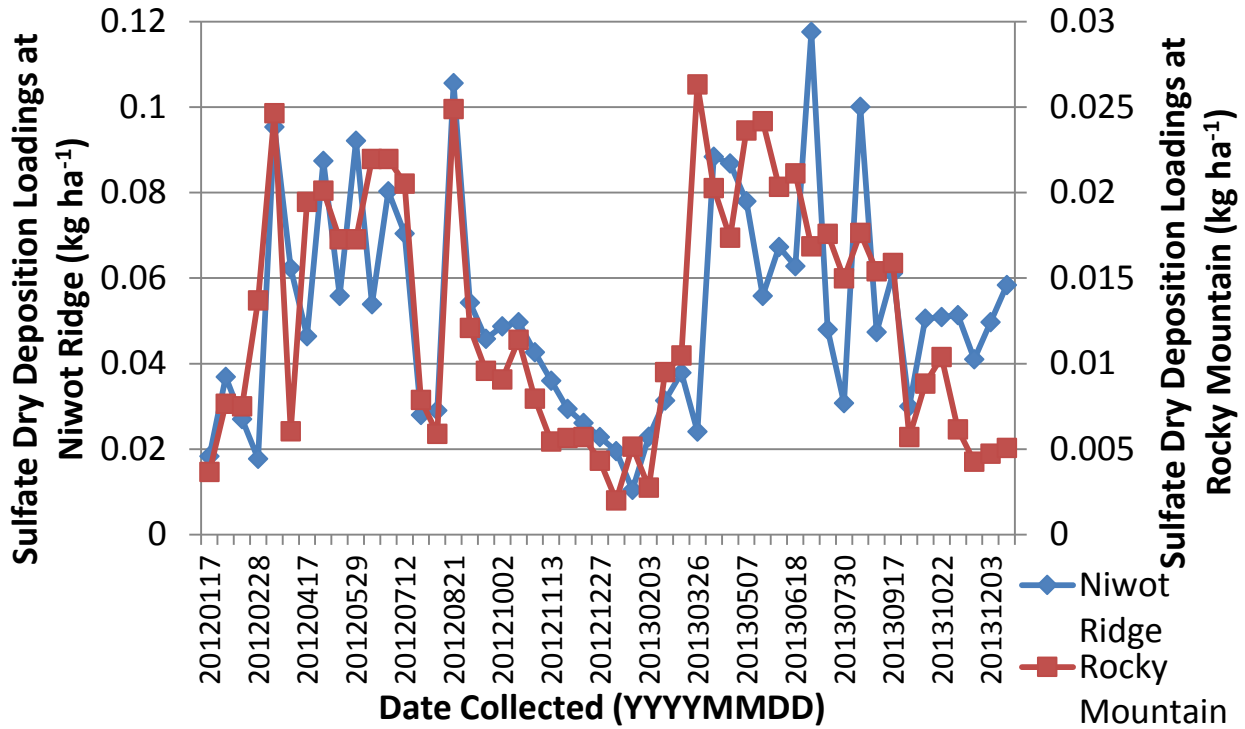
Figure 15. Sulfate Loadings in Dry Deposition for CASTNET at Rocky Mountain vs LTER Niwot Ridge.

4.7 Backwards Trajectories

Backwards trajectories using the NOAA HYSPLIT model showed that for the majority of the year, both wet and dry deposition trajectories are coming from the west/northwest, some reaching as far as the coast of Northern China, and from the southwest/Four Corners USA (Appendix A-4). A few trajectories showed several turbulent paths for some wet and dry deposition samples that appear to have started in the Rocky Mountains, west of the collection site. For both wet and dry deposition during the summer months, the majority of the trajectories originated off the Gulf of Mexico, moved west toward the Pacific Ocean and then moved northeast through the Four Corners USA before arriving at Niwot Ridge. Several summer wet and dry deposition samples showed trajectories that were moving directly north from the Gulf of

Mexico and then moving west across the Colorado Front Range or originating in the southwest off the coast of Baja California and traveling through the Four Corners.

Table 3. Numbers of Biweekly Collection Periods with Backwards Trajectories Originating from the Northwest, Northwest/Four Corners, South/Four Corners, and Rocky Mountain Directions*

	Northwest	Northwest/Four Corners	South/ Four Corners	Rocky Mountains
Winter	4	7	-	-
Spring	2	8	2	1
Summer	-	1	7	4
Fall	2	6	1	-

* Directions were determined by majority of the backwards trajectories.

4.8 Marbles vs. Bucket Collection Method

During the spring and summer of 2012 and the summer and fall 2013, 5-gallon buckets were used to collect dry deposition simultaneously while collecting dry deposition with the marble insert method. The purpose of collecting two samples of dry deposition by these two separate methods during the same collection period was to assess if the marble method was able to retain higher amounts of total particulate mass. A paired t-test revealed that the use of marble inserts does result in significantly higher (p value <0.02) amounts of total particulate mass than without marble inserts (Figure 16).
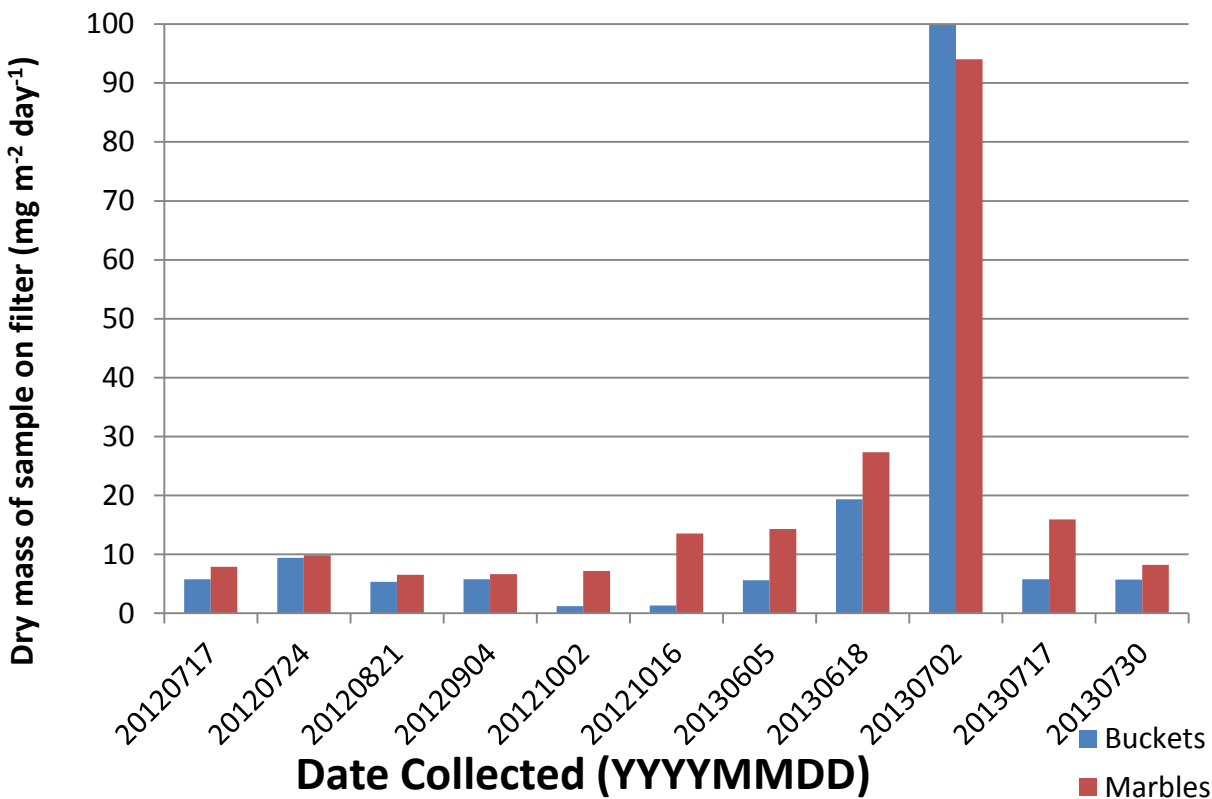
Figure 16. Dry Mass of Dry Deposition Bucket versus Marbles Collection Technique.

5. Discussion

Here, we present information about the chemical characteristics and the seasonality of atmospheric wet and dry deposition for a remote alpine environment. The results provide evidence that the atmospheric wet and dry deposition of C, N, P, and Ca^{2+} are important inputs of these elements to the carbon limited and undeveloped alpine soils at Niwot Ridge, and confirm earlier estimates posed by Mladenov et al. (2012). The annual VWM concentrations of DOC in this study, 1.10 mg C l^{-1} in 2012 and 0.84 mg C l^{-1} in 2013, are within the range 0.77 to 1.42 mg C l^{-1}, as previously determined by Mladenov (2012) and Ca^{2+} loadings in wet deposition during this study, 1.27 kg Ca^{2+} ha^{-1} in 2012 and 2.64 kg Ca^{2+} ha^{-1} in 2013, were also within the range 1.14 to 3.72 kg Ca^{2+} ha^{-1} yr^{-1} as determined by Mladenov et al. (2012) during the period of 2002

to 2010. Atmospheric dry deposition inputs have not been previously quantified by direct measurement, but had instead been estimated either by mass accumulation measurements in snow (Mladenov et al., 2012) or with atmospheric concentration measurements and deposition velocity models, such as the EPA CASTNET method. A revised C budget using the C budget from Mladenov et al., 2012 for the Green Lakes 4 watershed was recalculated using the dry deposition POC values determined from this study (Appendix A-6). Dry deposition for this alpine catchment nearly tripled; however, the dry deposition in the previous study was determined using the maximum accumulation of the snowpack. Maximum accumulation of the snowpack typically occurs in late April or early May, but these results show that dry deposition during the summer months are a substantial input to this alpine C budget.

The results of this study show that atmospheric deposition into alpine environments is variable from season to season and from year to year in both wet and dry deposition. Ca^{2+} and PO_4^{3-} annual loadings analyzed during this two-year period were not significantly different between wet and dry deposition. However, annual wet deposition loadings of NH_4^+, Mg^{2+}, NO_3^-, SO_4^{2-}, and DOC were significantly greater than loadings of those constituents in the water soluble fraction of dry deposition (p values <0.02). This is inconsistent with previous studies by Sievering et al. (1989), which showed that the atmospheric loading of NO_3^- by wet, dry, and fog deposition from the atmosphere to a lodgepole pine canopy at 3100 m elevation on Niwot Ridge was more than double that of NO_3^- wet deposition alone. Also Lovett and Kinsman (1990) showed that deposition decreases as the elevation gradient increases. However, the Soddie collection site, where our samples are collected, is at the upper limit of the treeline (bordering the alpine) so the inputs to the canopy found in the studies by Sievering et al. (1989) and Lovett and Kinsman (1990) could be different than a sparsely covered area such as in this study. If the

deposition is not significantly different from the upper limit of the treeline and the forest canopy, the lower values of those constituents in this study could likely reveal that the water soluble fraction of dry deposition contains less constituent mass than wet deposition and that the particulate fraction likely contributes additional mass that could not be measured in this study. Indeed, in the case of OC, for which POC mass was measured, the particulate form contributed an additional $60\% \pm 15\%$ to the total OC loading. The extraction method for the water soluble fraction of dry deposition calls for 20 minutes of contact time between water and particulates collected in the marble insert, and this may not be enough time for complete dissolution of the OC and nutrients. Therefore, the quantities measured here may be conservative or underestimate the water soluble fraction of dry deposition. Another difficult aspect to atmospheric deposition collection in this study is the unknown amount of cloud water or fog that may or may not have been captured in the collection process as either wet or dry deposition. Finally, even with the use of marble inserts, the turbulent conditions that exist at high elevation sites may prevent particulates from entering the collection container, and direct measures of dry deposition with bucket style collectors tend to underestimate this fraction of deposition (Goossens and Offer, 1995). Nevertheless, as will be discussed below, direct deposition measurements with NADP-style collectors are able to retrieve higher amounts of most dry deposition chemical constituents, compared to CASTNET filter packs.

Atmospheric wet and dry deposition showed a seasonal variability, which revealed wet deposition mainly had maximum loadings that would occur during the summer, except for Ca^{2+}, Mg^{2+}, and PO_4^{3-}, which occurred mainly in the spring. Dry deposition loadings often had maximum loadings occurring in the spring, except for PO_4^{3-}, which was highest in the summer. NO_3^- and DOC in 2012 and NH_4^+ and TOC in 2013 were also highest in the summer. Wet

deposition DOC concentrations in this study are in agreement with past quantitative results; such as those from Willey et al. (2000) who found that, overall, the highest DOC concentrations in wet deposition were from 'continental' rain, due to low-pressure systems, local thunderstorms and cold fronts in contrast to 'marine' rain. Avery et al. (1991) also found DOC concentrations were highest during local thunderstorms, suggesting that thunderstorms provide substantial vertical mixing in atmospheric regions with extreme sunlight and high ozone, and may therefore contribute to organic acid formation. Findings from both Willey and Avery are consistent with the typical summer weather patterns and conditions of the Colorado Front Range.

The significant relationship between NH_4^+ and SO_4^{2-} min both wet and dry deposition may reveal that SOA formation is occurring in the summer months, coinciding with the growing season when the vegetation is emitting the maximum amount of VOCs (Peñeulas et al., 1999) and upslope wind conditions (Brazel and Brazel, 1983) that may be delivering higher concentrations of SO_2 from the Denver-Boulder metro area and NH_4^+ from the Front Range area. Conifers exposed to high concentrations of SO_2 have been found to emit greater amounts of monoterpenes than control trees (Richter and Wild, 1992). Ehn et al. (2014) found ammonium sulphate (AS) seed addition causes a decrease in extremely low volatile organic carbons (ELVOCs), such as an terpenes, due to an increased particulate condensation sink, and a corresponding increase in SOA mass was detected (Appendix A-5). ELVOCs are a recently discovered highly oxidized group of multifunctional products, which are important for the nucleation and possibly make up 50–100% of SOA in early stages of particle growth in Hyytiälä (Ehn et al., 2012). Higher summer loadings of NH_4^+, Ca^{2+}, Mg^{2+}, NO^{3-}, SO_4^{2-}, and DOC in wet deposition compared to dry deposition suggest that some of these nutrients, such as NH_4^+, NO^{3-}, SO_4^{2-}, and DOC may be related to SOA formation which are elevated during the growing season

due to maximum VOCs being emitted from trees. SOA formation is important for cloud formation and may be additionally scavenging Ca^{2+} and Mg^{2+} from the atmosphere during the summer, which is often when this region experiences daily rainfall in the afternoons, especially during the month of July, which is that start of the monsoon season in the south.

Ca^{2+} and Mg^{2+} were strongly correlated in both wet deposition and dry deposition, especially during the spring. Additionally, TOC in the spring dry deposition is strongly correlated with PO_4^{3-}. These relationships may represent likely dust sources of these nutrients from the dust events that often occur during the spring in the arid west.

CASTNET dry deposition recorded less than 20 miles away at Rocky Mountain National Park, a U.S. EPA directed program, showed roughly a similar trend in maximum and minimum loadings during the same dates, but the data collected at Niwot Ridge for this study was an order of magnitude greater than the EPA directed CASTNET data collection for all constituents except for NH_4^+. This order of magnitude difference could be due to 1) the Rocky Mountain collector is located at an elevation that is 600 m lower than Niwot Ridge in a forested area, 2) Niwot Ridge is located closer to the Denver metropolitan area and therefore greater influence of atmospheric pollutants may be underway, or 3) CASTNET's filter pack technique is not able to capture larger particles that may instead be preferentially captured by gravitational deposition in the NADP-style collector. Previous studies have found that an increase in elevation gradient causes a decrease in chemical concentrations (Lovett and Kinsman, 1990); therefore, it is unlikely that the alpine area at Niwot Ridge would contain more nutrients than the CASTNET Rocky Mountain site which is located at a lower elevation. Additionally, previous studies have shown that CASTNET + NADP estimates of N deposition in semiarid forests of the West can be several-fold lower than throughfall fluxes (Kolian & Haeuber, 2004). This is likely due to the CASTNET

method is primarily obtaining the aerosol fraction of atmospheric constituents and not necessarily the larger particulate form of atmospheric constituents.

Backwards trajectories show that the majority of the year, both wet and dry deposition are coming from the west/northwest, with some samples originating as far as off the coast of Northern China, and the southwest/Four Corners USA. Both directions contain arid regions to the immediate west of the continental divide which could be contributing dust particles to the air masses as they move through these regions. These areas to the west have several coal-fired power plants, mining, oil and gas drilling, and millions of acres of farmland and large feedlots. Therefore, emissions from these sources could be contributing substantially to the nutrient loading to the alpine. Summer trajectories that originate off the Gulf Coast appear to be influenced by the summer monsoon season and some of these trajectories move directly north and along the Colorado Front Range, likely picking up pollutants such as NO_x and SO_x. As the air masses move across the subalpine forest, these pollutants may then interact with oxidized VOCs originating from vegetation, which contribute to new particle formation as SOAs.

This study directly confirmed that the use of marble inserts described in Goss et al. (2013) were more effective at retaining dry deposition than the use of a bucket that did not contain marbles (p value = 0.025). The marbles are likely providing a greater surface area for protecting the particulates from being blown out of the buckets during periods of high wind. It is likely that there is a large underestimate of the cumulative loading values in this study due to the missing of 72 days of data during this two year study (714 days). Additionally, it is unknown to what extent the nutrients in cloud and fog deposition contributed to either wet or dry deposition collection during this study.

6. Conclusion

Our results demonstrated that atmospheric deposition represents a substantial input of C, N, P, Ca^{2+} and Mg^{2+} to the alpine environment at Niwot Ridge. Overall, wet deposition loadings were significantly greater than dry deposition loadings of DOC, NH_4^+, Mg^{2+}, NO_3^-, and SO_4^{2-}. Mg^{2+} and PO_4^{3-} loadings were not significantly different in wet deposition than in dry deposition loadings. High summer loadings of DOC, NH_4^+, and SO_4^{2-}, as well as their strong summer correlation suggest SOA formation is occurring and implicate air pollutants and VOCs in the high summer DOC loading. Large increases in summer deposition loadings may reflect a combination of changing upslope wind patterns in the summer that would be expected to transport NO_x, SO_x, and possibly carbonaceous pollutants from the large urban Denver metro area and surrounding large agricultural areas. Indeed, backwards trajectories showed that, in the summer months, wind directions appear to change and storms occurring over the Gulf Coast in the south during the monsoon season tend to migrate north, often coming from the east over the Front Range, likely picking up NO_x and SO_x pollutants from urban and large agricultural areas. These summer trajectories also showed trajectories occurring over the Gulf Coast either moving directly north or sometimes moving initially west, but then moving northeast through the Four Corners of the USA before depositing at Niwot Ridge. These samples showing these trajectories during the summer, early July through early August, often had the highest loadings of nutrients, therefore the southern monsoon season may be influencing the increased nutrient loads during the summer. Backwards trajectories show that most air movements during the year come predominately from the west, mainly the northwest or southwest/Four Corners, USA, which may also bring dust and air pollutants.

Chapter 3 - Organic Matter Characterization of Atmospheric Wet and Dry Deposition Found in Alpine Environments in the Colorado Rocky Mountains

1. Introduction

In recent decades, extensive research has been conducted on aquatic dissolved organic matter (DOM) to better understand the biochemical structure of DOM and its role in the biogeochemistry of aquatic systems. Significant improvements in DOM characterization techniques have led to the understanding that DOM is a complex mixture of soluble organic compounds that differ in reactivity and ecological role, such as providing C (Wetzel, 1992) and nitrogen (Keil and Kirchman, 1991) in aquatic food webs. Advances in spectroscopic techniques with absorbance and fluorescence provide an alternative to traditional approaches for DOM characterization (Cobel et al., 1990; McKnight et al., 2001) Fluorescence characterization of DOM is a rapid, yet precise and inexpensive technique that provides information about the source, redox state, and biological activity of DOM (Miller et al., 2009; Mladenov et al., 2010). Recently studies have been using fluorescence spectroscopy to explore the characteristics of fog and rainwater DOM to improve the understanding of atmospheric organic matter chemistry and composition. These studies also examine how atmospheric organic matter affects the climate system, atmospheric processes, and human health, yet there are few studies that explore the spectral properties of atmospheric DOM in dry deposition.

Carbon (C) compounds, sometimes called 'carbonaceous aerosols' account for a large fraction of atmospheric particulate matter. The dominant fraction of carbonaceous aerosol is organic C, which includes all organic compounds present in the particle phase. Atmospheric fine

particulate matter can attribute 20 to 90% of aerosol mass in the lower troposphere (Kanakidou et al., 2005). It has been shown that a significant contribution to the total mass of organic compounds present in atmospheric aerosols is from macromolecular species (Zhang et al., 2007). The largest portion of these species were structurally similar to humic and fulvic acids and were, therefore, termed HUmic-LIke Substances (HULIS) (Havers et al., 1998; Zappoli et al., 1999; Decesari et al., 2000; Kiss et al., 2002). Atmospheric HULIS share some important features such as polyacidic nature, yet mounting evidence suggests that HULIS differ substantially from terrestrial and aquatic humic and fulvic substances, for example in surface activity and droplet activation efficiency (Graber and Rudich, 2006). HULIS can influence various aerosol properties, including optical parameters, cloud condensation nuclei (CCN) and ice nuclei (IN) action, surface tension and hygroscopicity (Kiss et al., 2005). Spectroscopic techniques in combination with air mass backward trajectories using the National Oceanic and Atmospheric Administration (NOAA) Hybrid Single Particle Lagrangian Integrated Trajectory Model (HYSPLIT) were used by Mladenov at al. (2009) support the notion that dust emitted in Africa and deposited in the Sierra Nevada Mountains of Spain contained significant amounts water soluble organic carbon (WSOC) with humic-like fluorescent compounds. The humic-like fraction of atmospheric aerosols is becoming a research topic that is gaining interest, yet sources and chemical quality of this fraction are not well defined (Graber and Rublich, 2006). Recent studies have indicated that the optical properties of chromophoric water soluble organic compounds in the atmosphere may be similar to chromophoric DOM (CDOM) in terrestrial and aquatic environments (Kiss et al., 2003; Kieber et al., 2006; Duarte et al., 2007). UV-vis absorbance and fluorescence spectra of WSOC found in atmospheric samples in the ultraviolet and visible (UV-vis) range have been shown to provide some evidence that terrestrial and aquatic

humic substances may be similar in chemical structure (Graber and Rudich, 2006 and references therein). Measurements of absorbance and fluorescence ratios and DOC-normalized specific UV absorbance (SUVA) may be used to further evaluate the similarities between atmospheric HULIS and terrestrial and aquatic humic substances (Kiss et al., 2003; Duarte et al., 2005, 2007; Kieber et al., 2006).

Irradiation from the sun can transform biologically recalcitrant DOM into labile substances that promote bacterial growth (Moran and Zepp, 1997; Miller et al., 2002; Obernosterer and Benner, 2004). These DOM phototransformations increase both bacterial respiration and biomass. The subsequent biomass transfers biologically recalcitrant, yet photochemically reactive DOM to higher trophic levels (Vähätalo et al., 2011). Solar radiation can also mineralize DOC directly to carbon dioxide (CO_2, in the form of dissolved inorganic carbon DIC) or to carbon monoxide (CO) (Mopper et al., 1991; Mopper and Kieber, 2000; White et al., 2010), of which DIC is the governing photoproduct (Miller and Zepp, 1995). Solar radiation may transform dissolved organic nitrogen (DON) to ammonium (NH_4^+), which increases bacteria and algal growth in nitrogen-limited surface waters (Bushaw et al., 1996; Morell and Corredor, 2001; Vähätalo and Zepp, 2005; Vähätalo et al., 2011).

In this study we compiled data for three consecutive years (2011 – 2013) of fluorescence and absorbance properties from atmospheric wet deposition and the water soluble (<0.7 μm) compounds found in atmospheric dry deposition. Our goal was to assess the spectral properties of fluorescent atmospheric organic matter for general characterization and evaluation of the similarity to signatures of aquatic DOM. This comparison is important to both verify the presence of humic- and protein- like signatures in atmospheric DOM fluorescence and to determine whether atmospheric DOM signatures differ from those observed in other natural

aquatic environments. This work seeks to develop a better understanding of atmospheric inputs of DOM for a remote, high-elevation watershed in the Colorado Rocky Mountains, USA by examining the optical spectroscopic properties to provide additional information on the quality and sources of DOM in atmospheric deposition.

2. Site Description

Niwot Ridge Long Term Ecological Research Station (NWT-LTER) located in the Colorado Front Range of the Rocky Mountains, manages three official National Atmospheric Deposition Program (NADP) sites, which collects long-term wet deposition (Figure 16). These sites are along an elevation gradient: CO94 at 2,524 m, CO91 at 3,287 m, and CO02 at 3,520 m, and a fourth, unofficial site at Soddie (3,345 m elevation), located on the leeward side of the Rocky Mountains. The research site is located at NWT-LTER approximately 25 km west of Boulder, Colorado, which also lies within the City of Boulder Watershed. The City of Boulder also operates the Boulder Creek Critical Zone Observatory at this research location because this site contains the headwaters of the North Boulder Creek. The meteorology of this site has been described extensively (Brazel and Brazel, 1983; Parish et al., 1990; Williams et al., 1996; Turnipseed et al., 2002). In summer months, NWT-LTER commonly exhibits a typical valley-mountain flow during the summer months: typical wind patterns are generally westerly at night (downslope drainage) bringing relatively clean air from the continental divide, whereas daytime heating creates easterly flow causing upslope wind conditions and bringing air from the Denver-Boulder metro area.

The NADP style wet and dry deposition collector used in this research is dedicated to the NWT LTER program at the Soddie site, which is located near the Continental Divide in the Colorado Front Range (40°03' N, 105°35' W). Soddie contains the same

instrumentation as official NADP sites, including an Aerometrics Wet and Dry Chemistry

system. Both wet deposition samples and dry deposition samples are analyzed for DOC, pH, and

other cations and anions. Weekly wet chemistry samples and bi-weekly dry chemistry samples

are analyzed at the NWT LTER Kiowa Environmental Chemistry Laboratory. Three official

NADP wet deposition sites are located in the surrounding area: CO02, CO94, and CO91. Trends

in DOC concentration measurements at Soddie and the 3 NADP sites were determined to be

statistically similar (Mladenov et al., 2012).
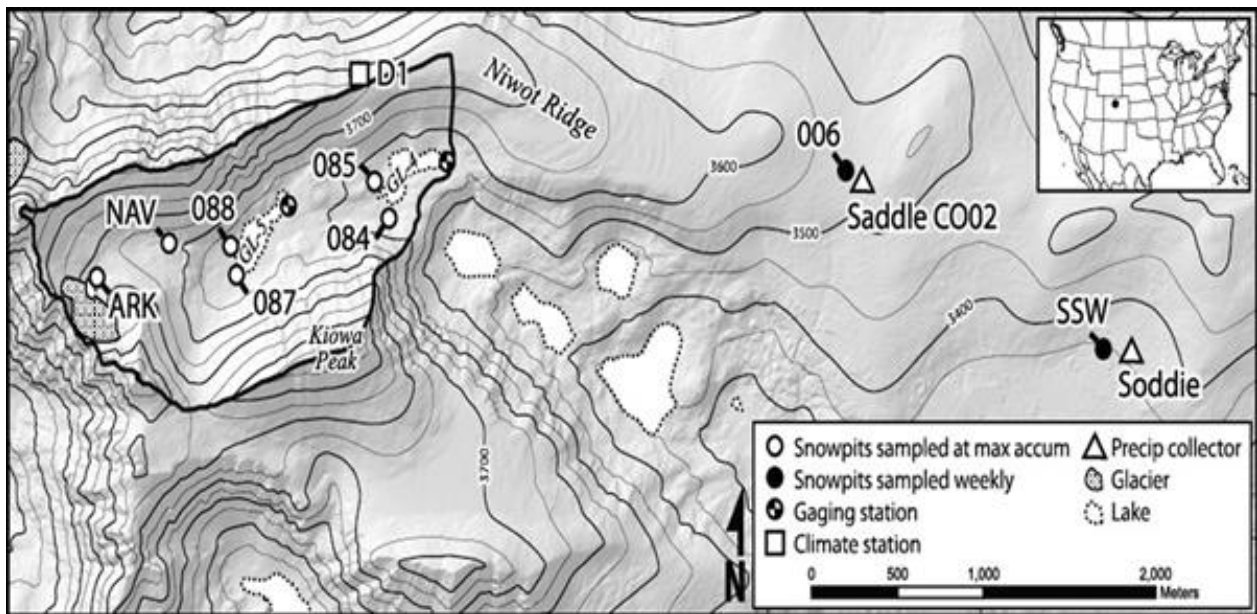
Figure 17. Site Map.

3. Methods

3.1 Sampling Collection

Physical and chemical properties of wet deposition and dry deposition are assessed in samples

collected in NADP style precipitation collectors at the Soddie site at Niwot Ridge. The quantity

of precipitation is measured as part of the NWT LTER program. Wet deposition is collected on a

weekly basis and dry deposition is collected on a biweekly basis. Wet deposition is collected

following NADP protocols. Dry deposition collectors are composed of approximately 800 g (~150) marbles that are placed into a plastic colander, which in turn rests inside a sealable Sterilite® container. This device sits on a platform that is 3.2 cm below the top of the 5-gallon dry deposition collection bucket and is exposed to dryfall for 14 days. After the collection period, the marble inserts are sealed with a leak-resistant Sterilite®lid, placed into a closed, transparent bag, and stored in a refrigerator at 4°C. Dry deposition (excluding visible insects) was collected by rinsing the bucket with 1000 mL of Milli-Q®, agitating for a minute, and then resting in the solution for 20 minutes. The aqueous solution is filtered through combusted, pre-weighed and pre-rinsed with 100 mL ultrapure water, 47 mm Whatman glass fiber (GFF) filters with an effective pore size of 0.7 μm. After filtration, the GFF filters are dried at 60°C for 24 hours. Once removed from the oven, the GFF filters are exposed to ambient air conditions for an hour before total particulate matter (PM) mass is recorded. To determine the particulate organic carbon (POC) fraction, GFF filters were combusted in a muffle furnace at 450°C for four hours to burn off all organic particulate mass. The GFF filters were exposed to ambient air conditions for one hour, and the mass was recorded. Particulate organic carbon, or water insoluble organic

carbon (WISOC), was determined as the difference between the mass of the filter before and

after combustion.

Figure 18. NADP Style Collector at the Soddie site at Niwot Ridge.

3.2 Water Chemistry Analysis

Both wet and dry deposition samples were analyzed for several specific chemical constituents

such as DOC at the Institute for Artic and Alpine Research (INSTAAR) Kiowa Environmental

Chemistry Laboratory in Boulder, CO. The dry deposition filtered samples were stored in the

dark at 4°C until analysis. Subsamples were immediately filtered through pre-combusted and

pre-rinsed (300 ml), 47-mm Whatman or Gelman A/E glass fiber filters with an effective pore

size of 0.7 μm. Filtered samples were stored in the dark at 4 C for subsequent analyses within 1

to 12 weeks. DOC concentrations were measured by high temperature catalytic oxidation with a

Shimadzu TOC-550A total organic carbon analyzer.

3.3 UV-vis Absorbance Measurements

Absorbance values were obtained using an Agilent 8453 ultraviolet (UV)– visible (vis) spectroscopy system. A 3-mL quartz cuvette with a path length of 1 cm was used and absorbance was measured at 1-nm intervals from 200 to 900 nm. UV-vis absorbance was measured in duplicate for each sample. For the wavelength range of interest (250 to 500 nm) the standard deviations always were < 1% of the measured absorbance. The photometric accuracy of the instrument is < ±0.005 arbitrary units (AU). Scattering effects were removed by subtracting the mean absorbance from 790 to 800 nm from all spectral absorbance values (Mitchell et al., 2003). Naperian absorption coefficients (a_{250} and a_{320}; m^{-1}) were used to indicate absorbance at 250 nm and 320 nm wavelengths. Absorption from 250 to 280 nm reflects absorbance by aromatic moieties (Weishaar et al., 2003). Absorption at 320 nm is, in general, used to signify UV transparency in the water column (Morris et al., 1995). The specific UV absorbance (SUVA; $m^2 g^{-1}$) was calculated as the UV absorbance value at 254 nm measured in inverse meters (m^{-1}) divided by the DOC concentration measured in milligrams per liter (mg L^{-1}) (Weishaar et al., 2003). SUVA is an "average" absorptivity for all the molecules that comprise the DOC and has been shown to be a useful parameter for estimating the dissolved aromatic carbon content, or humic fraction, of the DOC. The slope values of the linear regression of the log-transformed absorption spectra were used to calculate the spectral slopes from 275 to 295 nm and 350 to 400 nm (Helms et al., 2008). The spectral slope ratio (SR) is a dimensionless parameter that was calculated as the ratio of the slope of the shorter wavelength region (275–295 nm) to that of the longer wavelength region (350–400 nm) (Helms et al., 2008). Absorption spectral slope and slope ratios appear to be a good proxy for DOM molecular weight and provide further insight into the average characteristics about the chemistry, source, and diagenesis (Helms et al., 2008).

3.4 Fluorescence Spectral Acquisition

Fluorescence spectroscopy measures the intensity of photons emitted from a sample after it has absorbed photons. Fluorescence occurs when fluorescent capable material (fluorophores) in DOM become excited into a higher electronic state by absorbing an incident photon (UV and visible light) and cannot return to the ground state except by emitting energy as light or fluorescence. Therefore, the excitation and emission wavelengths upon which fluorescence occurs correspond to particular molecular structures. The fraction of chromophoric DOM that emits fluorescence when UV and visible light excite electrons of molecules is termed Fluorescent DOM (FDOM) (Coble, 2007). Fluorescence excitation emission (EEM) spectroscopy offers information about the chemical composition of the fluorescing DOM pool. EEMs are a 3-dimensional fluorescence illustration of fluorescence intensities scanned over a range of ex/em (ex/em) wavelengths. Humic-like fluorescent peaks have been identified as Peak A (ex/em at 260 nm/380–460 nm), Peak C (ex/em at 350 nm/420–480 nm), and a marine humic-like peak, Peak M (ex/em at 312 nm/380 - 420 nm) (Coble, 1996). Amino acid-like fluorescence peaks have been identified for tyrosine referred to as Peak B (ex/em at 275 nm/310 nm) and tryptophan referred to as Peak T (ex/em at 275 nm/340 nm) (Coble, 1996), but other compounds may also contribute to fluoresce in these low excitation/emission regions (Mladenov et al., 2011). EEMs were collected with a JY-Horiba Spex Fluoromax-3 spectrophotometer equipped with a 150-W xenon lamp. To ensure stable instrument function, a lamp scan, cuvette check, and water Raman scan were run during each time fluorescence was obtained. Samples were run at room temperature using 5 nm excitation and emission slit widths, an integration time of 0.25 s, an excitation range of 240–450 nm at 10 nm increments, and an emission range of 300–560 nm at 2 nm increments. Spectra were collected in signal-to-reference (S:R) mode with instrument-

specific excitation and emission corrections applied during post-processing in order to correct for lamp spectral properties and to compare results with those reported in other studies. EEMs were normalized to the area underneath the water Raman scan to account for decay in lamp output over time and to compare with other studies. Then, Raman-normalized Milli-Q blanks were subtracted to remove the Raman scattering signal. Instrument-specific corrections, Raman area normalization, blank subtraction, and generation of EEMs were completed using MATLAB (version R2012a). Results of the intensities of the fluorescent peaks were reported with both the mean and the median because a few samples fluoresced rather intensely which skews the mean upward. Two-dimensional fluorescence index (FI) was determined to facilitate the evaluation of microbial and terrestrial contributions to the DOM pool (McKnight et al., 2001). The FI was calculated as the ratio of emission wavelengths from 470 nm to 520 nm, obtained at excitation 370 nm. For aquatic systems, the 2-D graph of the curve from which FI values are calculated typically has a peak before 470 nm and the slope of the FI line after the peak (470 nm to 520 nm) at excitation wavelength 370 nm determines the FI value. Freshness index (FrI) is an indicator of the contribution of recently produced DOM (value closer to 1) or more decomposed DOM (value closer to 0) (Parlanti et al., 2000). FrI was calculated as the ratio of emission intensity at 380 nm dived by the emission intensity maximum observed between 420 nm and 435 nm, obtained at excitation 310 nm. Humification Index (HIX) is used as an indicator of humic substance content or extent of humification based on the idea that as humification of DOM proceeds, emission spectra of fluorescing molecules will shift to longer wavelengths due to lower H:C ratios (Zsonlay et al., 1999; Ohno, 2002). HIX is determined as the peak area under the emission spectra 435 to 480 nm divided by the peak area 300 to 445 nm, obtained at excitation 254 nm.
.

3.5 PARAFAC Modeling

Initially, PARAFAC modeling was performed for two separate data batches, wet deposition samples and dry deposition samples. EEMs were combined into two 3-dimensional data arrays: (105 samples×131 excitation×43 emissions) and (65 samples×131 excitation×43 emissions) and then each subgroup was assessed by PARAFAC individually according to the method described by Bro (1997) and Stedmon et al. (2003). PARAFAC separates the data signal into a series of three linear terms and a residual array.

$$x_{ijk} = \sum_{f=1}^{F} a_{if}\, b_{jf}\, c_{kf} + e_{ijk} \qquad\qquad i = 1\ldots K \qquad j = 1\ldots J \qquad k = 1\ldots K$$

In this application, x_{ijk} is the intensity of fluorescence for the ith sample at emission wavelength j and excitation wavelength k; a_{if} is directly proportional to the concentration (e.g., mM C) of the fth analyte in the ith sample. b_{jf} correlates linearly to the fluorescence quantum efficiency (fraction of absorbed energy emitted as fluorescence) of the fth analyte at emission wavelength j. Similarly, c_{kf} is linearly proportional to the specific absorption coefficient at excitation wavelength k. F defines the number of components in the model and the residual matrix e_{ijk} signifies variability not explained by the model. The model is calculated by minimizing the sum of squared residuals with an alternating least squares algorithm. This technique allows the signals from a complex mixture of compounds (in this case, fluorescent DOM) to be separated with no assumptions on their spectral shape or their number. The only assumptions in the PARAFAC algorithm are that each component has a unique spectra and there are no negative concentrations or spectra. The analysis was carried out in MATLAB with the "Nway toolbox for MATLAB" (Andersson and Bro, 2000). To define and validate the PARAFAC model, split-half validation was used according to Stedmon et al. (2003). The data array was divided into two halves and analyzed separately. PARAFAC models ranging from 2 to 8 components were then derived for

both data sets independently. Validation of the model was achieved by comparing the spectral shape of the components derived by the models.

The PARAFAC model returns only relative intensities of derived components called scores because the specific absorption and quantum yield of fluorescence of the components remains unknown. The intensity of the nth component in a given sample, I_n, was determined as the fluorescence intensity at the peak excitation and emission maximum of the nth component using the following equation:

$I_n = Score_n * Ex_n(\lambda_{max}) * Em_n(\lambda_{max})$

where $Score_n$ is the relative intensity of the nth component, $Ex_n(\lambda_{max})$ is the maximum excitation loading of the nth component, $Em_n(\lambda_{max})$ is the maximum emission loading of the nth component derived from the model. The total fluorescence intensity of a given sample was calculated as the sum of the components present in the (λ_{max}), which is the maximum excitation loading of the nth component, $Em_n(\lambda_{max})$, which is the maximum emission loading of the nth component calculated from the model. The total fluorescence intensity of a given sample was calculated as the sum of the components present in the sample:

$$I_{TOT} = \Sigma_1^n I_n$$

The percent contribution of each component toward the total fluorescence intensity was calculated as the ratio of the nth component intensity to a total fluorescence intensity of a given sample.

3.6 Solar Irradiation Experiment

Atmospheric constituents undergo intense solar irradiation; therefore an experiment was conducted to see how solar irradiation affects the spectral properties of fluorescent organic matter. Two different sample sets were irradiated: 1) a set of alpine soil microbes cultured by S.

Schmidt at the University of Colorado and 2) a set of commercially available compounds, including tryptophan, tyrosine, neopterin, pyridoxine, and pyridoxamine known to be present in biological aerosols (Poehlker et al., 2012). Fluorescence spectra of each sample were taken before the solar irradiation was conducted and again once the sample reached room temperature after each solar irradiation exposure to assess if any changes occurred. Samples were irradiated in a quartz tube with a rubber top at 545 W m^{-2}, roughly the average solar irradiation at Niwot Ridge determined by the program CESORA ® - Calculation of Effective Solar Radiation. Solar irradiation of samples lasted for 30 minutes and then again for 1 hour. Samples of commercially-available compounds tryptophan, tyrosine, neopterin, pyridoxine, and pyridoxamine were also irradiated for 30 min and again for 1 hour.

3.7 Statistical Analysis

Statistical analysis was conducted on the wet and dry deposition spectroscopic data. Two–sided t-test with unequal variances were conducted on the data to determine if there was statistical significance between the annual and seasonal average loadings of each constituent in wet and dry deposition using Microsoft Excel. Seasonal loadings and standard deviations were obtained using Microsoft Excel. Analytical precision for all solutes was assessed with spikes, blanks, and replicates. Detection limits can be found on the Kiowa Environmental Chemistry Laboratory website (http://snobear.colorado.edu Seiboldc/kiowa.html).

4. Results

4.1 General Spectral Features of Wet Deposition

The values of the fluorescent peaks as described in section 3.4 for the wet deposition can be found in Appendix B, Table B.1 and are summarized in Table 3 below. A leaching experiment

determined that the plain 5-gallon bucket leaches C into the sample in the bucket, therefore

affecting the fluorescence of spectra results. The use of a Teflon bag liner during the research

project prevented the plastic leaching. Unfortunately all samples before June 2012 could not be

analyzed because the previous protocol did not require a Teflon bag. Therefore, a total of 33

samples, out of 77 total wet deposition samples, were analyzed with fluorescence spectroscopy.

Additionally, some samples collected after June 2012 could not be analyzed for fluorescence

either due to not enough sample, missing sample, or the time after collection had been greater

than nine months and there was concern that the organic carbon may have been modified by

microorganisms that may be present in the sample even after filtration. The 3-D EEM spectra of

the wet deposition samples visually appeared to contain mainly characteristic peaks B and T as

described in section 3.4. Greater than 35% of wet deposition spectra contained an intense peak ,

which I will call Peak P, centered at approximately ex/em 290-310 nm/380-430 nm (Figure 19).

An additional 35% of the samples appeared to have a peak in the same area at the P Peak, but

with greater fluorescence occurring more near the ex 240 nm wavelength. Of the five

characteristic peaks (A, C, T, B, and M) described by Coble (1996), peak T was the dominant

peak in the majority of samples, with peak intensity values that ranged from 0.016 to 1291 R.U.,

with a mean peak intensity value of 43.6 ± 232 R.U. and a median peak intensity value 0.082

R.U. The greatest intensity of peak T was collected from 16 - 23 April 2013. The second most

dominant peak in most of the wet deposition samples using the fixed ex/em wavelengths for the

characteristic peaks was peak B which has peak intensity values that range from 0.012 to 1056

R.U., with a mean peak intensity value of 38.0 ± 190 R.U. and a median peak intensity value of

0.106 R.U. The sample with the most intense peak B was collected from 16 - 23 April 2013. The

third major peak exhibited in the wet deposition EEMs by the fixed excitation /emission

wavelengths of the main characteristic peaks was peak A, which has peak intensity values that range from 0.012 R.U. to 469 R.U., with a mean peak intensity value of 38.0 ± 190 R.U. and a median peak intensity value 0.168 R.U. The most intense peak A was also collected from April 16 – 23 April 2013. Finally, the two least dominant peaks using the fixed ex/em wavelengths of the characteristic peaks were peak M and peak C, with mean peak intensity values of 6.69 ± 29.4 R.U. and 1.32 ± 6.95 R.U., respectively, and median peak intensity values of 0.105 R.U. and 0.036 R.U., respectively. The most intense peaks for M and C occurred during the spring with mean values of 6.69 ± 29.4 R.U. and 1.32 ± 6.95 R.U., respectively. Each EEM appears to have an intense peak that exists at the excitation wavelength 240 nm, which is the lowest excitation wavelength of the spectrum range for fluorescence capabilities using the Flouromax-3 instrument. The peak generally appears to emit between 380 to 460 nm. Very few of the EEMs seem to fluoresce beyond the excitation wavelength of 350 nm.

Table 4. Average Seasonal Fluorescent Spectra Peaks in Wet Deposition.

	Peak A (R.U.)	Peak B (R.U.)	Peak T (R.U.)	Peak C (R.U.)	Peak M (R.U.)
Winter	0.047 ± 0.052	0.036 ± 0.021	0.035 ± 0.016	0.013 ± 0.015	0.026 ± 0.021
Spring	78.4 ± 191	176 ± 431.2	215 ± 527	6.5 ± 15.8	27.6 ± 66.6
Summer	27.1 ± 100.2	7.8 ± 26.1	3.78 ± 12.7	0.12 ± 0.21	2.1 ± 6.15
Fall	0.62 ± 0.79	0.14 ± 0.10	0.094 ± 0.076	0.08 ± 0.019	18.8 ± 1.81
Average	29.3 ± 109	38.0 ± 190	43.6 ± 232	1.32 ± 6.95	6.69 ± 29.4
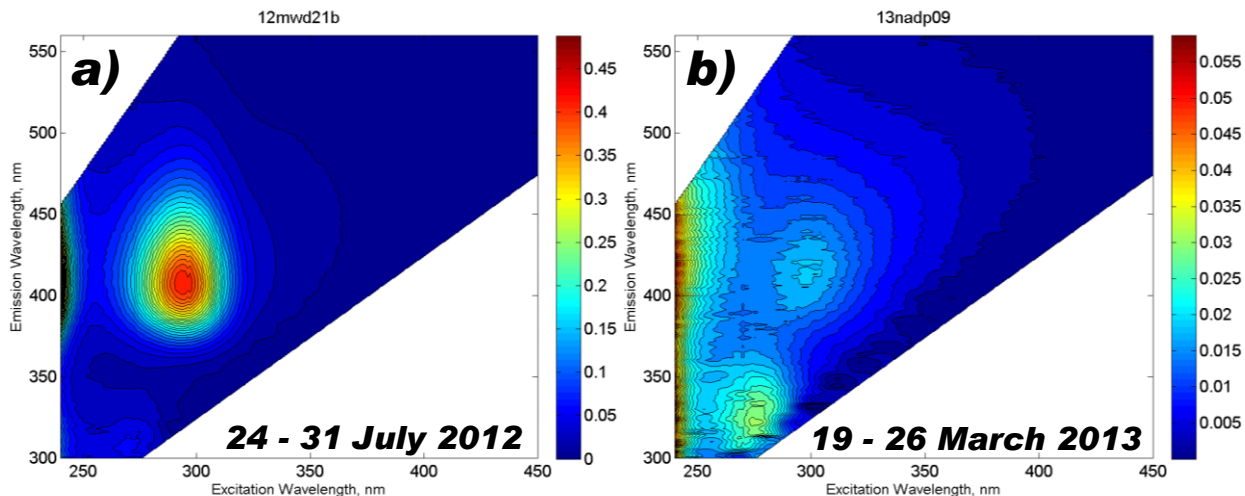
Figure 19. Representative EEMs of wet deposition samples during a) summer 2012 and b) spring 2013.

4.2 General Spectral Features of Dry Deposition

The values of the fluorescent peaks as described in section 3.4 for the dry deposition can be

found in Appendix B, Table B.2 and are summarized in Table 4 below. During the two-year

study, 40 of the 50 dry deposition samples could be analyzed for fluorescence. Ten of the

samples could not be analyzed due to either missing samples or contamination. The 3-D EEM

spectra of the dry deposition samples visually appeared to contain examples of mainly the

characteristic peaks B and T as described in section 3.4 and a slight presence of the P peak that

has an ex/em at 290-310 nm/380-430 nm (Figure 20). Of the characteristic peaks identified by

Coble (1996), the most common in the dry deposition samples was Peak B in the majority of the

samples with peak intensity values that range from 0.041 R.U. to 59.4 R.U., with a mean

intensity value of 3.7 ± 10.5 R.U. and a median intensity value of 0.306 R.U. The most intense

peak B was collected during the spring on 5 - 18 June 2013. The second most dominant peak in

the majority of the dry deposition samples was peak T, which has peak intensity values that

range from 0.025 R.U. to 39.1 R.U., with a mean peak intensity value of 2.04 ± 6.47 R.U. and a

median peak value of 0.254 R.U. The sample that contained the most intense peak T was also

collected from 5 - 18 June 2013. The third major peak exhibited in the dry deposition EEMs was

peak A, which has peak intensity values that range from 0.023 R.U. to 12.5 R.U., with a mean

peak intensity value of 0.85 ± 2.14 R.U. and a median peak intensity value of 0.170 R.U. The

most intense peak A was collected during the spring from 5- 18 June 2013. Finally the two least

dominant peaks were peak M and peak C, with a mean peak intensity value of 0.16 ± 0.24 R.U.

and 0.064 ± 0.099 R.U., respectively, and a median peak intensity value of 0.084 R.U. and 0.034

R.U., respectively. The most intense peaks for M and C occurred during the summer. Each EEM

appeared to have an intense peak that exists at the excitation wavelength 240 nm, which is the

lowest excitation wavelength of the spectrum range for fluorescence capabilities using the

Flouromax-3 instrument. Very few of the EEMs seemed to fluoresce beyond the excitation

wavelength 350 nm.

Table 5. Average Seasonal Fluorescent Spectra Peaks in Dry Deposition.

	Peak A (R.U.)	Peak B (R.U.)	Peak T (R.U.)	Peak C (R.U.)	Peak M (R.U.)
Winter	0.12 ± 0.071	0.32 ± 0.37	0.20 ± 0.16	0.028 ± 0.019	0.062 ± 0.049
Spring	2.12 ± 3.70	9.80 ± 18.1	5.31 ± 11.6	0.11 ± 0.17	0.28 ± 0.39
Summer	0.51 ± 047	0.72 ± 0.63	0.46 ± 0.43	0.066 ± 0.047	0.16 ± 0.12
Fall	0.33 ± 0.72	1.16 ± 2.76	0.53 ± 1.18	0.033 ± 0049	0.091 ± 0.16
Average	0.85 ± 2.14	3.35 ± 10.4	1.82 ± 6.47	0.064 ± 0.099	0.16 ± 0.24
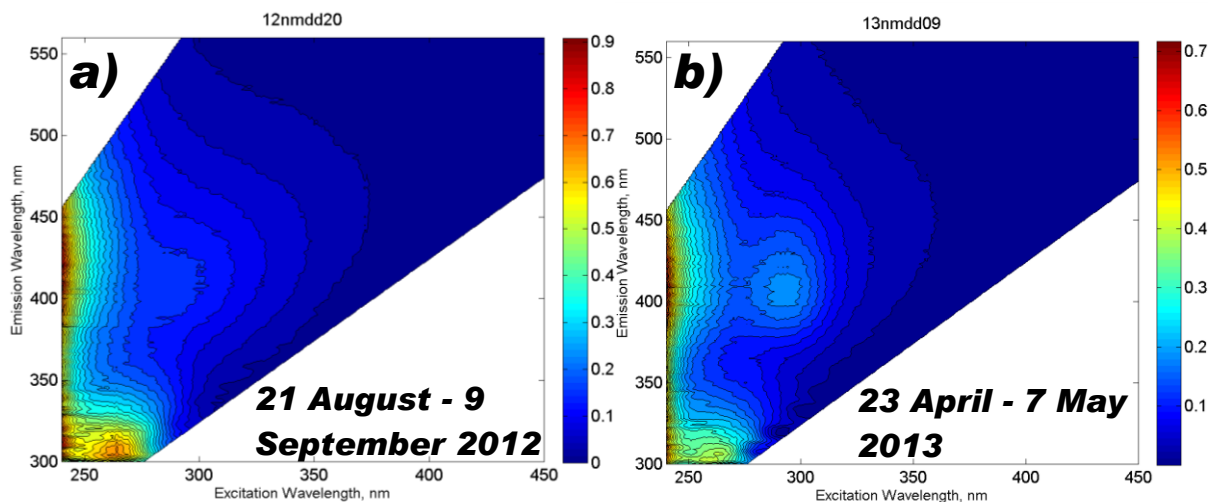
Figure 20. Representative EEMs of dry deposition samples extracted in water during a) summer 2012 and b) spring 2013.

4.3 Fluorescence Indices and UV-vis Absorbance Measurements for Wet Deposition

The values of the three fluorescence-derived indices described in section 3.4 and UV-vis absorbance measurements for the wet deposition can be found in the Appendices Table B.1 and are summarized in Table 5 below. The SUVA values range from 0.73 to 8.45 L mg C^{-1} m^{-1}, with a mean value of 1.42 ± 1.52 L mg C^{-1} m^{-1}. Only two wet deposition samples had SUVA values that were above 2.5 L mg C^{-1} m^{-1}, one from 9 – 16 April 2013 at 4.93 L mg C^{-1} m^{-1} and the other from 16 – 23 April 2013 at 8.45 L mg C^{-1} m^{-1}, which occurred during a spring. SUVA values were highest in the spring and fall. The FI values range 0.91 to 3.40, with a mean value of 1.38 ± 0.40. FI values were highest in the spring and fall. The FrI values range 0.36 to 1.33, with a mean value of 0.58 ± 0.17. FrI values were highest in the spring and fall. The HIX values range 0.018 to 3.06, with a mean value of 1.46 ± 0.83. HIX values were highest in the summer and winter.

Table 6. Summary of Fluorescent Indices in Wet Deposition.

	SUVA (L mg C^{-1} m^{-1})	FI	FrI	HIX
Winter	1.34 ± 0.42	1.29 ± 0.03	0.56 ± 0.09	1.38 ± 1.03
Spring	3.16 ± 2.99	1.73 ± 0.86	0.74 ± 0.30	1.36 ± 0.72
Summer	0.79 ± 0.33	1.28 ± 0.17	0.53 ± 0.11	1.60 ± 0.76
Fall	1.53 ± 0.71	1.39 ± 0.14	0.59 ± 0.07	1.23 ± 1.10
Average	1.42 ± 1.52	1.38 ± 0.40	0.58 ± 0.17	1.46 ± 0.83

4.4 Fluorescence Indices and UV-vis Absorbance Measurements for Dry Deposition

The values of the three fluorescence-derived indices described in section 3.4 and UV-vis absorbance measurements for dry deposition can be found in the appendices Table B.2 and are summarized in Table 6 below. The SUVA values range 0.18 to 4.32 L mg C^{-1} m^{-1}, with an annual mean value 1.60 ± 0.88 L mg C^{-1} m^{-1}. SUVA values were highest in the spring and fall (Figure 21). The 2-D graph of the intensity of the FI for aquatic systems typically has a peak before the emission wavelength of 470 nm and the slope of the FI line after the peak (470 nm to 520 nm) at excitation wavelength 370 nm determines the FI value. The FI values ranged from 1.00 to 1.65, with a mean value of 1.37 ± 0.16. FI values were highest in the winter and fall (Figure 22). The FrI values range 0.56 to 0.97, with a mean value of 0.71. FrI values were highest in the winter and spring (Figure 23). The HIX values range from 0.16 to 1.38, with an annual mean value 0.53. HIX values were highest in summer and winter (Figure 24). FrI values

were typically higher in dry than in wet deposition and HIX values were lower in dry than in wet deposition (Figures 23 and 24).

Table 7. Summary of Fluorescent Indices in Dry Deposition.

	SUVA (L mg C^{-1} m^{-1})	FI	FrI	HIX
Winter	1.36 ± 0.54	1.38 ± 0.14	0.74 ± 0.10	0.49 ± 0.24
Spring	1.96 ± 1.07	1.37 ± 0.18	0.74 ± 0.11	0.44 ± 0.21
Summer	1.17 ± 0.71	1.39 ± 0.18	0.71 ± 0.068	0.73 ± 0.29
Fall	1.85 ± 1.04	1.38 ± 0.033	0.65 ± 0.044	0.47 ± 0.14
Average	1.58 ± 0.90	1.38 ± 0.15	0.71 ± 0.09	0.53 ± 0.25
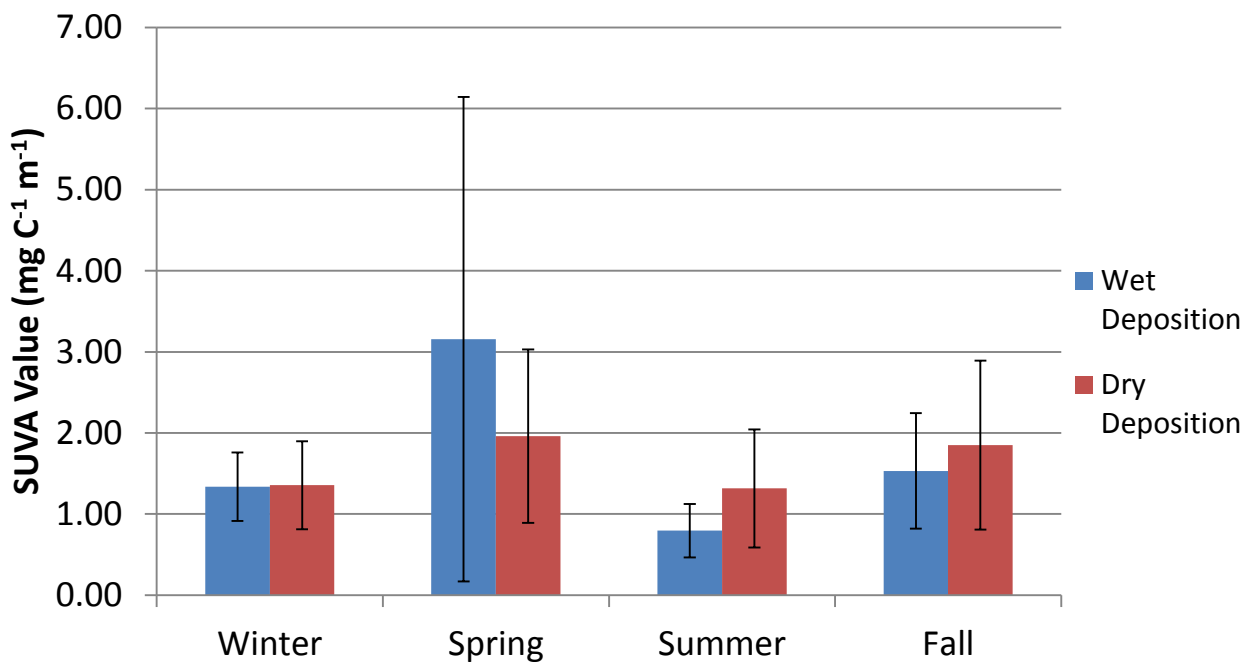
Figure 21. Seasonal Changes in the Average SUVA values for Wet and Dry Deposition.
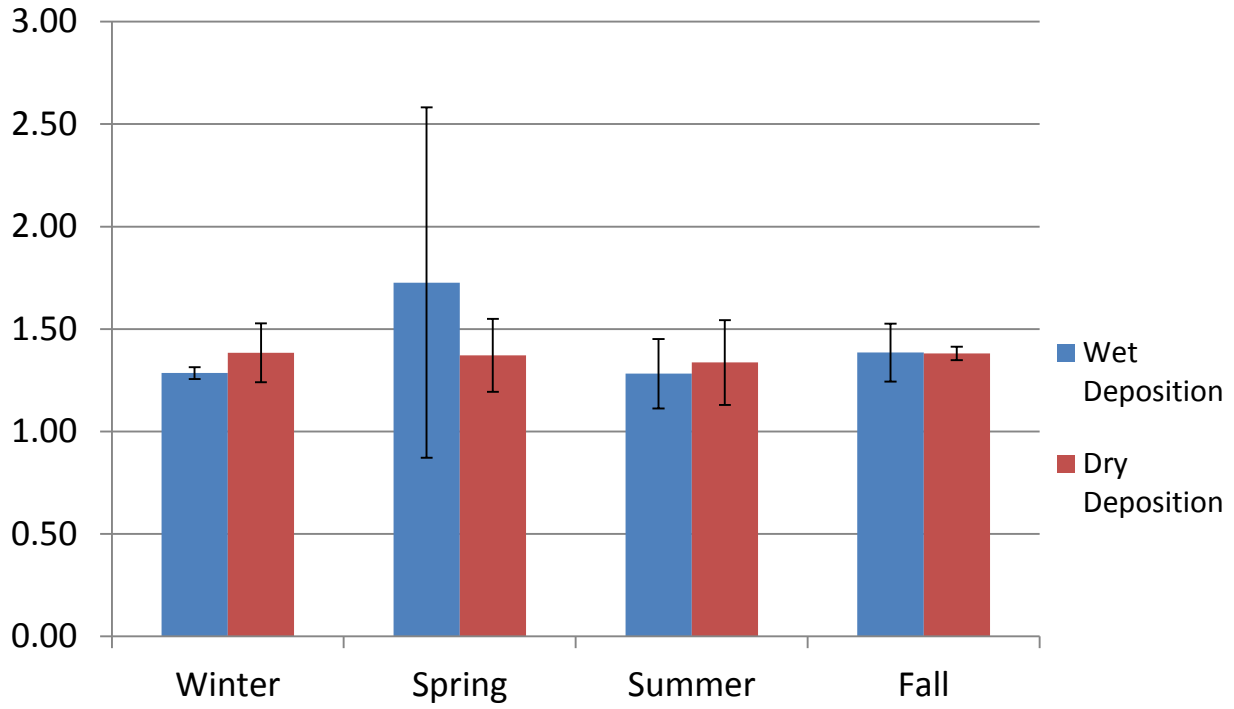
Figure 22. Seasonal Changes in the Average Fluorescence Indices for Wet and Dry Deposition.
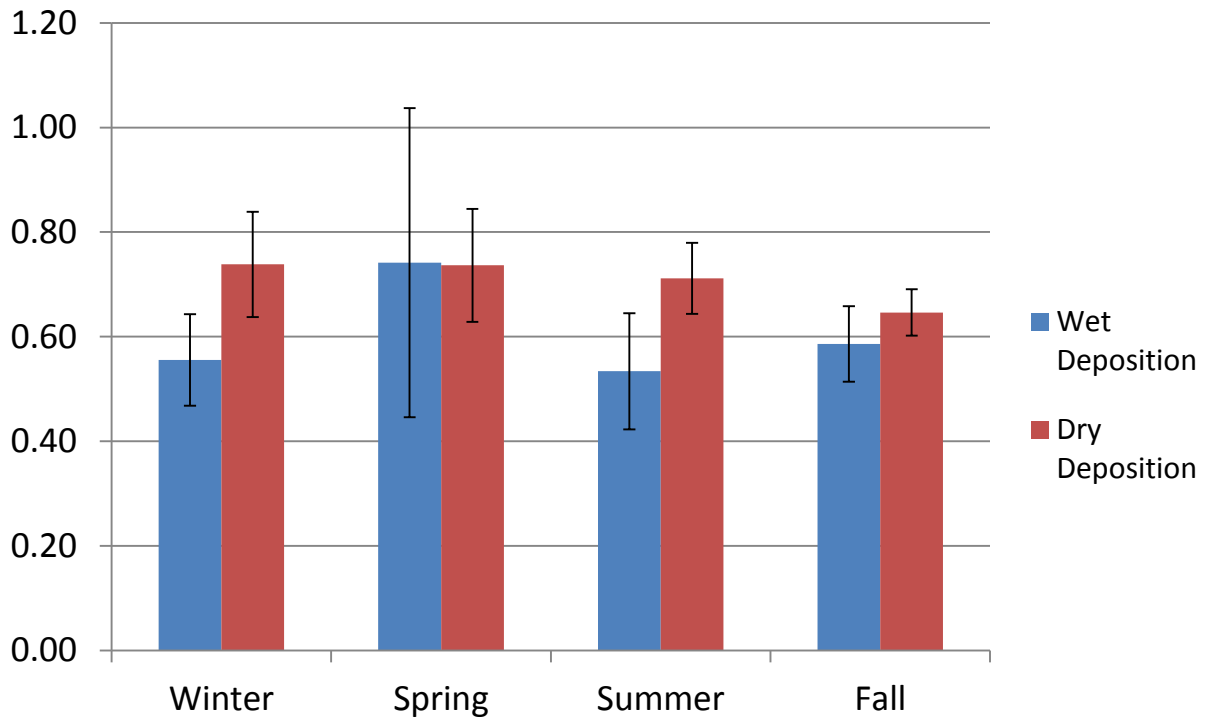
Figure 23. Seasonal Changes in the Average Freshness Indices for Wet and Dry Deposition.
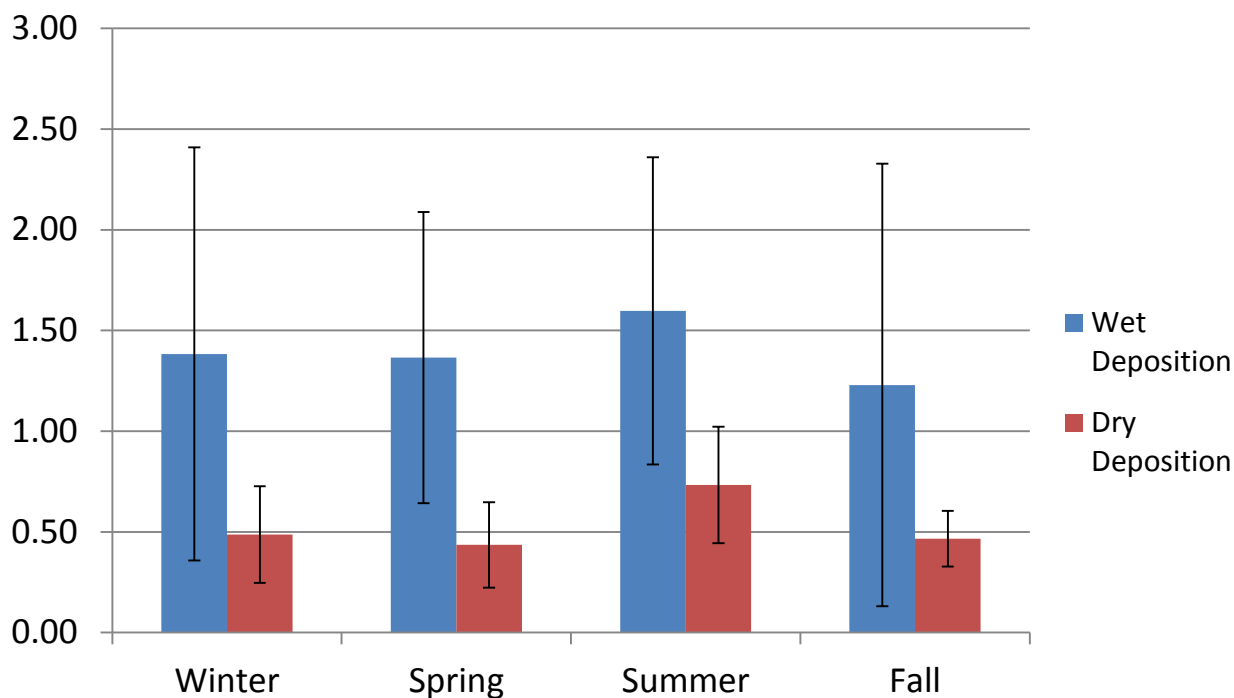
Figure 24. Seasonal Changes in the Average Humification Indices for Wet and Dry Deposition.

4.5 PARAFAC Modeling of EEMs from Wet and Dry Deposition

PARAFAC modeling was performed on the combined data set that contained samples with matching excitation and emission spectra. Final dimensions of the data array were: 68 samples×43 excitation wavelengths×149 emission wavelengths. The PARAFAC model identified 5 independently varying fluorescent components in each sample (Figure 25 and Table 7). Component 1 contains a peak that fluoresces in the same area as the humic-like peak A, except the peak is located at a lower excitation wavelength, around 230 nm and longer emission wavelength of 400-475 nm rather than at ex/em wavelengths of 260 nm/380-460 nm (for Peak A from Coble 1996). Component 2 contains a peak in a similar area as the tyrosine-like peak B, except that the emission wavelength appears to be at a lower wavelength around 300 nm instead of the emission wavelength of 310 nm. Component 3 contains the tryptophan peak, termed the T

peak, but this component also contains an additional peak that seems to fluoresce at about ex/em 230-240 nm/340 nm. Component 4 does not have a distinct peak and is unlike any fluorescent component that has been previously discovered or studied. Component 5 contains a peak in a similar area as the marine humic-like peak M, but the excitation wavelength is around 290 nm instead of 312 nm.

Wet deposition annual mean values for the 5 components are summarized in Table 7 below. The PARAFAC results revealed that component 4 was the most dominant in wet deposition samples, representing on average of 30.3% of the total fluorescence. The least common was component 3, representing on average of 11.3% of the fluorescence. Seasonal analysis revealed that, on average, summer samples contained the highest percentage of component 4 at 41.0%, fall samples contained the highest amount of component 5 at 44.8%, and winter samples contained roughly equal amounts of components 1, 2, and 3 at 32.4%, 21.4%, and 25.9% of the total fluorescence, respectively.
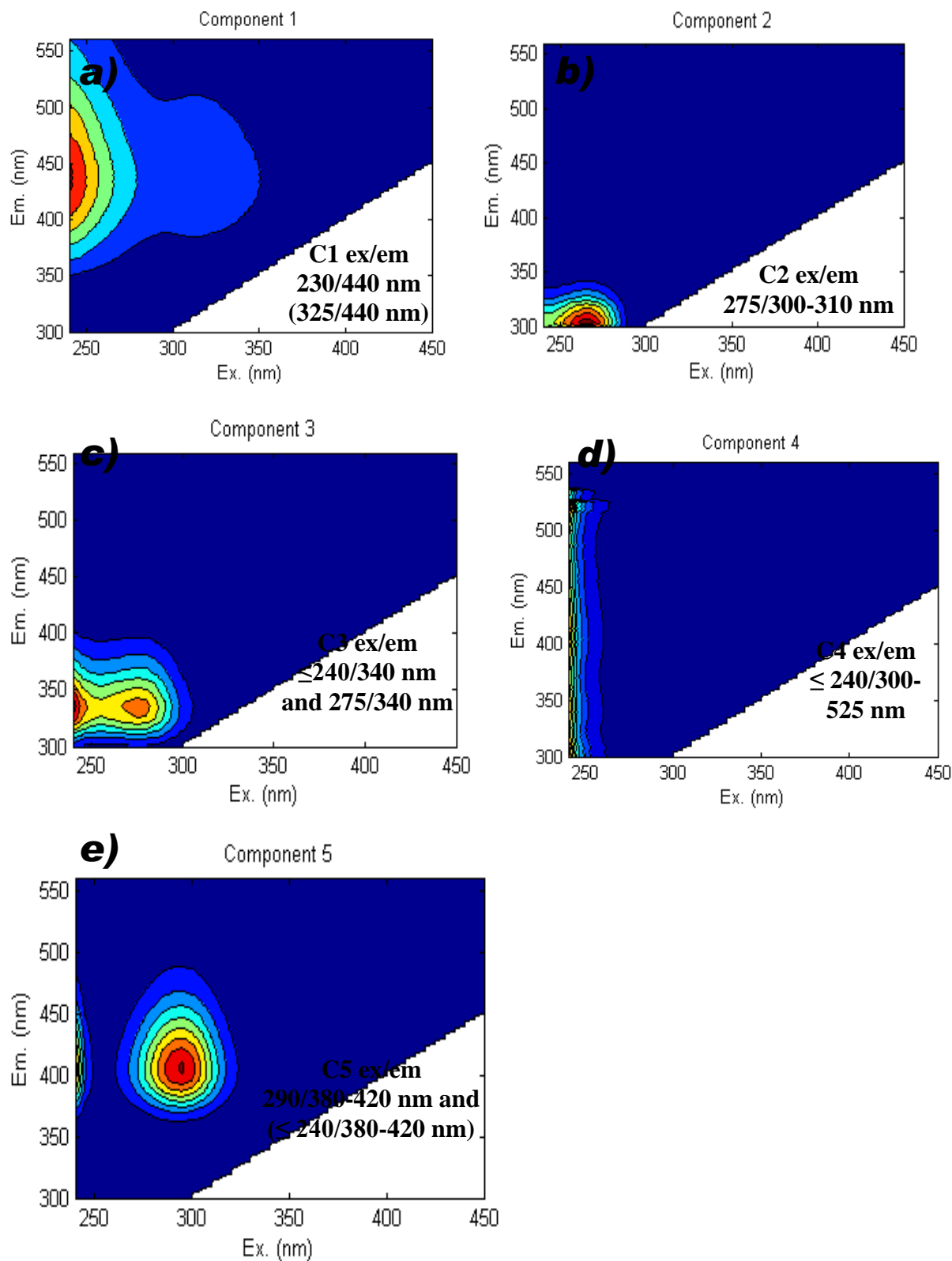
Figure 25. EEM spectra of fluorescent components identified by the PARAFAC model in wet and dry deposition samples.

Table 8. Summary of the relative amount (%) of each of five PARAFAC Components by Season in Wet Deposition.

	Component 1	Component 2	Component 3	Component 4	Component 5
Peak wavelengths (ex/em nm)	$\leq$ 230/440 (325/440)	275/300-310	275/340 and $\leq$ 240/340	$\leq$ 240/300-525	290/380-420 and $\leq$ 240/380-420
Winter	32.4	21.4	25.9	11.2	9.0
Spring	18.2	14.5	20.4	20.8	26.1
Summer	22.3	15.7	6.8	41.0	14.3
Fall	8.4	19.7	5.1	22.0	44.8
Average	20.2	16.9	11.3	30.3	21.3
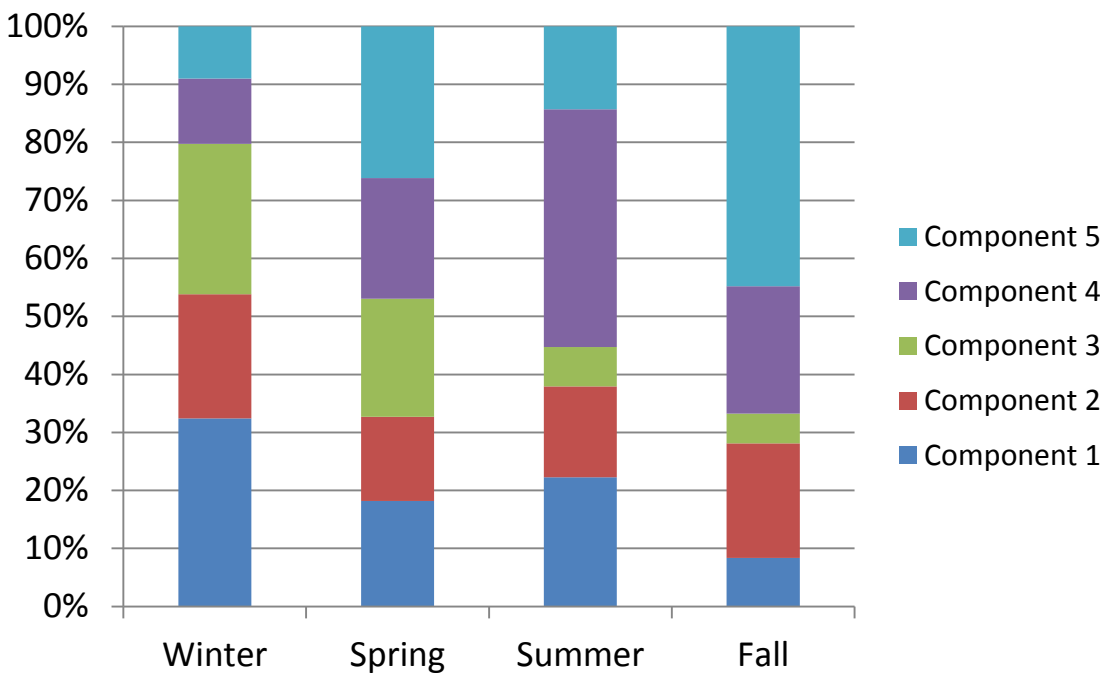
Figure 26. Seasonal Analysis of the 5 Components from the PARAFAC model in Wet Deposition.

Dry deposition annual mean values for the 5 components are summarized in Table 8 below. In all seasons, the two most dominant PARAFAC components were tyrosine-like component 2, representing between 27 and 47% of the total fluorescence, and unidentified component 4, representing between 19 and 42% of the total fluorescence (Figure 27).

Table 9. Summary of the relative amount (%) of each of five PARAFAC Components by Season in Dry Deposition.

	Component 1	Component 2	Component 3	Component 4	Component 5
Peak wavelengths (ex/em nm)	$\leq 230/440$ (325/440)	275/300-310	275/340 and $\leq 240/340$	$\leq 240/300$-525	290/380-420 and $\leq 240/380$-420
Winter	11.6	30.3	20.6	33.4	4.1
Spring	6.6	36.1	12.7	42.3	2.4
Summer	14.6	27.1	14.1	42.1	2.1
Fall	15.3	47.7	15.4	18.5	3.1
Average	11.9	34.4	15.4	35.5	2.8
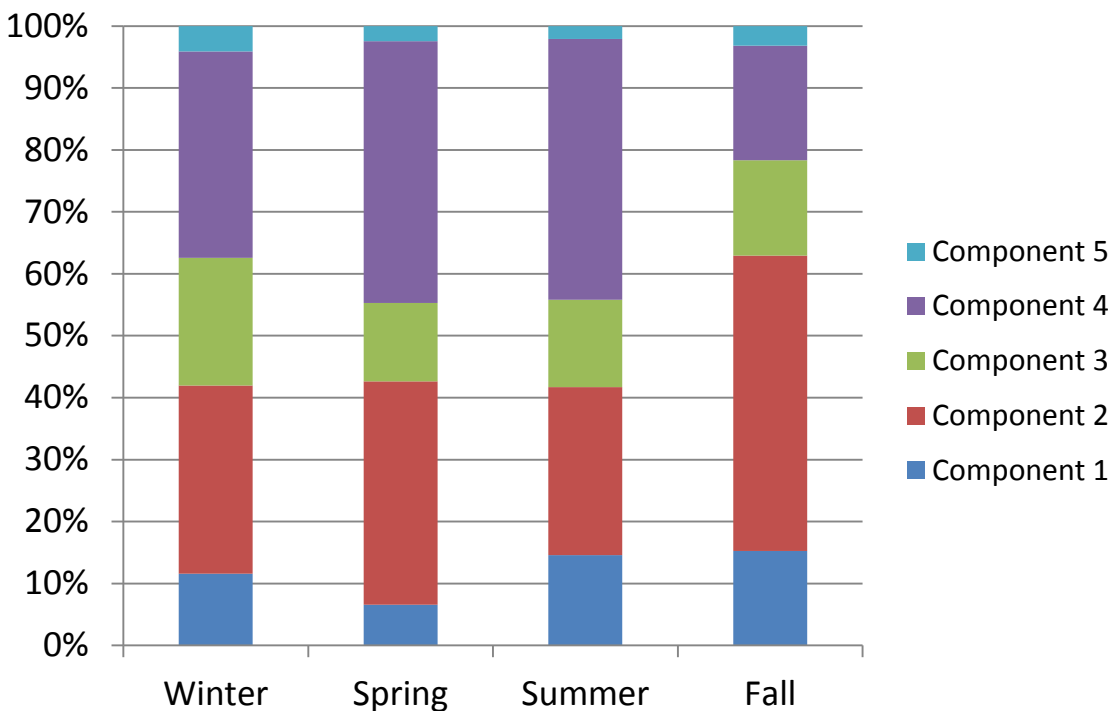
Figure 27. Seasonal Analysis of the 5 Components from the PARAFAC model in Dry Deposition.

4.6 Influence of Solar Irradiation on Fluorescence Properties

The solar simulation experiments exposed fluorescent organic compounds to solar irradiation for 30 minutes and then for 1 hour (Figure 28). Fluorescent peaks in the longer excitation wavelength region (> 300 nm) tended to readily disappear after the initial 30 minute exposure. Other initially dominant fluorescent peaks at shorter excitation wavelengths (< 300 nm) remained, but reduced in fluorescence intensity. Peak T fluorescence tends to be mostly resistant to solar irradiation, reducing only slightly in intensity compared to other fluorescent peaks. The fluorescence index, freshness index, and humification index were then analyzed to see if these indices would also change with irradiation. For most samples, the freshness index decreased with increased time of exposure to solar irradiation (p value ≤ 0.04; Figure 29) and the humification index increased under prolonged time of exposure to solar irradiation (p value ≤ 0.001; Figure

30). The fluorescence of the amino acid compounds, such as neopterin, tryptophan, tyrosine, pyridoxine, and pyridoxamine, was extremely photodegraded after 30 minutes; indeed so much that the freshness index and humification index could not be adequately determined due to all the noise (Figure 31).
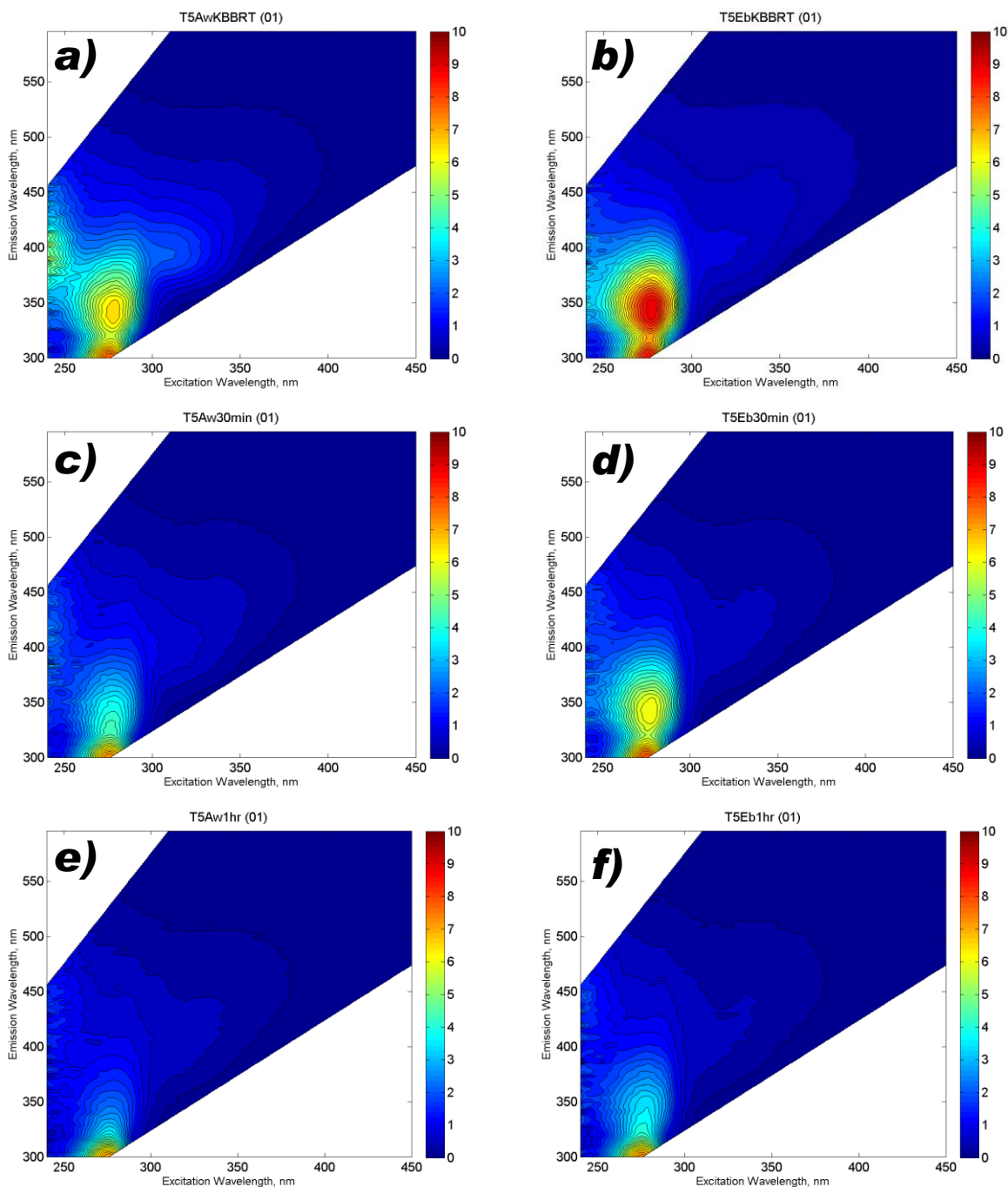
Figure 28. Solar Irradiation Experiment.

Solar Irradiation Experiment that exposed laboratory grown alpine soil microorganisms to 545 W m^2 $^{-1}$ for 30 minutes and then an hour. Figures a and b are the EEMs for two different samples before irradiation. Figures c and d are the EEMs of sample's a and b, respectively, after 30 minutes of solar exposure. Figures e and f are the EEMS for the two different samples after 1 hour of solar exposure.
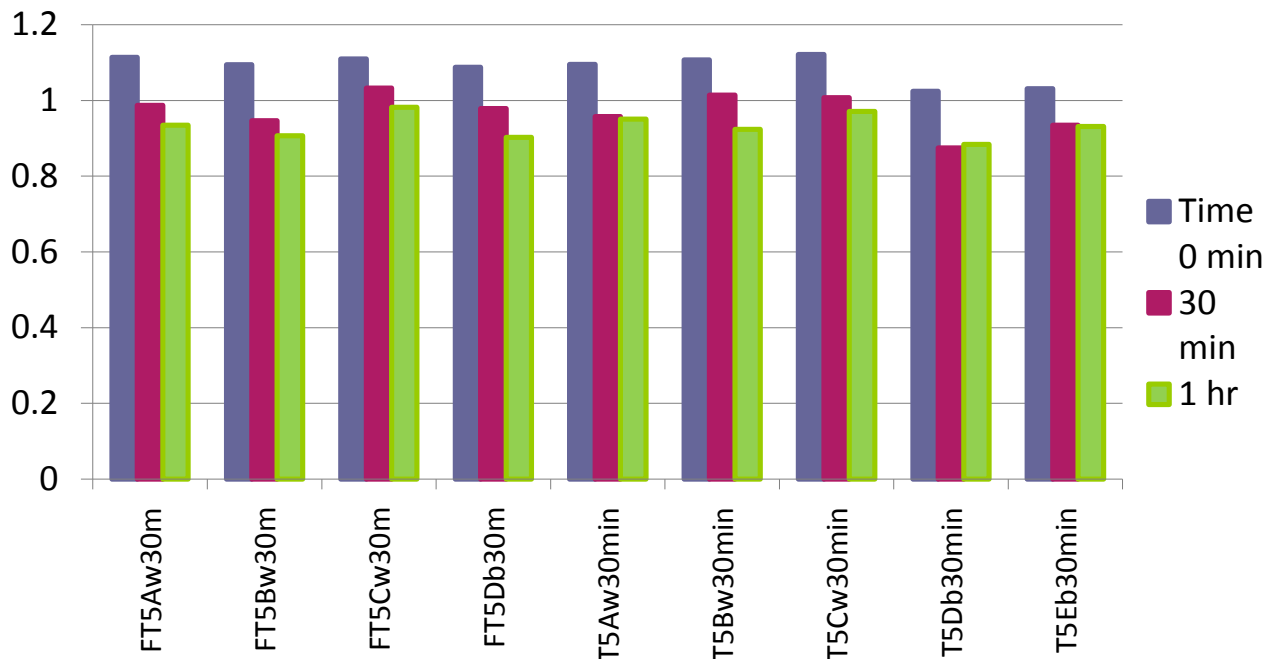
Figure 29. Changes in Freshness Index after Solar Irradiation. The freshness indices of various samples containing fluorescent compounds that were subjected to no solar irradiation (control), 30 minutes exposure to solar irradiation, and 1 hour solar irradiation.
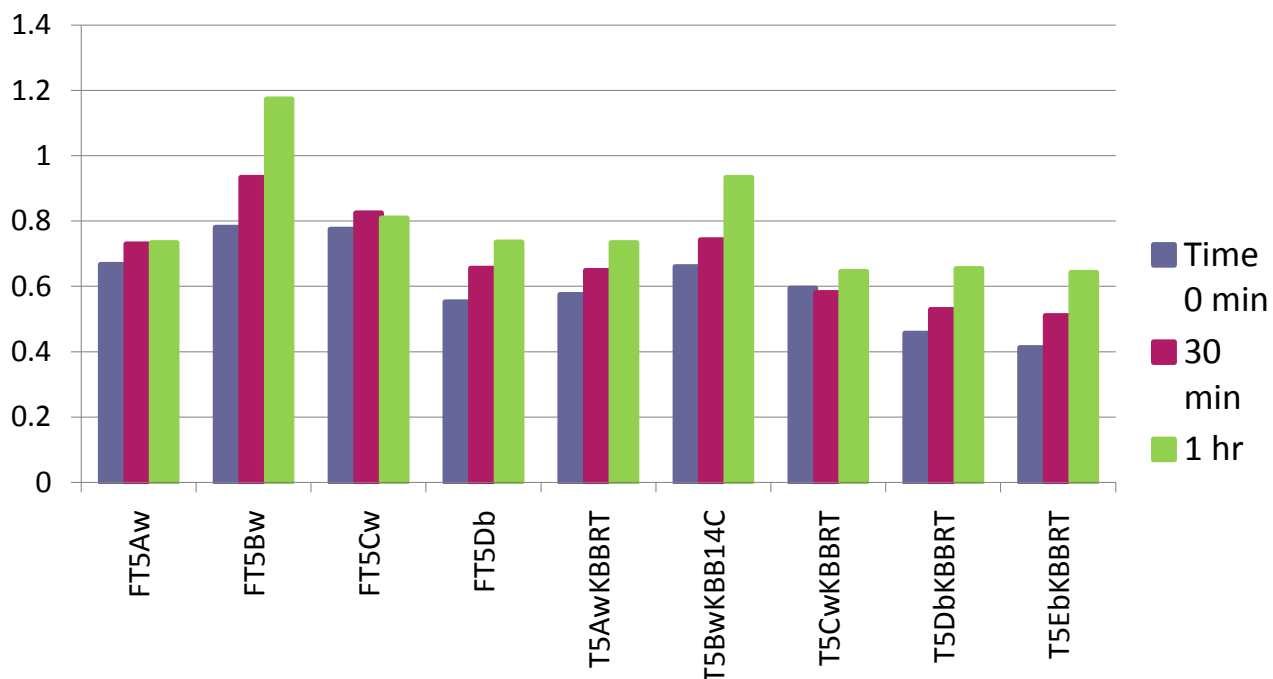
Figure 30. Changes in Humification Index after Solar Irradiation. The humification indices of various samples containing fluorescent compounds that were subjected to no solar irradiation (control), 30 minutes exposure to solar irradiation, and 1 hour solar irradiation.

mix10314 (01)

b)

o

mix130m0314 (01)
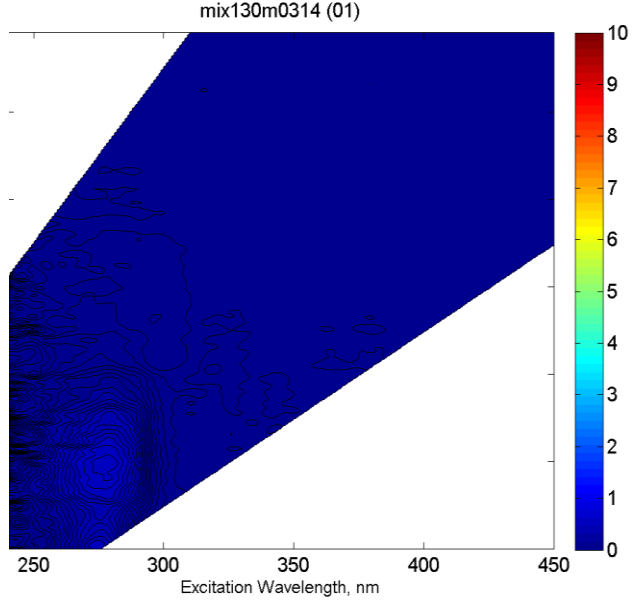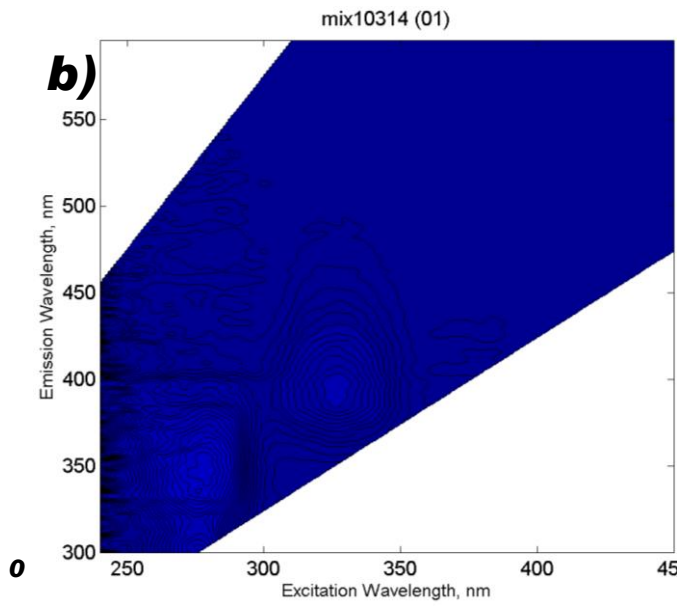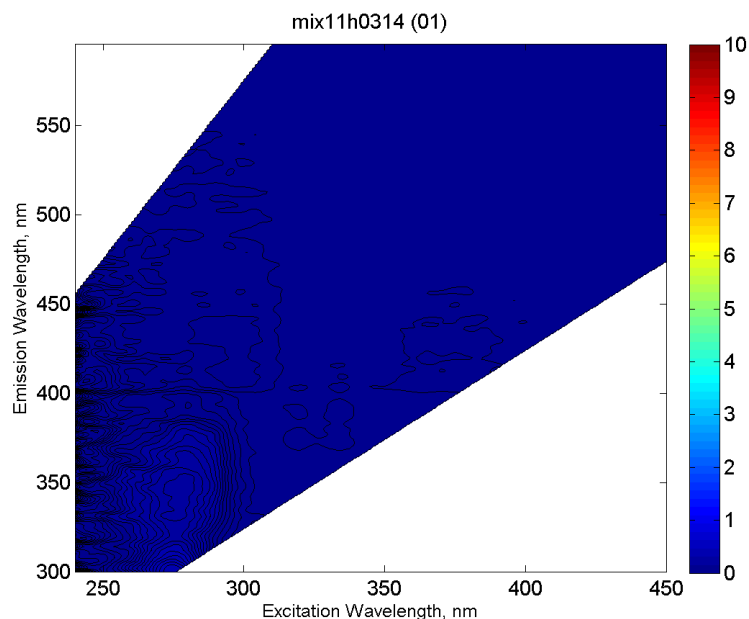
Figure 31. Mixture of neopterin, tryptophan, and pyridoxamine a) at time 0 minutes solar irradiation, b) at 30 minutes solar irradiation, and c) at 1 hour solar irradiation.

5. Discussion

Here, I present information about the optical properties of atmospheric wet and dry deposition of DOM. DOM in natural waters are quite susceptible to photodegradation by sunlight, resulting in a loss of absorbance and fluorescence (Kramer, 1979; Ertel 1990; Kieber et al., 1990). DOM in natural marine-transitional waters shows an absence, or destruction, of visible humic-like fluorescence at excitation wavelengths greater than 320 nm (Coble, 1996). This loss of absorbance and therefore fluorescence is believed to be primarily the result of photodegradation of humic substances and lignin-derived phenols (Ertel, 1990). Photodegradation, or photobleaching, has been shown to enhance lability of DOM (Moran and Zepp, 1997); therefore, it would be expected that atmospheric DOM may be an important source of bioavailable carbon and other nutrients to the alpine biota.

DOC concentrations peaked in the summer for wet deposition and mostly the spring and summer for dry deposition. High summer DOC concentrations in wet and dry deposition may be

related to the increased inputs of biological emissions and concentrations of biological particles in the atmosphere from terrestrial vegetation due to the growing season (Kieber et al., 2002). New particle formation in the Front Range of the Colorado Rocky Mountains is related to biological emissions of volatile organic compounds (VOCs), such as terpenes or sesquiterpenes from woody vegetation, which first are oxidized and then combine with sulphuric acid derived from sulfur dioxide (SO_2) possibly emitted from the urban environment, for example from fossil fuel combustion (Boy et al., 2008). New particle formation, or secondary organic aerosols (SOA), can also be formed from an oxidized VOC that combines with nitric acid which is derived from nitrogen oxides most likely emitted from the urban environment due to fossil fuel combustion (Graber and Rudich, 2006). In the spring, high DOC concentrations in wet and dry deposition may be attributed to dust deposition from the Colorado Plateau and Mojave Desert (Lawrence et al., 2010, Mladenov et al., 2012).

The most dominant peak in wet and dry deposition using the fixed ex/em wavelengths was peak B, which is a tyrosine-like, or protein-like peak. Tyrosine is an amino acid which is bound in proteins (Fellman et al., 2010). Peak B suggests biological activity, DOM availability, and cycling of fast and slow pools of DOM (Fellman et al., 2010). Generally the intensity of peak B was more intense in wet deposition than dry deposition; therefore water availability in wet deposition may stimulate biological activity and contribute to more microbially-derived fluorophores, like peaks B and M. The second most dominant peak in wet and dry deposition was the fixed ex/em peak T (ex/em at 275 nm/340 nm; Coble, 1996) which is a humic-like peak that is primarily derived from vascular plant sources, aromatic in nature, highly conjugated, and likely represents the higher-molecular-weight fraction of the DOM pool (Coble et al., 1998). The third most dominant peak in wet and dry deposition was the fixed ex/em peak A, which is a

humic-like peak. The EEM spectra show an intense peak occurring at ex/em of 240 nm/400-475 nm, therefore this observed peak at 240 nm could likely be a shifted peak A, which Birdwell and Valsaraj (2010) also observed a shift in excitation and emission wavelengths in fog water DOM, but it is unusual that the excitation wavelength is shifted lower, yet the emission wavelength shifted to longer wavelengths, therefore it could be a unique fluorophore signature for atmospheric deposition or it could be a blue-shifting of the peaks established by Coble (1996) due to intense solar irradiation during transport through the atmosphere.

Wet and dry deposition SUVA values were generally low, indicating that the DOM has low aromaticity. A few wet deposition samples collected from 2012 – 2013 had SUVA values that were above 2.5 mg C^{-1} m^{-1}, indicative of either high aromaticity or substantial amounts of non-DOM light-absorbing compounds, such as Fe or nitrate. Those samples, with SUVA values of 4.94 mg C^{-1} m^{-1} and 8.45 mg C^{-1} m^{-1}, were collected in the spring, both in April 2013. Dry deposition samples with SUVA values > 2.5 mg C^{-1} m^{-1} were collected in mid-Fall, 3.87 mg C^{-1} m^{-1} (October 2012), and in the spring, 2.51 mg C^{-1} m^{-1} and 3.35 mg C^{-1} m^{-1} , (from late April to mid-May 2013), and 4.32 mg C^{-1} m^{-1} (June 2013). These samples show a relatively high absorbance value (a_{254}), yet low DOC concentrations. Although iron was not measured, it does absorb light and may be responsible for the higher SUVA values in those samples (Weishaar et al., 2003) from spring dust events (Mladenov et al., 2011, 2012).

The 2-D graphs of the FI intensities for atmospheric wet and dry deposition samples were relatively flat with not much of a peak (Figure 32), likely because most of the organic compounds that absorb light at higher wavelengths have been photobleach. The lack of a distinct FI curve suggests that the FI may not be appropriate for the determination of DOM source in atmospheric samples.
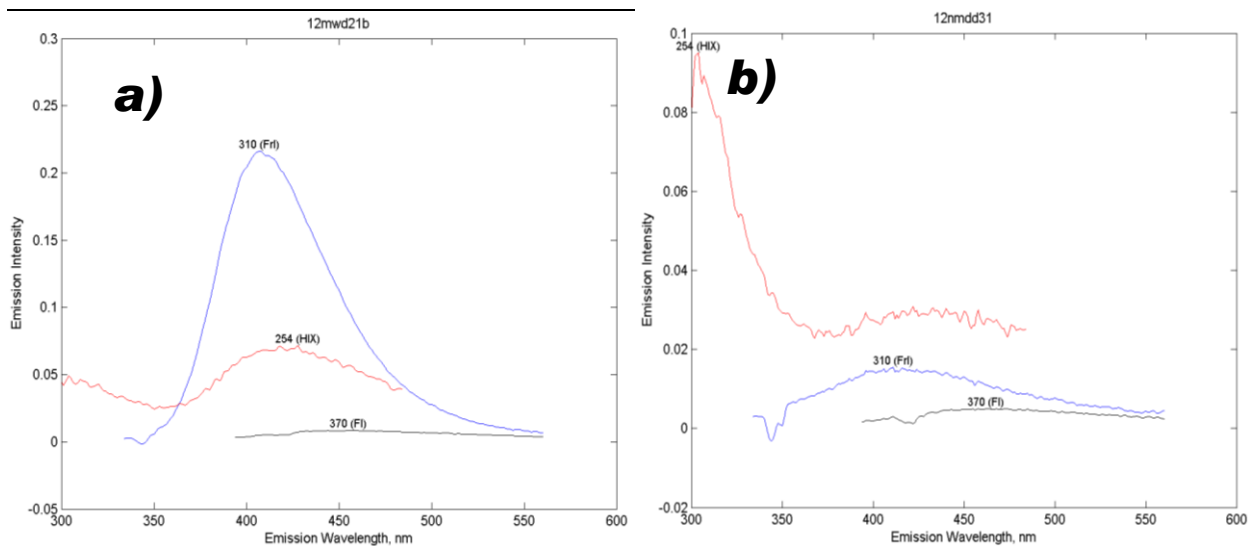
Figure 32. Two dimensional fluorescence curves at excitation of 254 nm (HIX; red), 310 nm (FrI; blue), and 370 nm (FI; black) acquired for a) wet deposition and b) dry deposition samples.

Mean FrI values of 0.58 and 0.71 for atmospheric wet and dry deposition, respectively, were both below 1. For aquatic environments, these low FrI values would suggest that the DOM is more decomposed (Parlanti et al., 2000). Organic matter in dry deposition is fresher, or less decomposed, than wet deposition organic matter (p value < 0.001). However, processes influencing aerosols during transport through the atmosphere may also act to decrease the FrI and may or may not reflect freshness or age of the sample. The solar irradiation experiment showed that often peaks at longer wavelengths (ex >300 nm) would readily disappear after a 30 minute exposure to 545 W m^{-2}. Irradiation experiments performed here did indeed act to significantly decrease the FrI after 1.5 hours exposure (p value = 0.016; Figure 29). By contrast, annual mean values of HIX (< 10), at 1.46 and 0.53 were low for wet and dry deposition, respectively, compared to aquatic samples for which the HIX can range from 5 to 35 (Williams et al. 2010). This low HIX in atmospheric deposition samples would suggest that atmospheric deposition is less humified or less processed. Irradiation experiments showed that HIX should

increase after irradiation (p value < 0.001). An increase in the humified nature of DOM after

irradiation has been observed for microbial compounds in the marine environment and is referred

to as photohumification (Kieber et al. 1997). HIX values peak in the summer for both wet and

dry deposition with mean values of 1.60 and 0.68, respectively. Dry deposition HIX values are

lower than wet deposition (p value < 0.001). Both FrI and HIX indicate that wet deposited

organic matter is more decomposed and processed than dry deposited organic matter, but still

much less humified than aquatic organic matter.

Results from the PARAFAC model revealed five individual fluorescent components in

each samples' EEM. These individual components' excitation and emission were described in

section 4.5 which found four of the five components to be similar to fluorescent peaks as

described by Coble (1996). Component 1 was similar to the humic-like peak A, except the peak

is located at a lower excitation wavelength and emits at a slightly longer wavelength than Coble

had demonstrated in a study on excitation-emission spectroscopy that was published in 1996.

Dry deposition samples contained a higher average percentage of component 1 than wet

deposition samples (Figure 24 and 25). Component 2 contains a peak in a similar area as the

tyrosine-like peak B, except that the emission wavelength in the samples collected appear to be

at a lower emission wavelength that that described by Coble (1996). Dry deposition samples

contained much more of tyrosine-like component 2 than wet deposition samples (Figure 24 and

25). Component 3 contained the tryptophan peak, termed the T peak, and dominated more of the

dry deposition samples than the wet deposition samples (Figures 24 and 25). Component 4 does

not have a distinct peak and is unlike any fluorescent component that has been previously

discovered or studied, yet interestingly the PARAFAC model reveals that component 4 seems to

dominate both the wet and dry deposition samples as the component with the highest average

77

percent. Component 5 contains a peak in a similar area as the marine humic-like peak M, but the

excitation wavelength is lower than Peak M described by Coble (1996), which I refer to as peak

P. Wet deposition samples contained a higher amount of component 5 than dry deposition

samples (Figure 24 and 25). Peak M has been found to be representative of low molecular weight

compounds, typically associated with biological activity in marine environments, but was also be

found in other aquatic environments such as wastewater, wetland, and agricultural environments

(Fellman et al., 2010). Therefore, if the wet deposition samples that contain high amounts of

component 5, or peak P, which may be similar to peak M, may indicate recently derived DOM or

biological activity. Though this peak could possibly be a shifted peak M, a shift in only the

excitation wavelength due to environmental factors (e.g., irradiation, microbial degradation) has

not been previously shown, therefore this peak could be a unique signature of atmospheric DOM.

The humic-like peak A may be attributed to HULIS, which has been described in aerosol, fog,

and cloud water samples (Graber and Rudich, 2006; Muller et al., 2008). Rainwater was

previously shown to have a dominant peak at ex/em of 300-340 nm/390-475 nm (Muller et al.,

2008), which was referred to as a HULIS peak similar to peak C (Coble, 1996) that is typically

characteristic of terrestrial fulvic acids. In rainwater, the HULIS peak was found to be more

blue-shifted than peak C. In our study, the humic-like peak A is also blue-shifted, fluorescing at

lower excitation wavelengths than freshwater or terrestrial humic substances, which may reflect

the lower content of aromatic structures and condensed unsaturated bond systems, and higher

aliphatic content in aerosol derived HULIS (Graber and Rudich, 2006 and references therein).

However, there are no components that resemble Peak C in our study like what Muller et al.

(2008) showed. Components 1, 2, 3, and 5 all appear to show similarities to peaks that have been

classified by Coble (1996), but show a shift either in the excitation wavelength or the emission

wavelength or both in the excitation and emission wavelengths. Blue-shifting of the fluorescence of organic matter in the atmosphere may be occurring due to intense solar irradiation.

This influence of photobleaching on organic compounds suggests that the fluorescence indices used to determine the sources and quality of DOM in aquatic environments may not be suitable for determining sources of DOM in atmospheric samples because photochemical processes in the atmosphere act to photobleach DOM, especially at excitation wavelengths greater than 300 nm. Also, irradiation experiments on bacterial cultures showed that photobleaching acted to increase the humification index and decrease the freshness index. Both of these would suggest that microbial DOM becomes more photo-humified upon irradiation. DOM extracted from dry deposition also was typically less photo-humified (lower HIX and higher FrI) than wet deposition, which is consistent with the potentially shorter atmospheric residence times of dry deposition as well as the short time of DOM leaching (20 min) during processing of marble collectors.

De Laurentiis, et al. (2013) demonstrated that a known fluorescent atmospheric compound is able to be photosensitized by another non-fluorescent compound and begin degradation upon solar irradiation in aqueous solution and may additionally create a new fluorescent band. Additionally, the new band coincides with the fluorescence spectrum of atmospheric HULIS (ex/em of 300-340 nm/390-475 nm), suggesting that supramolecular, or larger complexes of molecules, and photosensitizer–substrate interactions may have a role in HULIS fluorescence properties. Finally, De Laurentiis et al. (2013) analyzed the same interaction coated on silica particles (gas–solid system) under simulated sunlight and in the presence of variable relative humidity. The results revealed that the water molecules inhibited the degradation of the fluorescent compound, whereas the coated particles were more degraded. This

finding is relevant for my study in that the degradation processes of fluorescent DOM could be even faster on the surface of particles than in solution, but this is not consistent with this study because the low HIX and high FrI in dry deposition indicates that dry deposition organic matter is less degraded and more fresh, therefore likely more labile. However, the influence of solar irradiation on the freshness index and humification index make it difficult to draw definitive conclusions based these indices. Caution should be used when applying fluorescence indices to atmospheric organic matter.

6. Conclusion

The fluorescence analysis of atmospheric wet and dry deposition collected in the alpine at Niwot Ridge identified relatively similar components to fluorescent aquatic DOM, but none were identical. These peaks could be shifted fluorescent peaks as defined by Coble (1996) or they could be unique atmospheric fluorescent DOM components. Atmospheric wet and dry deposition samples both peak in fluorescence intensities mainly during the spring (some summer), which may be derived from dust sources, air pollution, and bioaerosols. Applying SUVA, freshness index, and humification index values to characterize wet and dry deposition, dry deposition samples could be described as having lower aromaticity, and being less humified or less processed than wet deposition samples.

Also the strong presence of tyrosine-like peak B in both wet and dry deposition samples suggests biological activity, DOM availability, and cycling of fast and slow pools of DOM. Peak B was more dominant in the dry deposition samples than the wet deposition samples. Since the amounts of both Peak B and T were shown to be well correlated with biodegradable DOM (Fellman et al., 2009) this result may suggest that the DOM extracted from dry deposition is more

labile or contains more microbes or microbial compounds than wet deposition. Our results also demonstrate that some aquatic DOM indices, such as the fluorescence index, may not be suitable for the analysis of atmospheric DOM quality or sources.

Chapter 4 - Summary and Conclusions

Alpine ecosystems are often characterized as remote, "pristine" environments that contain undeveloped soils and are carbon (C) and phosphorus (P) limited. Currently a switch to nitrogen (N) saturation is occurring in several alpine areas throughout the Rocky Mountains in the USA. The atmosphere controls the Earth's climate and ultimately influences the circumstances in which humans live by affecting our supply of food and water, our health and our economy. The atmosphere has the potential to greatly influence nutrient cycles in N sensitive alpine ecosystems not only by warming temperatures, but also by the various amounts of C and other nutrients that are contained in particles and/or water vapor via wind movements and in rain and snow. Nitrate concentrations in the alpine stream exiting from the outlet of Green Lakes 4 at Niwot Ridge have been increasing by 0.27 μmole N year^{-1}. C and other nutrients may be a factor in this increasing trend because C is a necessary source of food for heterotrophs that produce ammonia as a waste product, which then can be nitrified by nitrifying bacteria, producing nitrate, which is exported in the alpine streams.

This study tested the following hypotheses: 1) dry deposition is just as significant as wet deposition as a source of C and other nutrients to alpine environments in the Rocky Mountains, 2) atmospheric pollutants, NO_x and SO_x, and organic C from Front Range sources contribute substantially to the high summer atmospheric load in the remote alpine environment of the Rocky Mountains, 3) dust particles, especially during the spring season, are being transported in the atmosphere long distances and are largely responsible for nutrient and DOC deposition in the alpine, and 4) the quality of atmospheric organic compounds reflects photodegradation during transport through the atmosphere. My work also evaluated the chemical composition and optical

properties of inorganic and organic constituents, such as dissolved organic matter (DOM), for a remote, high-elevation watershed in the Colorado Rocky Mountains, USA. A national atmospheric deposition program (NADP) style wet and dry deposition collector was used to collect both wet deposition and dry deposition on a weekly and bi-weekly basis, respectively. Dry deposition was collected within the 5-gallon buckets typically used for wet deposition collection by the NADP, but containing a marble insert, which proved to be more effective at collection of dry deposition mass than a plain 5-gallon bucket with no marble insert.

Overall, wet deposition loadings represented a significantly larger input than dry deposition loadings of DOC, NH_4^+, Mg^{2+}, NO_3^-, and SO_4^{2-}, however DOC, Mg^{2+}, and NO_3^- wet deposition loadings were only significantly greater than dry deposition in the summer months. Therefore, as proposed in Hypothesis 1, dry deposition is just as significant as wet deposition throughout the year, except for NH_4^+ and SO_4^{2-} and during the summer months. Additionally, summer C and P loadings were particularly high in dry deposition. Annual C loadings as TOC in dry deposition were generally greater than annual C loadings in wet deposition as DOC. Together wet and dry deposition represented an annual flux of 3.0 g m^{-2} day^{-1}, or 6500 kg to the Green Lake 4 catchment at Niwot Ridge. Wet and dry deposition values for C loadings are comparable to those estimated from autotrophic C production.

During the summer months, especially July, C loadings in both wet and dry deposition were at the maxima, with mean wet deposition C loadings being significantly greater in the summer than in other seasons. The significant relationships between DOC, ammonium, nitrate, and sulfate, particularly in the summer, provide strong support for Hypothesis #2 and suggest that secondary organic aerosol formation, driven by nitrogen and sulfur compounds derived from air pollution, may be responsible for the peaks in summer DOC concentrations in wet deposition.

83

Synchrony between dry deposition observations with CASTNET in Rocky Mountain National Park and this study at Niwot Ridge further indicates this is not local, but a regional phenomenon.

Backwards trajectory analysis were consistent with Hypothesis #3 and suggested that arid regions with known dust sources may have been a source of aerosols in dry deposition to Niwot Ridge. Most air masses originated from the far distances in the west, often the northwest or the southwest which is characterized by arid regions, such as the Four Corners of the USA, as well as Arizona and Idaho that produce dust storm. Backwards trajectories from this study through these regions likely brought dust particles that were eventually deposited into the alpine zone of the Rocky Mountains. Ca^{2+} and Mg^{2+} were highly correlated, especially during the spring months, and suggest deposition during the spring could be from dust storms originating to the west. Increases in summer deposition are likely related to the monsoon season occurring in the south over the Gulf Coast influencing air masses, which often brought weather systems from the south and then east, moving through the polluted urban and large agricultural areas of the Colorado Front Range before depositing at Niwot Ridge. Although arid regions likely provided substantial aerosol mass that was deposited to Niwot Ridge, dust transport is not the only source of aerosol deposition. SOA formation and summer upslope conditions were also found to be important for wet and dry deposition in the alpine.

Fluorescent DOM in atmospheric wet and dry deposition has been shown to likely be composed of both humic-like and protein-like fluorophores, which is consistent with DOM contributions from terrestrial sources and biological substances generated by various macro- and microorganisms. However, atmospheric wet and dry deposition fluorescence is also subject to intense irradiation in the atmosphere. Some typical peaks found in aquatic DOM (e.g., peak B and peak T) were also found in atmospheric DOM. However, EEMs of atmospheric DOM were

quite different than those of aquatic DOM in terms of having higher amounts and more intense peaks in the protein-like region. The lower excitation wavelength shifting of humic-like peaks A and M could possibly be unique signatures, like peak P, that might be attributed to secondary organic aerosols or organic matter that are formed or transformed by atmospheric processes such as photooxidation or photodegradation. The 2-D graphs of the FI intensities for atmospheric wet and dry deposition samples were relatively flat with no distinct peak, indicating that the FI may not be appropriate to determine the origin of DOM for atmospheric samples as it is for aquatic environments. Solar irradiation experiments demonstrated that the freshness index and the humification index (HIX) did change in response to irradiation. HIX increases reflect stronger irradiation in the summer. Photo-resistant compounds with unique fluorescence remain after irradiation. The findings above are consistent with Hypothesis #4 and indicate that photodegradation influences organic compounds in wet deposition during transport through the atmosphere. Organic matter appears to be more photo-labile when in solute form (i.e. wet deposition). However, for dry deposition, the less variable seasonal distribution of PARAFAC model components reflects a minor influence of photodegradation on organic matter in dry deposition.

These results showing that organic carbon in atmospheric deposition is linked to dust and air pollution sources has broader implications for nitrogen sensitive ecosystems. Recent evidence of increased dust emissions due to extensive grazing and prolonged drought in the Western US suggests an increase in nutrient loading to nearby alpine watersheds (Neff et al., 2008; Munson et al., 2011). It is not currently known whether the increasing dust emissions are also increasing the amount of organic carbon in the atmosphere and organic carbon loading to alpine watersheds. Although the biodegradability of organic carbon in atmospheric deposition is still in question, the

potential for organic aerosols to fuel alpine heterotrophs, which produce ammonium and other byproducts needed by autotrophic nitrifiers, is an important link to the nitrogen cycle and nitrification in alpine ecosystems. The currently increasing trend of nitrate export from alpine streams will likely continue to rise and possibly at a faster rate especially once the alpine watershed reaches full N saturation and with increasing atmospheric deposition. Nitrate is regulated as a drinking water standard at 10 ppm (mg l^{-1}) because excess nitrate consumption, especially for infants, can starve the blood of oxygen, known as "blue baby syndrome," and if gone untreated, the infant could die. This research location is near the continental divide, therefore this region contains the headwaters to the majority of the Western US population and the quality of their drinking water source may be threatened.

The amount of organic carbon in wet and dry deposition represents a substantial input of carbon to alpine ecosystems, such as Niwot Ridge, and little is known about how this constituent is changing over the long term, especially in dry deposition. The results of this study suggest that there is a need for regular monitoring of C and P in NADP or EPA CASTNET dry deposition programs to evaluate long-term trends in deposition of these limiting nutrients for the alpine.

References

Andersson, C. A. and Bro, R. (2000). The N-way Toolbox for MATLAB. Chemometrics Intelligent Lab. Syst., 52, 1–4.

Andreae, M.O., Talbot, R. W., Andreae, T. W., and Harris, R. C. (1988). Formic and acetic acid over the central Amazon Region, Brazil : 1. Dry season. Journal of Geophysical Research, 93, 1616–1624.

Avery, G. B., Willey, J. D., and Wilson, C. A. (1991). Formic and acetic acids in coastal North Carolina rainwater. Environmental Science and Technology, 25, 1875-1880.

Avery, G. B., Kieber, R. J., Witt, M., and Willey, J. D. (2006). Rainwater monocarboxylic and dicarboxylic acid concentrations in southeastern North Carolina, USA, as a function of air-mass backtrajectory. Atmospheric Environment, 40, 1683–1693.

Baron, J. S., Schmidt, T. M., and Hartman, M. D. (2009). Climate induced changes in high elevation stream nitrate dynamics. Global Change Biology, 15, 1777–1789.

Birdwell, J. E., and Valsaraj, K. T. (2010). Characterization of dissolved organic matter in fogwater by excitation–emission matrix fluorescence spectroscopy. Atmospheric Environment, 44 (27), 3246-3253.

Barnes, R. T., Williams, M. W., Parman, J. N., Hill, K., Caine, N. (2013). Thawing glacial and permafrost features contribute to nitrogen export from Green Lakes Valley, Colorado Front Range, USA. Biogeochemistry, DOI 10.1007/s10533-013-9886-5.

Boy, M., Karl, T., Turnipseed, A., Mauldin, R. L., Kosciuch, E., Greenberg, J., Rathbone, J., Smith, J., Held, A., Barsanti, K., Wehner, B., Wiedensohler, A., Bonn, B., Kulmala, M., and Guenther, A. (2008). New particle formation in the Front Range of the Colorado Rocky Mountains. Atmos. Chem. Phys., 8, 1577-1590.

Brazel, A. and Brazel, P. (1983). Summer diurnal wind patterns at Niwot Ridge, CO. Phys. Geog. 4, 53–61.

Brooks, P. D. and Williams, M. W. (1999). Snowpack controls on nitrogen cycling. Hydrological Processes, 13, 2177–2190.

Caine, N. (2011). Recent hydrologic change in a Colorado alpine basin: an indicator of permafrost thaw?. Annals of Glaciology, 51, 130–134.

Coble, P. G. (1996). Characterization of marine and terrestrial DOM in seawater using excitation-emission matrix spectroscopy. Mar. Chem., 51, 325–346.

Coble, P. G, Del Castillo, C. E., and Avril, B. (1998). Distribution and optical properties of CDOM in the Arabian Sea during the 1995 SW monsoon. Deep-Sea Res. II, 45, 2195 – 2223.

Coble, P. G. (2007). Marine Optical Biogeochemistry: The Chemistry of Ocean Color. Chem. Rev., 107, 402–418.

Cory, R. M., and McKnight, D. M. (2005). Fluorescence spectroscopy reveals ubiquitous presence of oxidized and reduced quinones in DOM. Environmental Science and Technology, 39, 8142–8149.

De Laurentiis, E., Socorro, J., Vione, D., Quivet, E., Brigante, M., Mailhot, G., Wortham, H., and Gligorovski, S. (2013). Phototransformation of 4-phenoxyphenol sensitised by 4-carboxybenzophenone: Evidence of new photochemical pathways in the bulk aqueous phase on the surface of aerosol delinquent particles. Atmospheric Environment, 81, 569 – 578.

Decesari, S., Facchini, M. C., Fuzzi, S., and Tagliavini, E. (2000). Characterization of water-soluble organic compounds in atmospheric aerosol: A new approach. J. Geophys. Res., 105, 1481–1489.

Decesari, S., Mircea, M., Cavalli, F., Fuzzi, S., Moretti, F., Tagliavini, E., and Facchini, M. C. (2007). Source attribution of water-soluble organic aerosol by nuclear magnetic resonance spectroscopy. Environ. Sci. Technol., 41, 2479–2484.

Duarte, R. M. B. O., Pio, C. A., and Duarte, A. C. (2005). Spectroscopic study of the water-soluble organic matter isolated from atmospheric aerosols collected under different atmospheric conditions. Anal. Chim. Acta, 530, 7–14.

Duarte, R. M. B. O., Santos, E. B. H., Pio, C. A., and Duarte, A. C. (2007) Comparison of structural features of water-soluble organic matter from atmospheric aerosols with those of aquatic humic substances. Atmos. Environ., 41, 8100–8113.

Ehn, M., Kleist, E., Junninen, H., Petäjä, T., Lönn, G., Schobesberger, S., Dal Maso, M., Trimborn, A., Kulmala, M., Worsnop, D. R., Wahner, A., Wildt, J., and Mentel, T. F. (2012). Gas phase formation of extremely oxidized pinene reaction products in chamber and ambient air. Atmos. Chem. Phys., 12, 5113–5127.

Ehn, M., Thornton, J. A., Kleist, E., Sipilä, M., Junninen, H., Pullinen, I., Springer, M., Rubach, F., Tillmann, R., Lee, B., Lopez-Hilfiker, F., Andres, S., Acir, I., Rissanen, M., Jokinen, T., Schobesberger, S., Kangasluoma, J., Kontkanen, J., Nieminen, T., Kurtén, T., Nielsen, L. B., Jørgensen, S., Kjaergaard, H. G., Canagaratna, M., Dal Maso, M., Berndt, T., Petäjä, T., Wahner, A., Kerminen, V., Kulmala, M., Worsnop, D. R., Wildt, J. and Mentel, T. F. (2014). A large source of low-volatility secondary organic aerosol. Nature, 506, 476-479.

Ertel, J. R. (1990). Photochemistry of dissolved organic matter: An organic geochemical perspective, in *Effects of solar ultraviolet radiation on geochemical dynamics in aquatic environment*. (ed. N. V. Blough and R. G. Zepp), Woods Hole Oceanogr. Inst. Tech. Rep. 90-09, 79-81.

Favez, O., Sciare, J., Cachier, H., Alfaro, S. C., and Abdelwahab, M. M. (2008). Significant formation of water-insoluble secondary organic aerosols in semi-arid urban environment. Geophysical Research Letters, 35, L15801.

Fellman, J. B., Hood, E., D'Amore, D.V., Edwards, R. T., and White, D. (2009). Seasonal changes in the chemical quality and biodegradability of dissolved organic matter exported from soils to streams in coastal temperate watersheds. Biogeochemistry, 95, 277–293.

Fellman, J. B., Hood, E., and Spencer, R. G. M. (2010). Fluorescence spectroscopy opens new windows into dissolved organic matter dynamics in freshwater ecosystems: A review. Limon. Oceanogr., 55 (6), 2452 – 2562.

Goossens, D. and Offer, Z. Y. (1995). Comparisons of day-time and night-time dust accumulation in a desert region. Journal of Arid Environments, 31, 253–281.

Goss, N. R., Mladenov, N., Seibold, C. M., Chowanski, K., Seitz, L., Wellemeyer, T. B., and Williams, M. W. (2013). Quantifying particulate matter deposition in Niwot Ridge, Colorado:Collection of dry deposition using marble inserts and particle imaging using the FlowCAM. Atmospheric Environment, 80, 549 – 558.

Graber, E. R. and Rudich, Y. (2006). Atmospheric HULIS: How humic-like are they? A comprehensive and critical review. Atmos. Chem. Phys., 6, 729–753.

Green M. J. and Helliwell P. R. (1972) The effect of wind on the rainfall catch. *In Distribution of Precipitation in Mountainous Areas*, Vol. II, pp. 27--46. WMO/OMM No. 326, World Meteorological Organization, Geneva, Switzerland.

Havers, N., Burba, P., Lambert, J., and Klockow, D. (1998). Spectroscopic characterization of humic-like substances in airborne particulate matter. J. Atmos. Chem., 29 (1), 45–54.

Helms, J. R., Stubbins, A., Ritchie, J. D., and Minor, E. C., Kieber, D. J., and Mopper, K. (2008) Absorption spectral slopes and slope ratios as indicators of molecular weight, source, and photobleaching of chromophoric dissolved organic matter. Limnol. Oceanogr., 53, 955-969.

Kanakidou, M., Seinfeld, J. H., Pandis, S. N., Barnes, I., Dentener, F. J., Facchini, M. C., Van Dingenen, R., Ervens, B., Nenes, A., Nielsen, C. J., Swietlicki, E., Putaud, J. P., Balkanski, Y., Fuzzi, S., Horth, J., Moortgat, G. K., Winterhalter, R., Myhre, C. E. L., Tsigaridis, K., Vignati, E., Stephanou, E. G., and Wilson, J. (2005). Organic aerosol and global climate modelling: a review. Atmospheric Chemistry and Physics, 5, 1053–1123.

Kieber, R.J., Zhou, X., and Mopper, K. (1990). Formation of carbonyl compounds from UV-induced photodegradation of humic substances in natural waters: Fate of riverine carbon in the sea. Limnol. Oceanogr., 35 (7), 1503-1515.

Kieber , R ., Hydro, L., and Seaton , F. (1997). Photooxidation of triglycerides and fatty acids in seawater: Implication toward the formation of marine humic substances. Limnol. Oceanogr. 4 (2), 1454 – 1462.

Kieber, R. J., Peake, B., Willey, J. D., and Avery, G. B. (2002). Dissolved organic carbon and organic acids in coastal New Zealand rainwater. Atmos. Environ., 36, 3557–3563.

Kieber, R. J., Willey, J. D., Whitehead, R. F., and Reid, S. N. (2007). Photobleaching of chromophoric dissolved organic matter (CDOM) in rainwater. J. Atmos. Chem., 58, 219–235.

Kiss, G., Tomb´acz, E., Varga, B., Alsberg, T., and Persson, L. (2003). Estimation of the average molecular weight of humic-like substances isolated from fine atmospheric aerosol. Atmos. Environ., 37, 3783–3794.

Kolian, M., and Haeuber, R. (2004). Clean air status and trends network (CASTNet)—Airquality assessment and accountability. In: Wiersma, G.B., ed. Environmental monitoring. CRC Press, Boca Raton, FL, pp. 685–718.

Kramer, C. J. M. (1979). Degradation by sunlight of dissolved fluorescing substances in the upper layers of the eastern Atlantic Ocean, Neth. J. Sea Res., 13, 325-329.

Lawrence, C. R. and Neff, J. C. (2009). The physical and chemical flux of eolian dust across the landscape: A synthesis of observations and an evaluation of spatial patterns. Chem. Geol., 267, 46–63.

Lawrence, C. R., Neff, J. C., Painter, T., and Landry, C. (2010). Contemporary composition of Aeolian dust deposited in the San Juan Mountains, Colorado, USA. J. Geophys. Res-Biogeo., 115.

Ley, R. E., Lipson D.A., and Schmidt S.K. (2001). Microbial biomass levels in barren and vegetated high altitude talus soils. Soil Sci. Soc. Am. J., 65, 111-117.

Ley, R., Williams, M. W., and Schmidt, S. (2004). Microbial population dynamics in an extreme environment: controlling factors in talus soils at 3750m in the Colorado Rocky Mountains. Biogeochemistry, 68, 297–311.

Litaor, M. I. (1987). The influence of eolian dust on the genesis of alpine soils in the Front Range, Colorado. Soil Sci. Soc. Am. J., 51, 142–147.

Lovett, G. M. and Kinsman, J. D. (1990). Atmospheric pollutant deposition to high-elevation ecyostems. Atmospheric Environment, 24 (11), 2767-2786.

McKnight, D. M., Boyer, E. W., Westerhoff, P. K., Doran, P. T., Kulbe, T., and Andersen, D. T. (2001). Spectrofluorometric characterization of dissolved organic matter for indication of precursor organic material and aromaticity. Limnol. Oceanogr., 46, 38–48.

Mitchell, B. G., Kahru, M.,Wieland, J., and Stramska, M. (2003). Determination of spectral absorption coefficients of particles, dissolved material and phytoplankton for discrete water samples, in: Ocean optics protocols for satellite ocean color sensor validation. Revision 4. Vol. IV, edited by: Mueller, J. L., Fargion, G. S., and Mc-Clain, C. R., NASA/TM-2003-211621/R, Goddard Space Flight Center, Greenbelt, Md., 39–56.

Mladenov, N., L´opez-Ramos, J., McKnight, D. M., and Reche, I. (2009). Alpine lake optical properties as sentinels of dust deposition and global change. Limnol. Oceanogr., 54, 2386–2400.

Mladenov, N., Reche, I., Olmo-Reyes, F. J., Lyamani, H., and Alados-Arboledas, L. (2010). Relationships between spectroscopic properties of high altitude organic aerosols and sun photometry from ground-based remote sensing. J. Geophys. Res.-Biogeo., 115.

Mladenov, N., Sommaruga, R., Morales-Baquero, R., Laurion, I., Camarero, L., Diéguez, M. C., Camacho, A., Delgado, A., Torres, O., Chen, Z., Felip, M., and Reche, I. (2011). Dust inputs and bacteria influence dissolved organic matter in clear alpine lakes. Nature Communications, 2 (405).

Mladenov, N., Williams, M.W., Schmidt, S. K., and Cawley, K. (2012). Atmospheric Deposition as a Source of Carbon and Nutrients to an Alpine Catchment of the Colorado Rocky Mountains. Biogeosciences, 9 (8), 3337-3355.

Moran , M. and Zepp, R. G. (1997). Role of Photoreactions in the Formation of Biologically Labile Compounds from Dissolved Organic Matter. Limnology and oceanography, 42 (6), 1307 - 1316.

Morris, D. P., Zagarese, H.,Williamson, C. E., Balseiro, E. G., Hargreaves, B. R., Modenutti, B., Moeller, R., and Queimalinos, C. (1995). The attenuation of solar UV radiation in lakes and the role of dissolved organic carbon. Limnol. Oceanogr., 40, 1381–1391.

Muller, C. L., Baker, A., Hutchinson, R., Fairchild, I. J., and Kidd, C. (2008). Analysis of rainwater dissolved organic carbon compounds using fluorescence spectrophotometry. Atmospheric Environment, 42, 8036 – 8045.

Munson, S. M., Belnap, J., and Okin, G. S. (2011). Responses of wind erosion to climate-induced vegetation changes on the Colorado Plateau, Proc. Natl. Acad. Sci. USA, 108, 3854–3859.

Neff, J. C., Ballantyne, A. P., Farmer, G. L., Mahowald, N.M., Conroy, J. L., Landry, C. C., Overpeck, J. T., Painter, T. H., Lawrence, C. R., and Reynolds, R. L. (2008). Increasing aeolian dust deposition in the western United States linked to human activity. National Geosciences, 1, 189–195.

Nelson, D.W. and L.E. Sommers. (1996). Total carbon, organic carbon, and organic matter. In: Methods of Soil Analysis, Part 2, 2nd ed., A.L. Page et al., Ed. Agronomy. 9:961-1010. Am. Soc. of Agron., Inc. Madison, WI.

Parlanti, E., Orz, K., Geoffroy, L., and Lamotte, M. (2000). Dissolved organic matter fluorescence spectroscopy as a tool to estimate biological activity in a coastal zone submitted to anthropogenic inputs. Organic Geochemistry, 31, 1765–1781.

Parrish, D. D., Hahn, C. H., Fahey, D. W., Williams, E. J., Bollinger, M. J., Hubler, G., Buhr, M. P., Murphy, P. C., Trainer, M., Hsie, E. Y., Liu, S. C., and Fehsenfeld, F. C. (1990).

Systematic variations in the concentrations of NOx (NO Plus NO2) at Niwot Ridge. Colorado, J. Geophys. Res., 95, 1817–1836.

Parry, M.L., Canziani, O.F., Palutikof, J.P., van der Linden, P.J. & Hanson, C.E. (2007) Contribution of Working Group II to the Fourth Assessment Report of the Intergovernmental Panel on Climate Change. Cambridge University Press, New York.

Pena, R. M., Garcia, S., Herrero, C., Losada, M., Vazquez, A., Lucas, T. (2002). Organic acids and aldehydes in rainwater in a northwest region of Spain. Atmospheric Environment, 36, 5277 - 5288.

Peñuelas, J., Llusiá, J. and Gimeno, B. S. (1999). Effects of ozone concentrations on biogenic volatile organic compounds emission in the Mediterranean region. Environmental Pollution, 105, 17- 23.

Poehlker, C., Huffman, J. A., and Poeschl, U. (2012). Autofluorescence of Atmospheric Bioaerosols - Fluorescent Biomolecules and Potential Interferences. Atmospheric Measurement Techniques, 5 (1), 37-71.

Psenner, R. (1999). Living in a dusty world: airborne dust as a key factor for alpine lakes. Water Air & Soil Pollution, 112, 217–227.

Reche I., Ortega-Retuerta, E., Romera, O., Pulido-Villena, E., Morales-Baquero, R., and Casamayor, E. O. (2009). Effect of Saharan dust inputs on bacterial activity and community composition in Mediterranean lakes and reservoirs. Limnol. Oceanogr., 54, 869 – 879.

Richter, C. M. and Wild, A. (1992) Phenolic compounds in needles of Norway spruce trees in relation to novel forest decline. I. Studies on trees from a site in the northern Black Forest. Biochemie und Physiologie der Pflanzen, 188, 305-320.

Santos, P. S. M., Otero, M., Duarte, R. M. B. O, and Duarte, A. C. (2009). Spectroscopic characterization of dissolved organic matter isolated from rainwater. Chemosphere, 74 (8), Pages 1053-1061.

Sievering, H., Braus, J., and Caine, J. (1989). Dry deposition of nitrate and sulfate to coniferous canopies in the Rocky Mountains. In *Transactions on effects of air pollution on western forests,* edited by Olson, R. K. and Lefohn, A. S. Pittsburg, PA: Air and Waste Management Assoc.

Sievering, H. and Burton, D. (1992). Atmospheric loading of nitrogen to alpine tundra in the Colorado Front Range. Global Biogeochemical Cycles, 6 (4), 339-346.

Sullivan, A. P., Weber, R. J., Clements, A. L., Turner, J. R., Bae, M. S., and Schauer, J. J. (2004). A method for on-line measurement of water-soluble organic carbon in ambient aerosol particles. Results from an urban site. Geophys. Res. Lett., 31, L13105.

Thomas, C. D., Cameron, A., Green, R. E., Bakkenes, M., Beaumont, L. J., Collingham, Y. C., Erasmus, B. F. N., Ferreira De Siqueira, M., Grainger, A., Hannah, L., Hughes, L., Huntley, B., Van Jaarsveld, A. S., Midgley, G. F., Miles, L., Ortega-Huerta, M. A., Peterson, A. T., Phillips, O. L., Williams, S. E. (2004). Extinction risk from climate change. Nature, 427, 145–148.

Theurillat, J.-P. & Guisan, A. (2001). Potential impact of climate change on vegetation in the European Alps: a review. Climate Change, 50, 77–109.

Turnipseed, A. A., Blanken, P. D., Anderson, D. E., and Monson, R. K. (2002). Energy budget above a subalpine forest in complex terrain. Agric. Forest Meteorol., 110, 177–201.

Weishaar, J. L., Aiken, G. R., Bergamaschi, B. A., Fram, M. S., Fujii, R., and Mopper K. (2003) Evaluation of Specific Ultraviolet Absorbance as an Indicator of the Chemical Composition and Reactivity of Dissolved Organic Carbon. Environ. Sci. Technol., 37, 4702–4708.

Willey, J. D., Kieber, R. J., Eyman, M. S., and Avery Jr., G. B. (2000). Rainwater dissolved organic carbon: concentrations and global flux. Global Biogeochemical Cycles, 14, 139–148.

Williams, C. J., Yamashita, Y., Wilson, H. F., Jaffe , R., and Xenopoulos, M. A. (2010). Unraveling the role of land use and microbial activity in shaping dissolved organic matter characteristics in stream ecosystems. Limnol. Oceanogr., 55(3), 1159–1171.

Williams, M.W., Baron, J.S., Caine, N., Sommerfeld, R., Sanford Jr., R. (1996). Nitrogen saturation in the Rocky Mountains. Environmental Science and Technology 30, 640–646.

Williams, M.W., Davinroy, T., and Brooks, P. D. (1997). Organic and inorganic nitrogen pools in talus soils and water, Green Lakes Valley, Colorado Front Range, Hydrological Processes, 11, 1747–1760.

Williams, M. W., Knauf, M., Cory, R., Caine, N., and Liu, F. J. (2007). Nitrate content and potential microbial signature of rock glacier outflow, Colorado Front Range. Earth Surface Processes, 32 (7), 1032-1047.

Williams, M. W., Barnes, R. T., Parman, J. N., Freppaz, M., and Hood, E. (2011). StreamWater Chemistry along an Elevational Gradient from the Continental Divide to the Foothills of the Rocky Mountains. Vadose Zone J., 10, 900–914.

Willoughby, A. S., Wozniak, A. S., and Hatcher, P. G. (2014). A molecular-level approach for characterizing water-insoluble components of ambient organic aerosol particulates using ultrahigh-resolution mass spectrometry. Atmos. Chem. Phys., 14, 10299–10314.

Wozniak, A. S. (2009). Characterization and Deposition of Aerosol Organic Matter in the Eastern United States: A dissertation. The College of William and Mary in Virginia

Zappoli, S., Andracchio, A., Fuzzi, S., Facchini, M. C., Gelencs´er, A., Kiss, G., Krivacsy, Z., Molnar, A., Meszaros, E., Hansson, H. C., Rosman, K., and Zebuhr, Y. (1999). Inorganic, organic and macromolecular components of fine aerosol in different areas of Europe in relation to their water solubility. Atmos. Environ., 33, 2733– 2743.

Zhang, Q., Jimenez, J. L., Canagaratna, M. R., Allan, J. D., Coe, H., Ulbrich, I. M., Alfarra, M. R., Takami, A., Middlebrook, A. M., Sun, Y. L., Dzepina, K., Dunlea, E., Docherty, K., DeCarlo, P. F., Salcedo, D., Onasch, T. B., Jayne, J. T., Miyoshi, T., Shimono, A., Hatakeyama, S., Takegawa, N., Kondo, Y., Schneider, J., Drewnick, F., Borrmann, S. L.,

Weimer, S., Demerjian, K., Williams, P., Bower, K. N., Behreini, R., Cottrell, L., Griffin, R. J., Rautiainen, J., Sun, J. Y., Zhang, Y. M., Worsnop, D. R. (2007) Ubiquity and dominance of oxygenated species in organic aerosols in anthropogenically—influenced northern hemisphere mid-latitudes. Geophysical Resource Letters, 34, (13), L13801.

Zsolnay, A., Baigar, E., Jimenez, M., Steinweg, B., and Saccomandi, F. (1999). Differentiating with fluorescence spectroscopy the sources of dissolved organic matter in soils subjected to drying. Chemosphere, 38, 45–50.

Appendix A - Supplemental Information for Chapter 2. Seasonality and Chemical Characteristics of Atmospheric Wet and Dry Deposition to Alpine Environments in the Colorado Rocky Mountains

A-1. Determination of Water Insoluble Organic Carbon by Combustion from Remaining Particulate Mass on Filters

Total organic carbon (TOC) was calculated as the sum of DOC and 60 percent of the weight of organic matter on the glass fiber filter which was lost during combustion at 450° C. Unfortunately there is no evidence in the literature about the loss of ignition to determine only the water insoluble portion of organic carbon. It is not known what fraction of the water insoluble constituents is due to organic carbon, organic nitrogen, and other organics (sulfur and phosphorus). Traditionally, for soils, a conversion factor of 1.724 has been used to convert organic matter that was lost on ignition to organic carbon based on the assumption that organic matter contains 58% organic carbon (C) (i.e., g organic matter/l .724 = g organic C), of which greater than 90% of the dissolved organic matter (DOM), which includes the water soluble organic carbon (WSOC) fraction, is extracted within the first few minutes when introduced to water (Nelson and Sommers, 1996). Additionally, atmospheric deposition contains secondary organic aerosols that also may include organic nitrogen and other non-carbonaceous organic compounds. Therefore, since the particulate matter that remains on the filter contains almost entirely just the insoluble fraction of the organic matter, using the findings of Nelson and Sommers (1996), I assume that, of the insoluble organic matter lost on ignition, 60 percent is organic C. This is believed to be a conservative number.

A-2. Wet and Dry Deposition Data

Table A.1. Loadings in Wet Deposition in kg ha^{-1}

Sample Name	Date ON	Date OFF	Season	NH$_4^+$	Ca^{2+}	Mg^{2+}	NO$_3^-$	SO$_4^{2-}$	PO$_4^{3-}$	DOC
F12MWNADP1	20120103	20120110	W	0.009	0.002	0.0003	0.034	0.016	0.0003	0.031
F12MWNADP2	20120110	20120117	W	0.007	0.005	0.0006	0.033	0.026	0.0002	0.029
F12MWNADP3	20120117	20120124	W	0.006	0.013	0.0035	0.040	0.040	0.0019	0.024
F12MWNADP4	20120124	20120131	W	0.004	0.003	0.0003	0.008	0.017	0.0001	0.014
F12MWNADP5	20120131	20120207	W	0.038	0.018	0.0016	0.043	0.036	0.0009	0.051
F12MWNADP6	20120207	20120214	W	0.005	0.003	0.0004	0.019	0.026	0.0006	0.019
F12MWNADP8	20120328	20120403	Sp	0.083	0.058	0.0062	0.077	0.133	0.0014	0.089
F12MWNADP9	20120403	20120410	Sp	0.002	0.005	0.0004	0.010	0.008	0.0000	0.019
F12MWNADP10	20120410	20120417	Sp	0.133	0.062	0.0064	0.331	0.382	0.0014	0.152
F12MWNADP11	20120417	20120424	Sp	0.009	0.009	0.0013	0.021	0.033	0.0008	0.074
F12MWNADP12	20120424	20120502	Sp	0.010	0.035	0.0038	0.074	0.074	0.0013	0.076
F12MWNADP13	20120502	20120508	Sp	0.071	0.057	0.0066	0.234	0.235	0.0009	0.145
F12MWNADP14	20120508	20120515	Sp	0.066	0.112	0.0131	0.223	0.405	0.0004	0.168
F12MWNADP15	20120515	20120522	Sp	0.027	0.042	0.0048	0.099	0.113	0.0004	0.162
F12MWNADP16	20120522	20120529	Sp	0.024	0.051	0.0057	0.070	0.130	0.0016	0.115
F12MWNADP17	20120529	20120605	Sp	0.025	0.060	0.0063	0.079	0.132	0.0014	0.107
F12MWNADP18	20120626	20120703	Su	0.094	0.086	0.0088	0.205	0.228	0.0019	0.392
F12MWNADP19	20120703	20120710	Su	0.680	0.141	0.0164	1.403	1.046	0.0157	1.694
F12MWNADP20	20120710	20120717	Su	0.133	0.059	0.0053	0.489	0.514	0.0061	0.488
F12MWNADP21	20120724	20120731	Su	0.081	0.041	0.0044	0.359	0.318	0.0008	0.358
F12MWNADP22	20120731	20120807	Su	0.034	0.037	0.0047	0.183	0.143	0.0003	0.226
F12MWNADP23	20120807	20120821	Su	0.094	0.062	0.0072	0.203	0.208	0.0063	0.405
F12MWNADP24	20120821	20120828	Su	0.049	0.029	0.0033	0.153	0.121	0.0026	0.284
F12MWNADP25	20120828	20120904	Su	0.101	0.052	0.0053	0.281	0.223	0.0017	0.261
F12MWNADP26	20120904	20120911	Su	0.031	0.024	0.0033	0.109	0.105	0.0024	0.133
F12MWNADP27	20120911	20120918	Su	0.078	0.058	0.0080	0.261	0.250	0.0050	0.273
F12MWNADP28	20120918	20120926	F	0.069	0.014	0.0016	0.142	0.202	0.0007	0.072
F12MWNADP29	20120926	20121002	F	0.030	0.005	0.0006	0.131	0.134	0.0004	0.170
F12MWNADP30	20121002	20121009	F	0.021	0.056	0.0059	0.082	0.123	0.0029	0.081
F12MWNADP31	20121009	20121016	F	0.005	0.010	0.0015	0.017	0.035	0.0022	0.052
F12MWNADP32	20121016	20121023	F	0.003	0.009	0.0013	0.011	0.021	0.0003	0.018
F12MWNADP33	20121023	20121030	F	0.019	0.010	0.0015	0.066	0.085	0.0024	0.061
F12MWNADP34	20121106	20121113	F	0.000	0.002	0.0002	0.005	0.004	0.0001	0.009
F12MWNADP35	20121205	20121205	F	0.033	0.044	0.0055	0.251	0.323	0.0070	0.122
F12MWNADP36	20121218	20121227	W	0.003	0.007	0.0019	0.049	0.020	0.0023	0.015
F13MWNADP1	20130108	20130115	W	0.000	0.000	0.0000	0.006	0.002	0.0001	0.000
F13MWNADP2	20130122	20130129	W	0.004	0.000	0.0001	0.014	0.002	0.0002	0.011

F13MWNADP3	20130205	20130212	W	0.004	0.006	0.0008	0.025	0.011	0.0008	0.018
F13MWNADP4	20130212	20130219	W	0.006	0.004	0.0006	0.042	0.015	0.0003	0.030
F13MWNADP5	20130219	20130226	W	0.007	0.007	0.0009	0.043	0.012	0.0012	0.031
F13MWNADP6	20130226	20130305	W	0.016	0.009	0.0011	0.070	0.053	0.0025	0.064
F13MWNADP7	20130305	20130313	W	0.022	0.007	0.0006	0.062	0.024	0.0014	0.051
F13MWNADP8	20130313	20130319	W	0.013	0.076	0.0082	0.039	0.055	0.0047	0.031
F13MWNADP9	20130319	20130326	Sp	0.025	0.023	0.0028	0.083	0.054	0.0026	0.067
F13MWNADP10	20130326	20130402	Sp	0.037	0.038	0.0041	0.135	0.060	0.0014	0.052
F13MWNADP11	20130402	20130409	Sp	0.071	0.197	0.0155	0.179	0.194	0.0073	0.093
F13MWNADP12	20130409	20130416	Sp	0.047	0.174	0.0155	0.092	0.063	0.0009	0.084
F13MWNADP13	20130416	20130423	Sp	0.076	1.022	0.0574	0.196	0.328	0.0199	0.171
F13MWNADP14	20130430	20130507	Sp	0.142	0.337	0.0369	0.400	0.242	0.0253	0.240
F13MWNADP15	20130507	20130514	Sp	0.273	0.073	0.0093	0.371	0.279	0.0079	0.358
F13MWNADP16	20130514	20130520	Sp	0.018	0.017	0.0021	0.054	0.027	0.0004	0.046
F13MWNADP17	20130520	20130528	Sp	0.041	0.023	0.0027	0.076	0.041	0.0006	0.063
F13MWNADP18	20130528	20130605	Sp	0.032	0.052	0.0065	0.084	0.046	0.0022	0.045
F13MWNADP20	20130625	20130702	Su	0.096	0.057	0.0110	0.191	0.096	0.0198	0.356
F13MWNADP21	20130702	20130709	Su	0.109	0.051	0.0092	0.229	0.092	0.0164	0.396
F13MWNADP22	20130709	20130717	Su	0.145	0.027	0.0037	0.389	0.145	0.0020	0.477
F13MWNADP23	20130717	20130723	Su	0.048	0.016	0.0019	0.144	0.036	0.0005	0.148
F13MWNADP24	20130723	20130730	Su	0.048	0.050	0.0056	0.150	0.063	0.0016	0.300
F13MWNADP25	20130730	20130806	Su	0.045	0.032	0.0049	0.212	0.115	0.0019	0.218
F13MWNADP26	20130806	20130813	Su	0.093	0.036	0.0045	0.208	0.130	0.0005	0.272
F13MWNADP27	20130813	20130820	Su	0.020	0.016	0.0022	0.089	0.053	0.0003	0.123
F13MWNADP28	20130820	20130827	Su	0.044	0.021	0.0022	0.269	0.108	0.0071	0.488
F13MWNADP29	20130827	20130903	Su	0.089	0.040	0.0046	0.305	0.183	0.0036	0.335
F13MWNADP30	20130903	20130910	Su	0.206	0.111	0.0102	0.676	0.296	0.0015	0.673
F13MWNADP31	20130910	20130917	Su	0.077	0.017	0.0015	0.391	0.169	0.0041	0.492
F13MWNADP32	20130917	20130924	F	0.025	0.014	0.0021	0.127	0.115	0.0026	0.148
F13MWNADP33	20130924	20131001	F	0.005	0.004	0.0005	0.020	0.013	0.0007	0.038
F13MWNADP34	20131001	20131008	F	0.053	0.038	0.0035	0.133	0.067	0.0003	0.052
F13MWNADP36	20131015	20131022	F	0.016	0.005	0.0007	0.048	0.043	0.0005	0.051
F13MWNADP37	20131029	20131105	F	0.006	0.010	0.0010	0.052	0.050	0.0010	0.034
F13MWNADP38	20131112	20131119	F	0.006	0.006	0.0006	0.040	0.017	0.0003	0.026
F13MWNADP39	20131119	20131126	F	0.013	0.005	0.0010	0.061	0.010	0.0033	0.052
F13MWNADP40	20131126	20131203	F	0.003	0.010	0.0013	0.027	0.016	0.0005	0.011
F13MWNADP41	20131203	20131210	F	0.011	0.006	0.0008	0.045	0.059	0.0003	0.197

Table A.2. Loadings in Dry Deposition in kg ha^{-1}

Sample Name	Date ON	Date OFF	Season	NH_4^+	Ca^{2+}	Mg^{2+}	NO_3^-	SO_4^{2-}	PO_4^{3-}	DOC
F12NMDD2	20120131	20120214	W	0.0118	0.034	0.0045	0.065	0.027	0.0011	0.166
F12NMDD3	20120103	20120117	W	0.0043	0.017	0.0017	0.037	0.018	0.0015	0.062
F12NMDD4	20120117	20120131	W	0.0022	0.020	0.0023	0.064	0.037	0.0015	0.051
F12NMDD5	20120214	20120228	W	0.0084	0.031	0.0047	0.034	0.018	0.0027	0.285
F12NMDD6	20120228	20120327	W	0.0017	0.096	0.0080	0.111	0.095	0.0026	0.119
F12NMDD7	20120327	20120403	Sp	0.0174	0.065	0.0074	0.050	0.062	0.0016	0.159
F12NMDD8	20120403	20120417	Sp	0.0178	0.099	0.0045	0.054	0.046	0.0022	0.225
F12NMDD9	20120417	20120502	Sp	0.0084	0.051	0.0063	0.136	0.087	0.0016	0.203
F12NMDD10	20120502	20120515	Sp	0.0088	0.056	0.0055	0.109	0.056	0.0069	0.133
F12NMDD11	20120515	20120529	Sp	0.0111	0.184	0.0134	0.120	0.092	0.0011	0.284
F12NMDD12	20120529	20120612	Sp	0.0076	0.059	0.0069	0.067	0.054	0.0045	0.406
F12NMDD13	20120612	20120626	Sp	0.0103	0.095	0.0114	0.147	0.080	0.0115	0.271
F12NMDD14	20120626	20120712	Su	0.0017	0.081	0.0100	0.140	0.070	0.0171	0.166
F12NMDD15	20120712	20120717	Su	0.0017	0.024	0.0029	0.097	0.028	0.0022	0.072
F12NMDD17	20120717	20120724	Su	0.0052	0.028	0.0029	0.100	0.029	0.0047	0.153
F12NMDD19	20120724	20120821	Su	0.0053	0.114	0.0124	0.262	0.106	0.0307	0.401
F12NMDD20	20120821	20120904	Su	0.0022	0.056	0.0059	0.157	0.054	0.0038	0.232
F12NMDD21	20120904	20120918	Su	0.0055	0.066	0.0057	0.215	0.046	0.0033	0.141
F12NMDD22	20120918	20121002	F	0.0033	0.049	0.0039	0.214	0.049	0.0017	0.196
F12NMDD23	20121002	20121016	F	0.0048	0.045	0.0037	0.084	0.050	0.0025	0.136
F12NMDD24	20121016	20121030	F	0.0070	0.028	0.0035	0.076	0.043	0.0014	0.171
F12NMDD31	20121113	20121127	F	0.0007	0.014	0.0033	0.073	0.029	0.0024	0.055
F13NMDD1	20121227	20130109	W	0.0044	0.010	0.0010	0.079	0.020	0.0025	0.872
F13NMDD2	20130109	20130122	W	0.0021	0.011	0.0040	0.037	0.010	0.0042	0.714
F13NMDD3	20130122	20130203	W	0.0006	0.012	0.0014	0.052	0.023	0.0013	0.812
F13NMDD4	20130203	20130219	W	0.0007	0.026	0.0023	0.073	0.031	0.0024	1.055
F13NMDD5	20130219	20130305	W	0.0053	0.050	0.0053	0.092	0.038	0.0017	1.253
F13NMDD6	20130305	20130326	W	0.0033	0.045	0.0025	0.030	0.024	0.0026	0.710
F13NMDD7	20130326	20130409	Sp	0.0017	0.087	0.0070	0.145	0.088	0.0017	1.633
F13NMDD8	20130409	20130423	Sp	0.0056	0.269	0.0250	0.093	0.087	0.0006	1.052
F13NMDD9	20130423	20130507	Sp	0.0006	0.047	0.0039	0.107	0.078	0.0020	0.643
F13NMDD10	20130507	20130520	Sp	0.0061	0.046	0.0046	0.079	0.056	0.0023	1.219
F13NMDD11	20130520	20130605	Sp	0.0006	0.065	0.0062	0.114	0.067	0.0025	1.343
F13NMDD17	20130605	20130618	Sp	0.0035	0.039	0.0065	0.059	0.063	0.0089	1.263
F13NMDD18	20130618	20130702	Su	0.0866	0.026	0.0094	0.021	0.118	0.1290	6.464
F13NMDD19	20130702	20130717	Su	0.0156	0.019	0.0049	0.084	0.048	0.0612	4.107
F13NMDD20	20130717	20130730	Su	0.0020	0.021	0.0030	0.077	0.031	0.0210	1.321
F13NMDD24	20130730	20130813	Su	0.0006	0.020	0.0030	0.091	0.100	0.0188	1.346

F13NMDD25	20130813	20130827	Su	0.0006	0.030	0.0036	0.098	0.047	0.0179	0.922
F13NMDD26	20130827	20130917	Su	0.0048	0.006	0.0003	0.027	0.061	0.0271	0.501
F13NMDD27	20130917	20130924	F	0.0125	0.026	0.0004	0.036	0.030	0.0176	2.016
F13NMDD28	20130924	20131008	F	0.0006	0.021	0.0010	0.046	0.051	0.0059	0.994
F13NMDD30	20131022	20131105	F	0.0031	0.023	0.0004	0.049	0.051	0.0046	0.873
F13NMDD31	20131105	20131119	F	0.0006	0.014	0.0006	0.051	0.041	0.0031	0.480
F13NMDD33	20131203	20131217	F	0.0020	0.001	0.0001	0.031	0.058	0.0029	0.324

A-3. Correlation of Nutrients
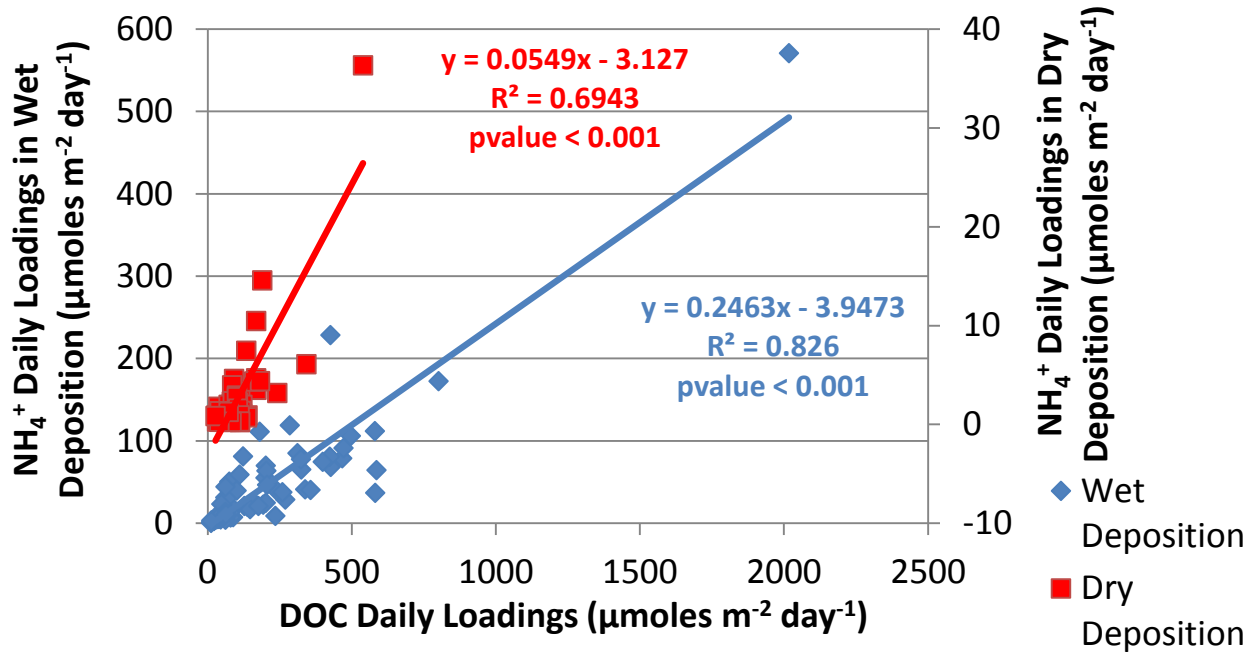
Figure A.1. Scatterplot of average daily NH_4^+ Loadings vs. DOC Loadings in Atmospheric Wet and Dry Deposition in 2012 and 2013. This relationship was used to determine a spring DOC value in wet deposition (F12MWNADP9).
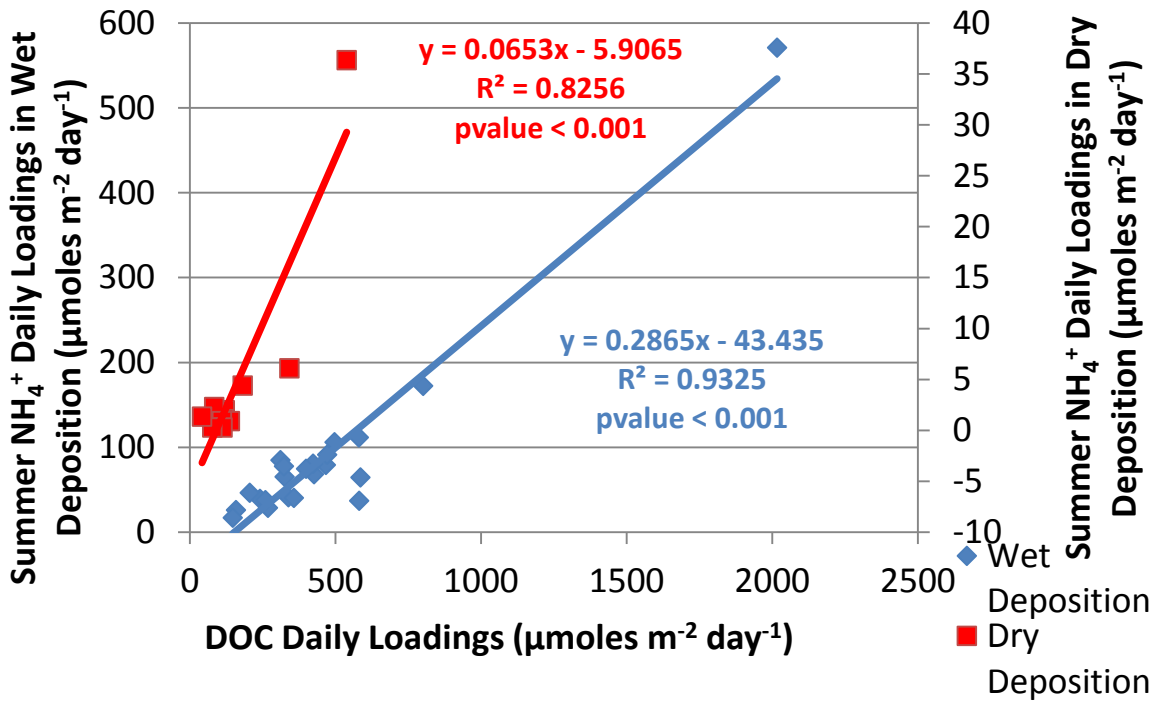
Figure A.2 Scatterplot of average daily NH_4^+ Loadings vs. DOC Loadings in Summer Atmospheric Wet and Dry Deposition in 2012 and 2013.
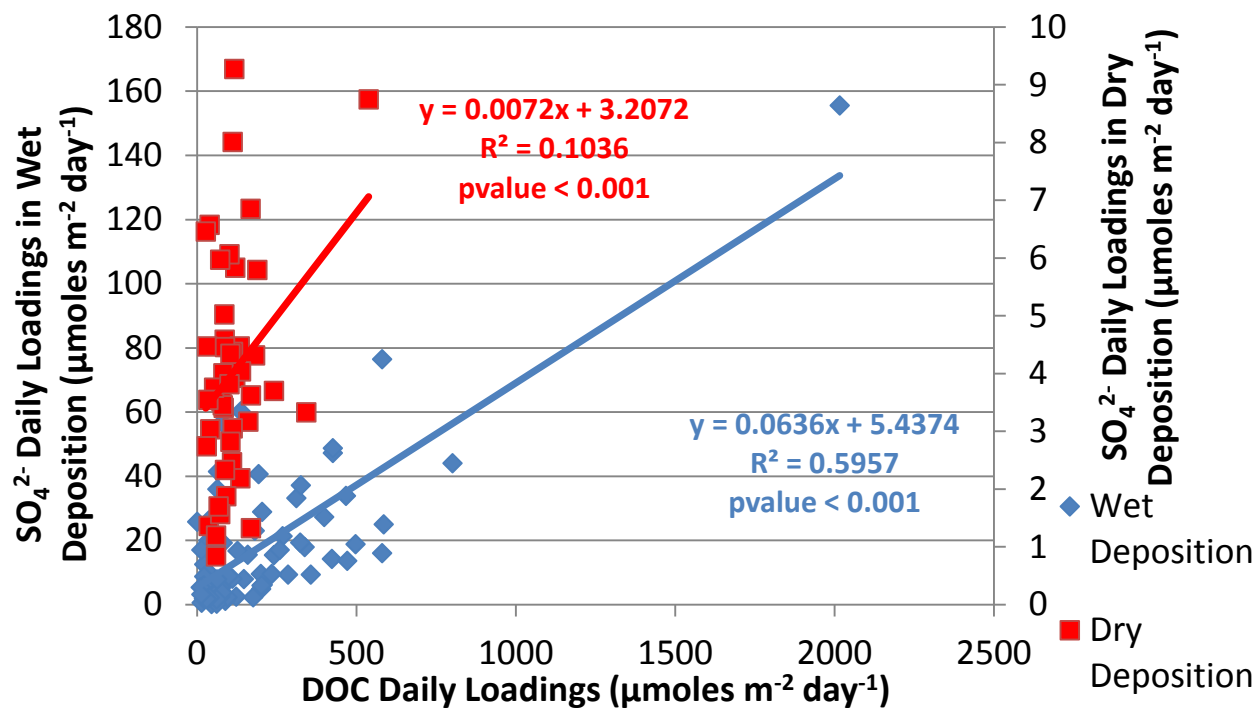
Figure A.3 Scatterplot of average daily SO_4^{2-} Loadings vs. DOC Loadings in Atmospheric Wet and Dry Deposition in 2012 and 2013.
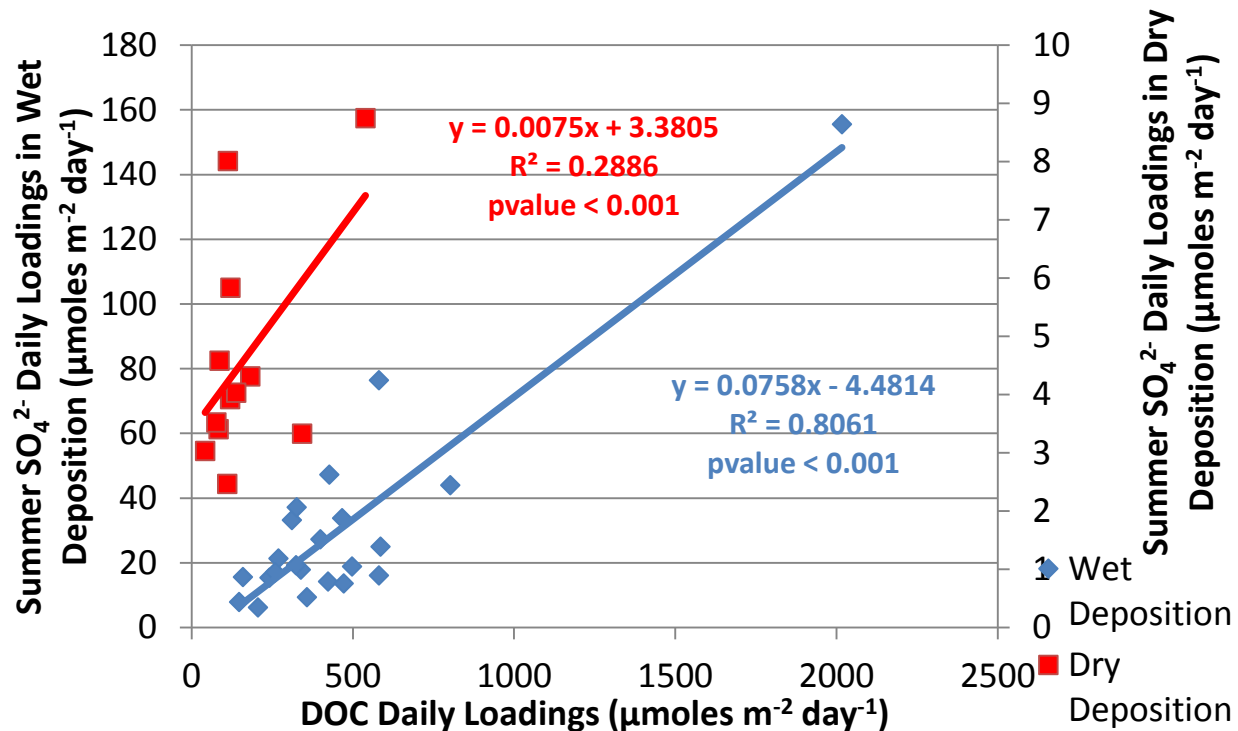
Figure A.4 Scatterplot of average daily SO_4^{2-} Loadings vs. DOC Loadings in Summer Atmospheric Wet and Dry Deposition in 2012 and 2013.
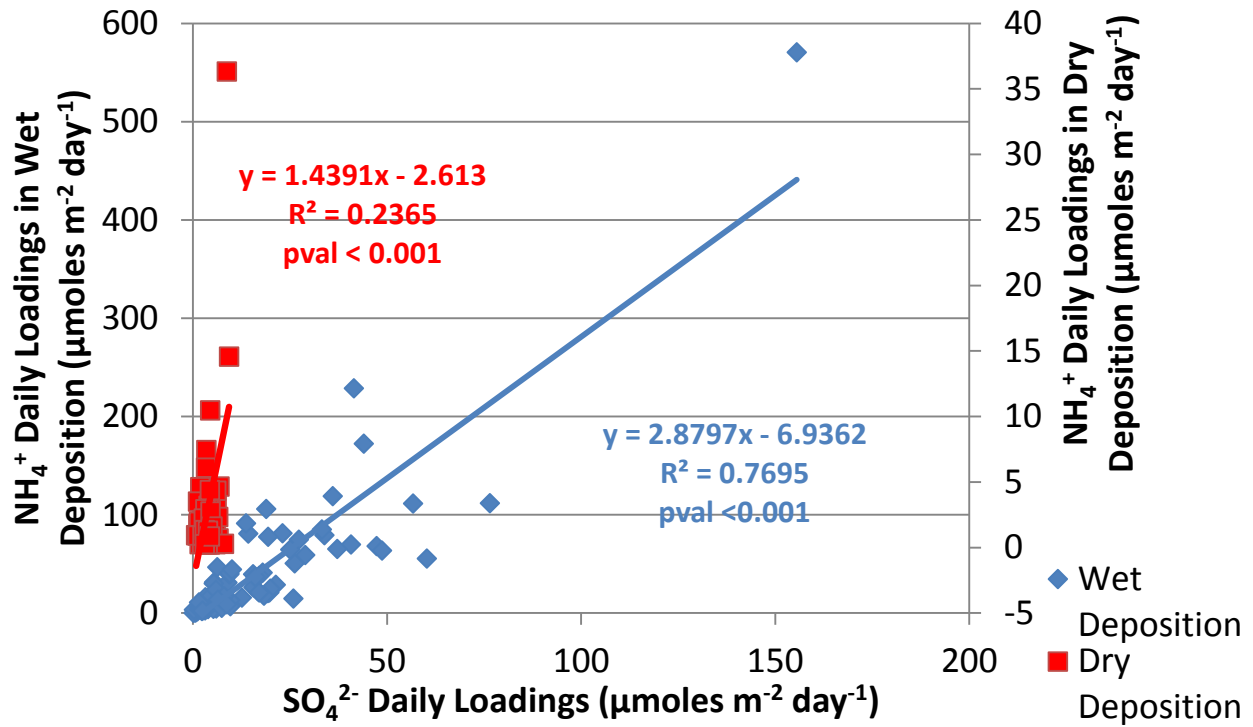
Figure A.5 Scatterplot of NH_4^+ Loadings vs. SO_4^2 Loadings in Atmospheric Wet and Dry Deposition in 2012 and 2013.
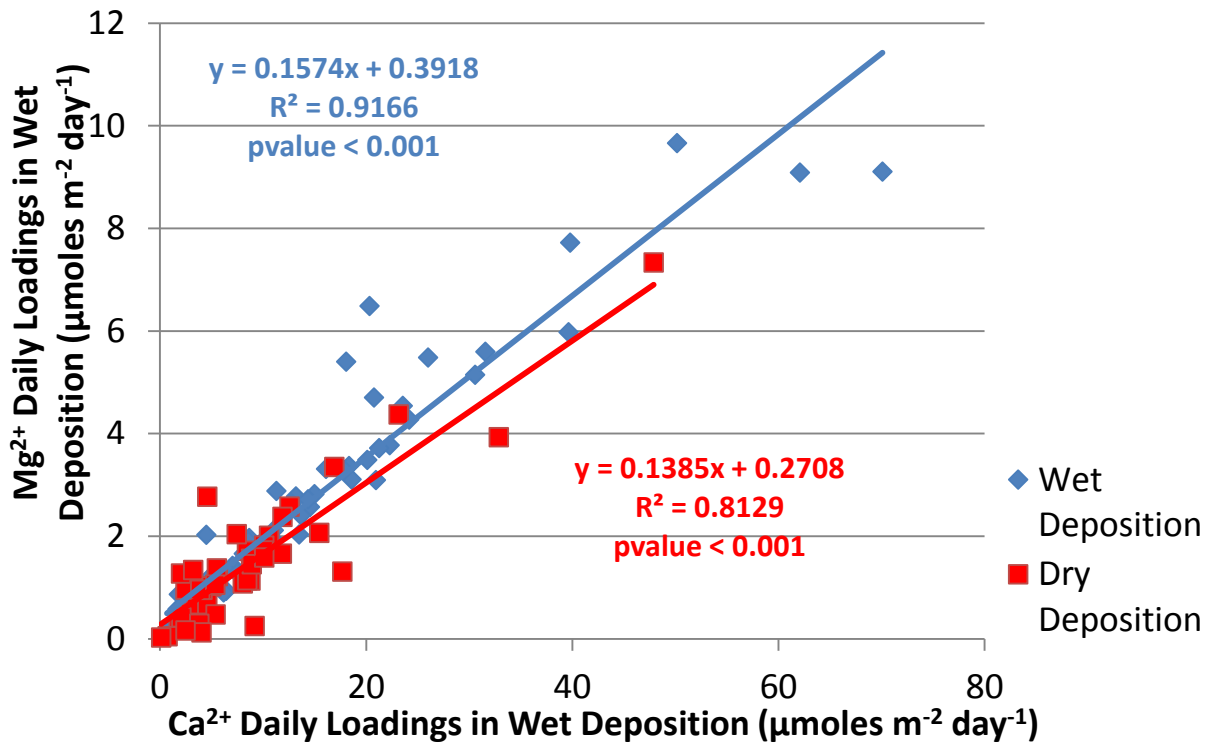
Figure A.6 Scatterplot of Ca^{2+} Loadings vs. Mg^{2+} Loadings in Wet and Dry Deposition in 2012 and 2013.
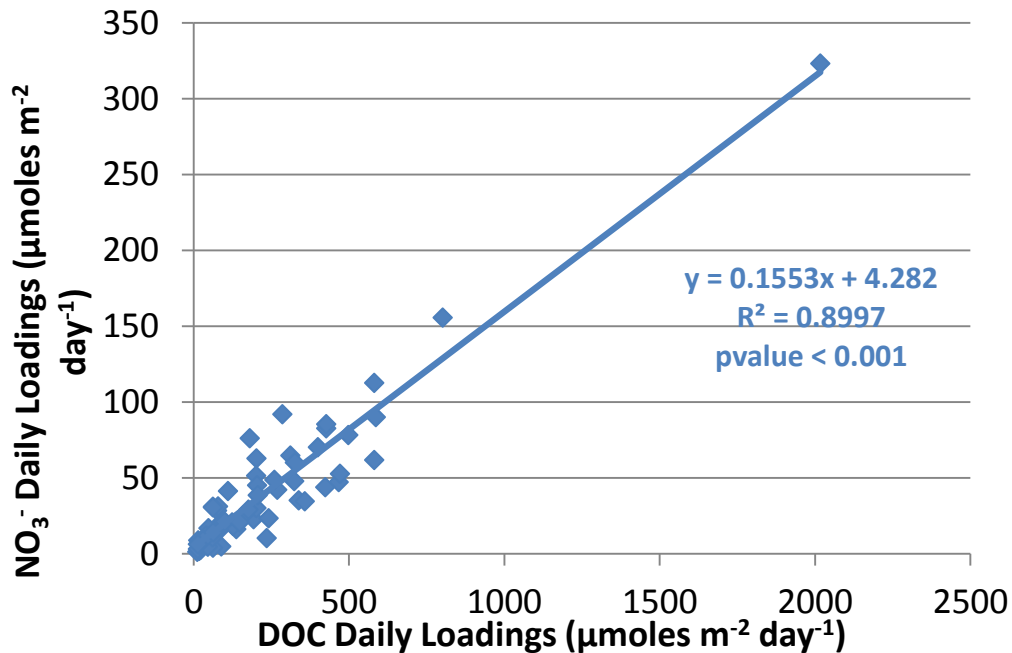
Figure A.7 Scatterplot of nitrate vs DOC collected in atmospheric wet deposition in 2012 and 2013. This relationship was used to determine a winter DOC loading in wet deposition (F12MWNADP30) and four winter NO_3^- loadings in wet deposition (F13MWNADP4-7).
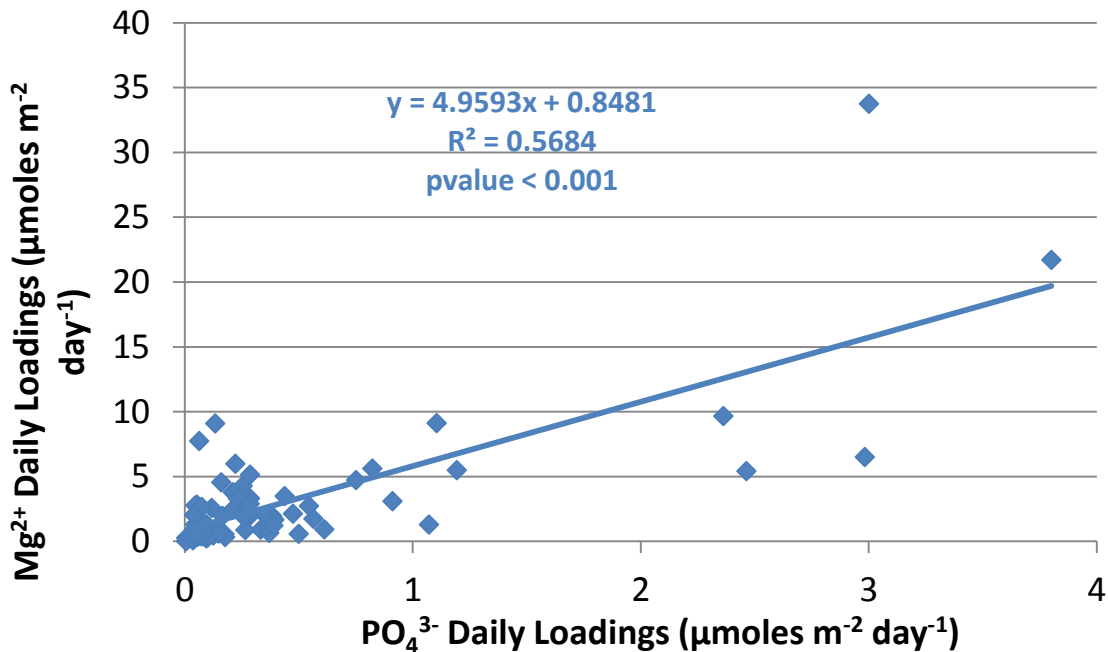
Figure A.8 Scatterplot of Mg^{2+} Loadings vs. PO_4^{3-} Loadings in Atmospheric Wet Deposition in 2012 and 2013. This relationship was used to determine a winter Mg^{2+} loading (F13MWNADP1).

A-4. Backwards Trajectories
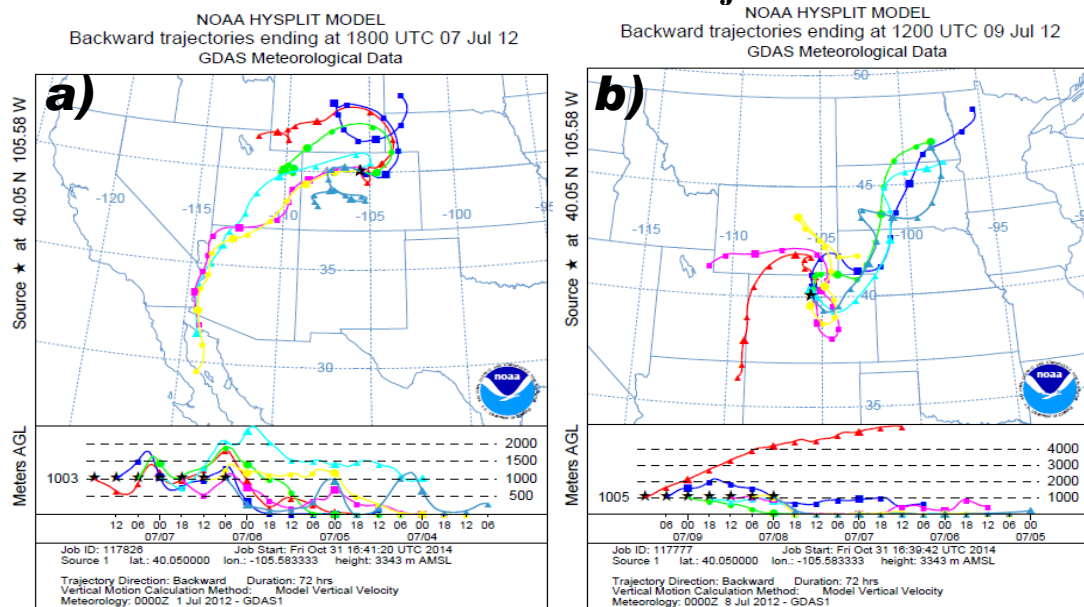
Figure A.9 a) and b) Backwards trajectory of the rain event for sample F12MWNADP19 collected 3 – 10 July 2012, representing the highest wet deposition rate of DOC, NH_4^+, NO_3^-, and SO_4^{2-} loadings and the second highest wet deposition rate of Ca^{2+} loadings, depositing 1.69 kg C ha^{-1}, 0.68 kg NH_4^+ ha^{-1}, 1.40 kg NO_3^- ha^{-1}, 1.05 kg SO_4^{2-} ha^{-1}, and 0.14 kg Ca^{2+} ha^{-1}, respectively.
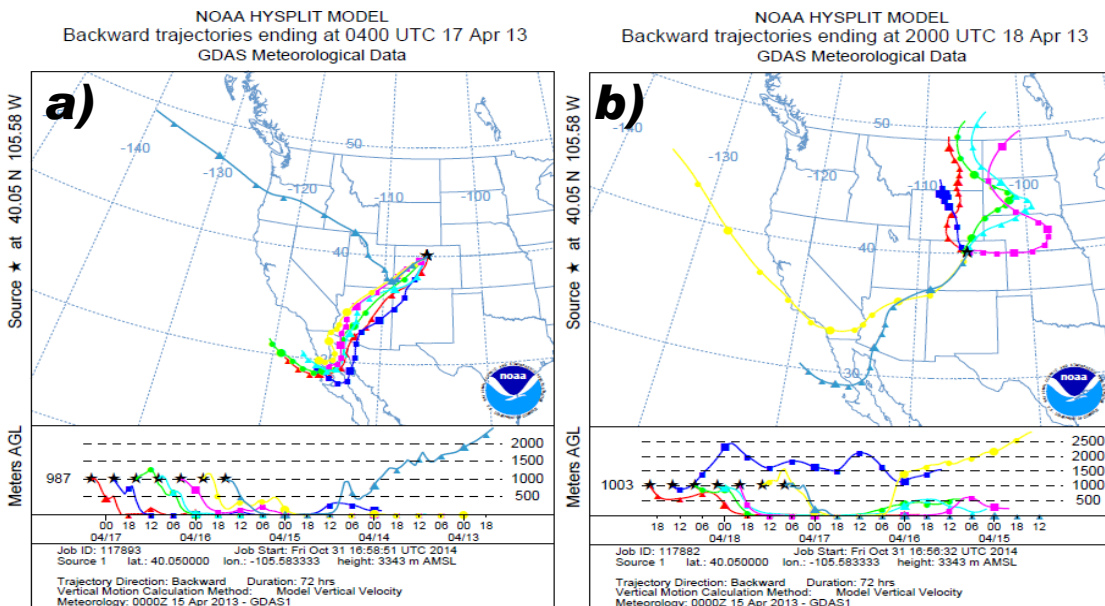
Figure A.10 a) and b) Backwards trajectory of the rain event for sample F13MWNADP13 collected from 16 – 23 April 2013, representing the highest wet deposition rate of Ca^{2+} and Mg^{2+} loadings and the second highest wet deposition rate of PO_4^{3-} loadings, with 1.02 kg Ca^{2+} ha^{-1}, 0.057 kg Mg^{2+} ha^{-1}, and 0.020 kg PO_4^{3-} ha^{-1}, respectively, deposited during that week.
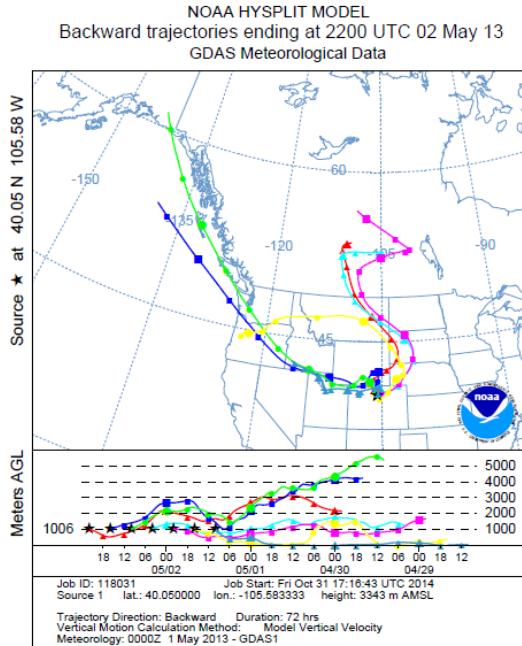
Figure A.11 Backwards trajectory of the rain event for sample F13MWNADP14 collected from 30 April – 7 May 2013, representing the highest wet deposition rate of PO_4^{3-} loadings and the second highest wet deposition rate of Mg^{2+}, depositing 0.025 kg PO_4^{3-} ha^{-1} and 0.037 kg Mg^{2+} ha^{-1}, respectively, during that week.
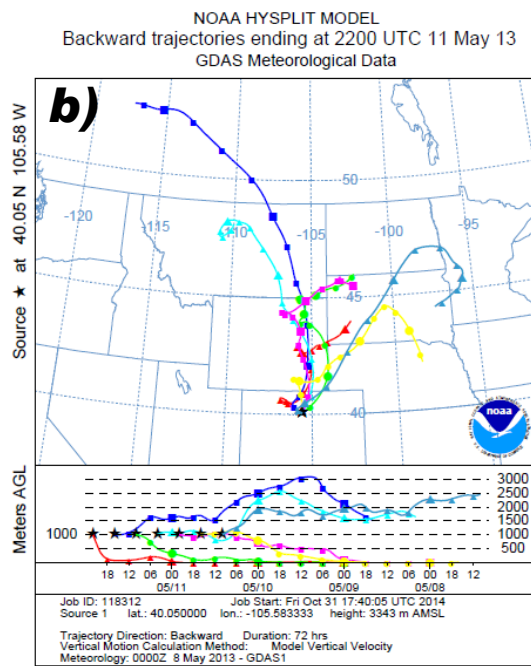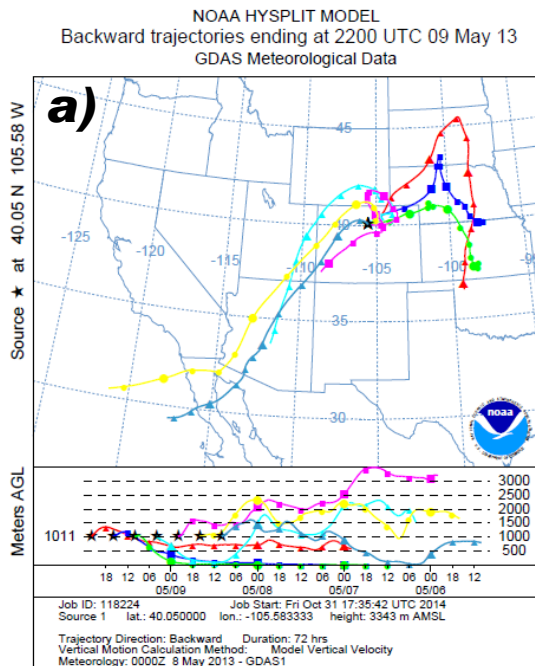
Figure A.12 a) and b) Backwards trajectory of the rain event for sample F13MWNADP15 collected from 7 – 14 May 2013, representing the second highest wet deposition rate of NH_4^+ loadings, depositing 0.27 kg NH_4^+ ha^{-1} during that week.
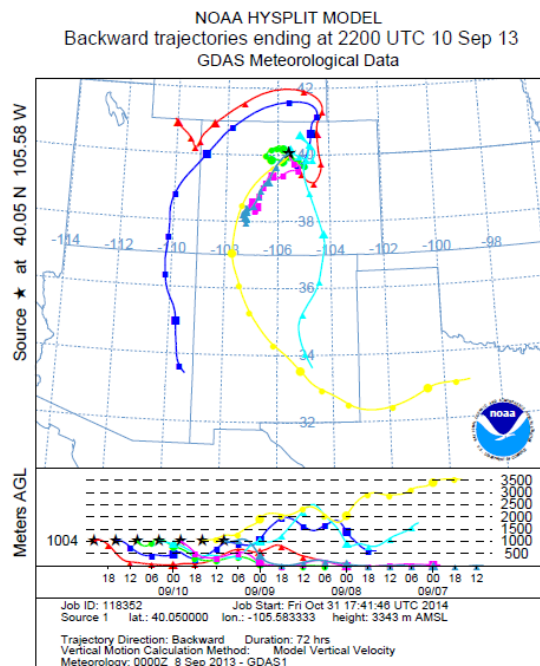
Figure A.13 Backwards trajectory of the rain event for sample F13MWNADP30 collected from 3 – 10 September 2013, represented the second highest deposition rate of NO_3^- loadings, depositing 0.68 kg NO_3^- ha^{-1} during that week.
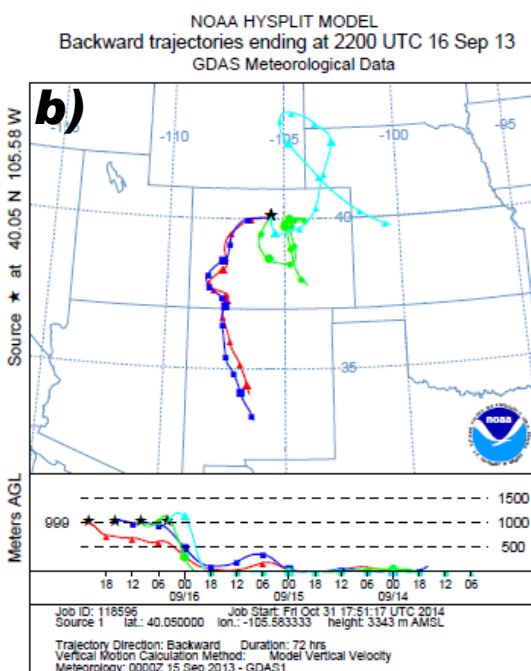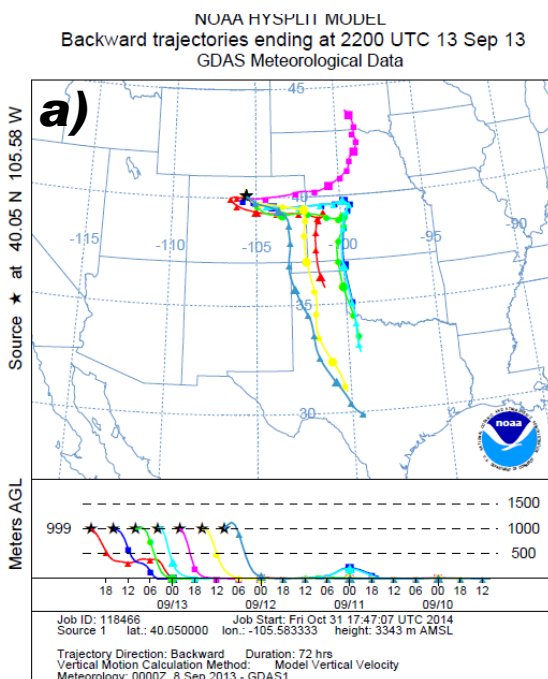
Figure A.14 a) and b) Backwards trajectory of the rain event for sample F13MWNADP31 collected from 10 – 17 September 2013, representing the second highest wet deposition rate of DOC loadings depositing 0.49 kg DOC ha^{-1} that week.

109
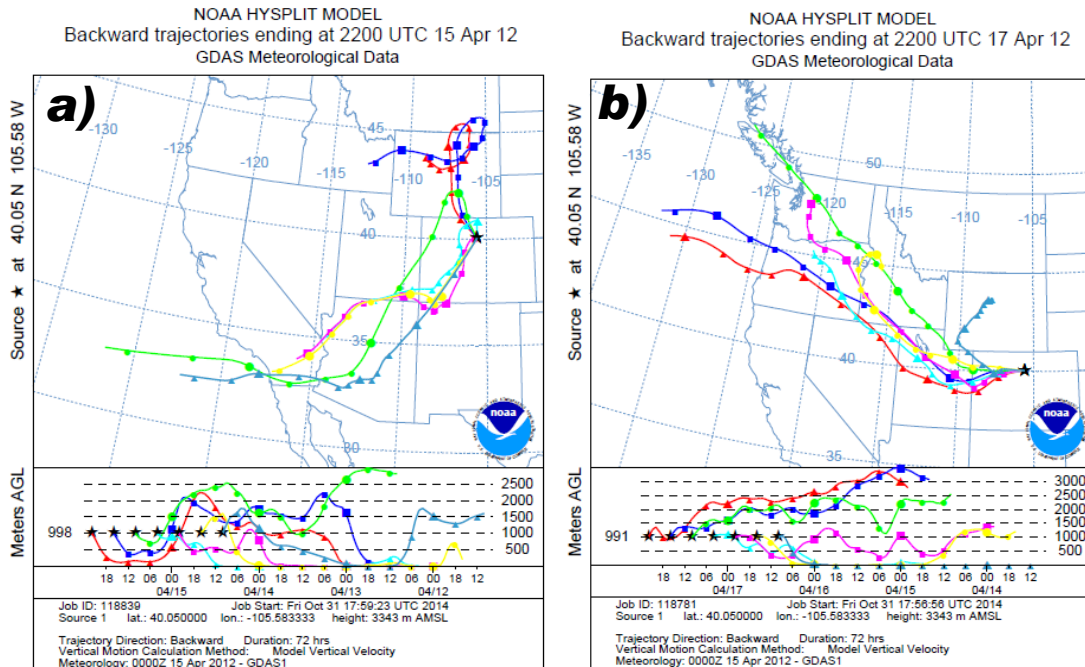
Figure A.15 a) and b) Backwards trajectory of the rain event for sample F12MWNADP10 collected from 10 – 17 April 2012, representing the second highest wet deposition rate of SO_4^{2-} loadings, depositing 0.038 kg SO_4^{2-} ha^{-1} during that week.
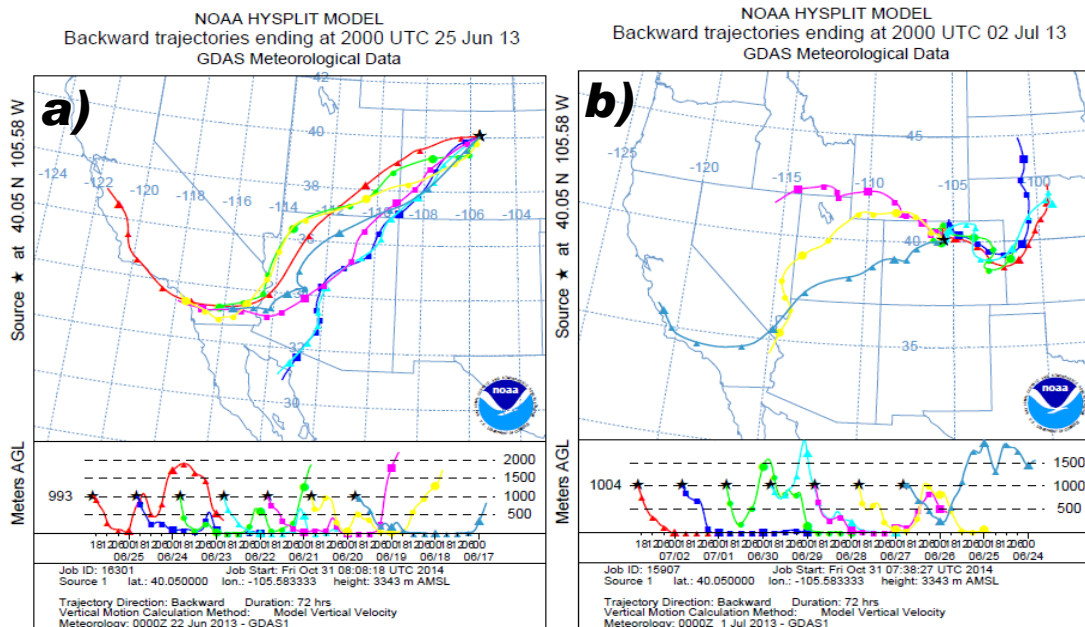
Figure A.16 a) and b) are backwards trajectories for sample F13NMDD18 collected from 18 June – 2 July 2013, representing the highest dry deposition of DOC, NH_4^+, and PO_4^{3-} loadings, and second highest SO_4^{2-} loadings, 0.90 kg C ha^{-1}, 0.087 kg NH_4^+ ha^{-1}, 0.13 kg PO_4^{3-} ha^{-1}, and 0.12 kg SO_4^{2-} ha^{-1}, respectively, deposited during those 2 weeks.
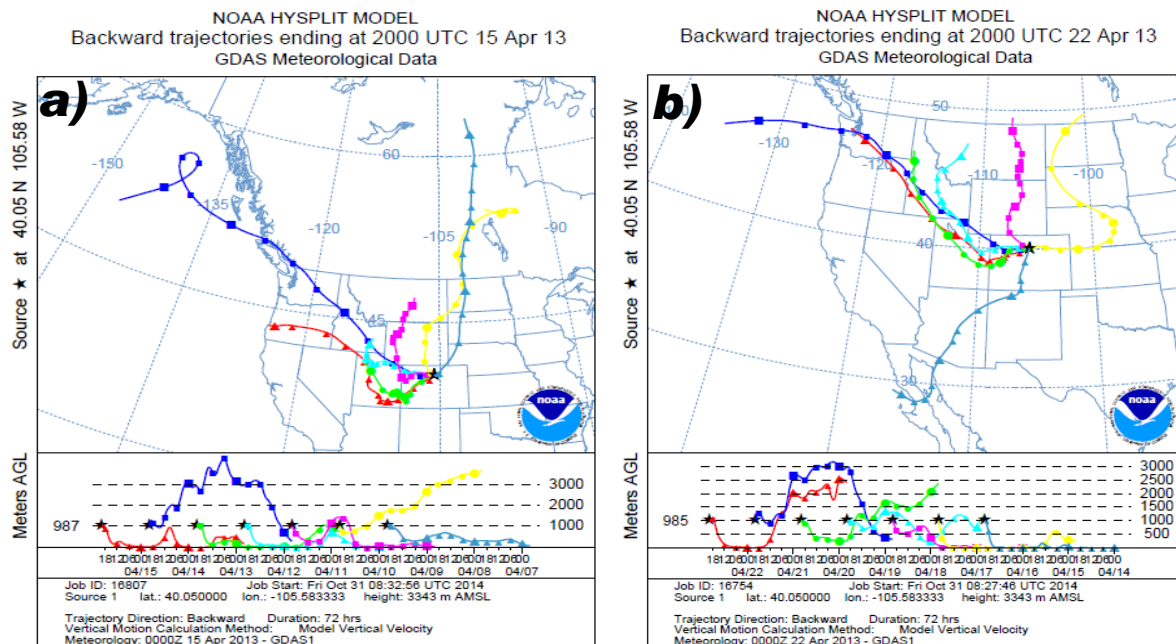
Figure A.17 a) and b) are backwards trajectories for sample F13NMDD8 collected from 9-23 April 2013, representing the highest dry deposition of Ca^{2+} and Mg^{2+} loadings, with 0.27 kg Ca^{2+} ha^{-1} and 0.025 kg Mg^{2+} ha^{-1}, respectively, deposited over those 2 weeks.
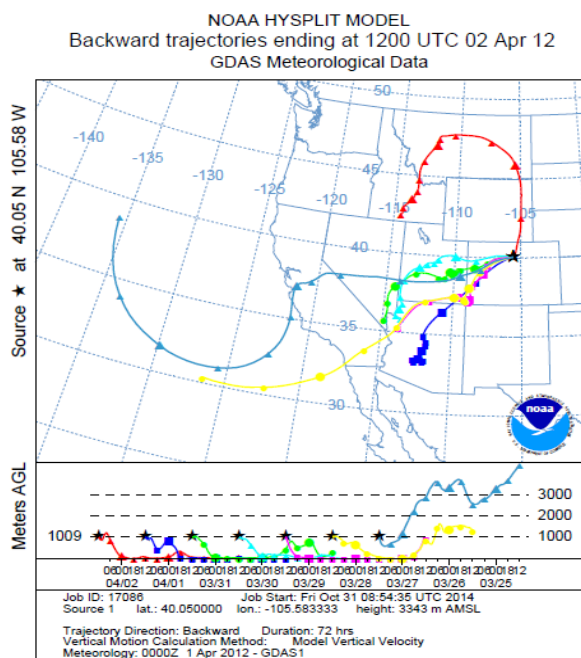
Figure A.18 Backwards trajectories for sample F12NMDD7 collected from 27 March – 3 April 2012, representing the highest dry deposition rate of SO_4^{2-} and the second highest NH_4^+ and Mg^{2+}, with 0.062 kg SO_4^{2-} ha^{-1}, 0.017 kg NH_4^+ ha^{-1}, and 0.0074 kg Mg^{2+} ha^{-1}, respectively, deposited during the 7 day period.
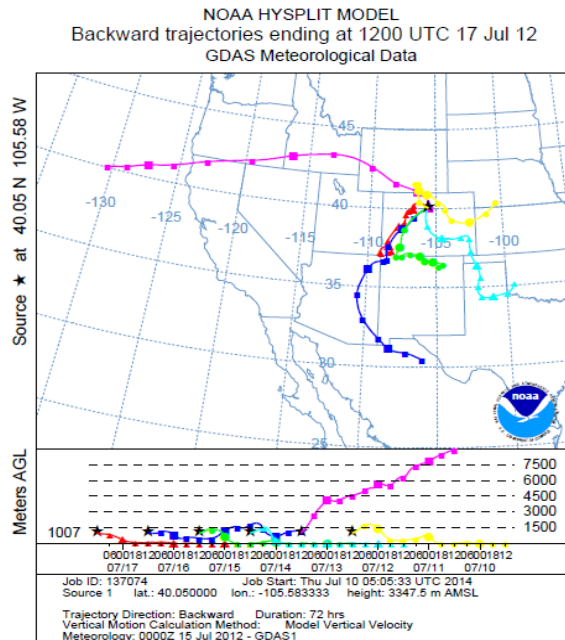
Figure A.19 Backwards trajectories for F12NMDD15 collected from 12-17 July 2012, represents the highest NO_3^- in dry deposition with 0.097 kg NO_3^- ha^{-1} deposited during the 5 days.
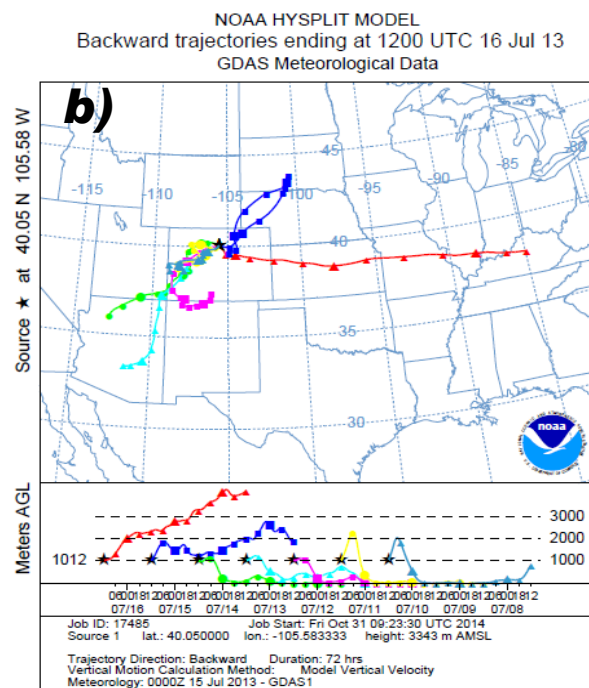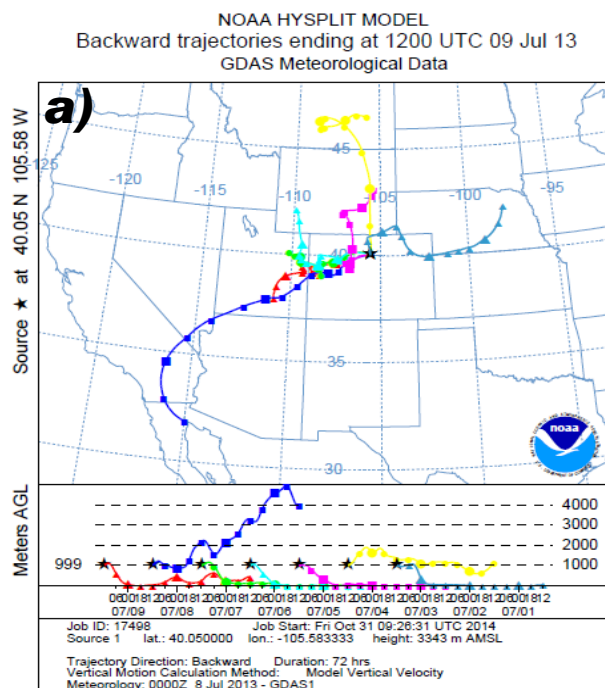
Figure A.20 a) and b) backwards trajectories for sample F13NMDD19 collected from 2-17 July 2013, representing the second highest dry deposition rate of DOC and PO_4^{3-} loadings, 0.62 kg C ha^{-1} and 0.06 kg PO_4^{3-}, respectively, deposited during these 2 weeks.
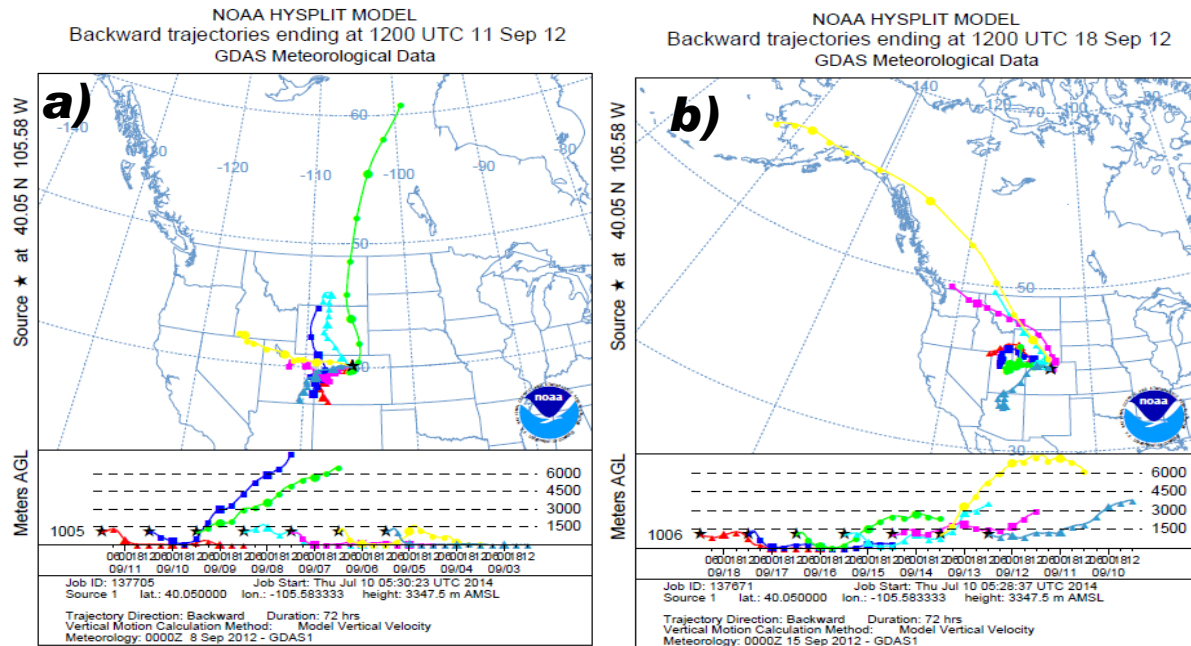
Figure A.21 a) and b) backwards trajectories for F12NMDD21 collected from 4-18 September 2012, represents the second highest dry deposition rate of NO$_3^-$ in dry deposition with 0.22 kg NO$_3^-$ ha^{-1} deposited during the 2 weeks.
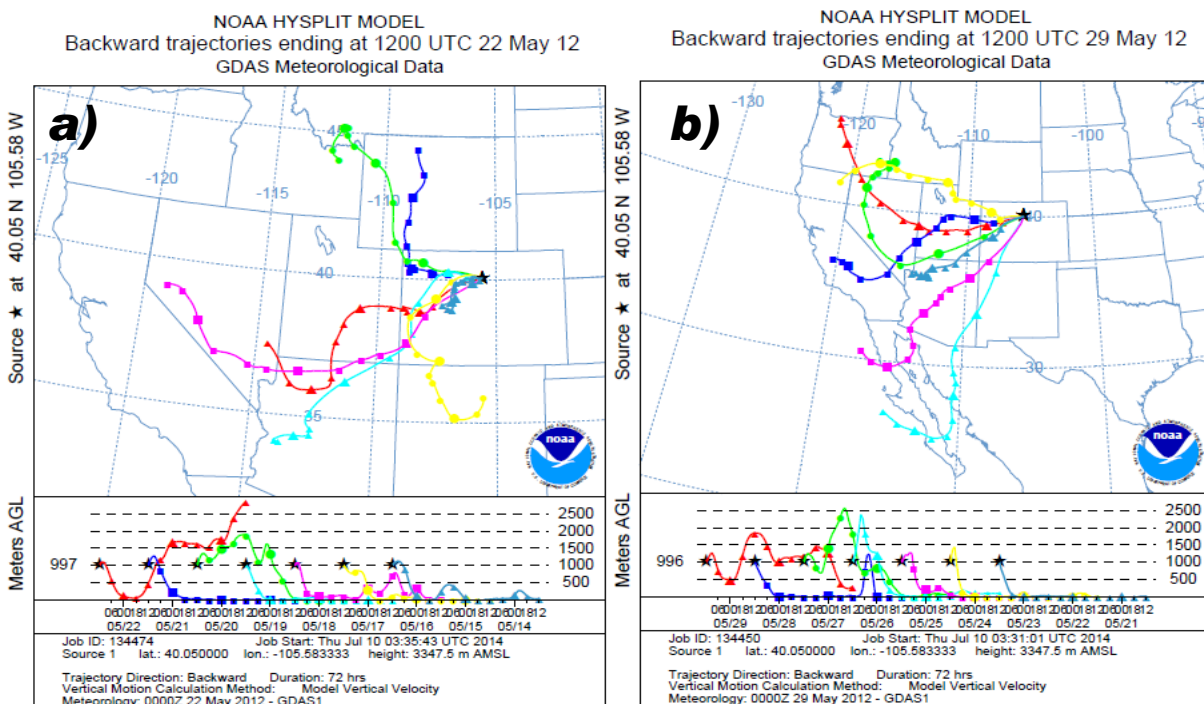
Figure A.22 a) and b) backwards trajectories for sample F12NMDD11 collected from 15-29 May 2012, represents the second highest dry deposition Ca^{2+} with 0.18 kg Ca^{2+} ha^{-1} deposited during these 2 weeks.

A-5. Ammonium Sulphate Relation to Increase in SOA Mass
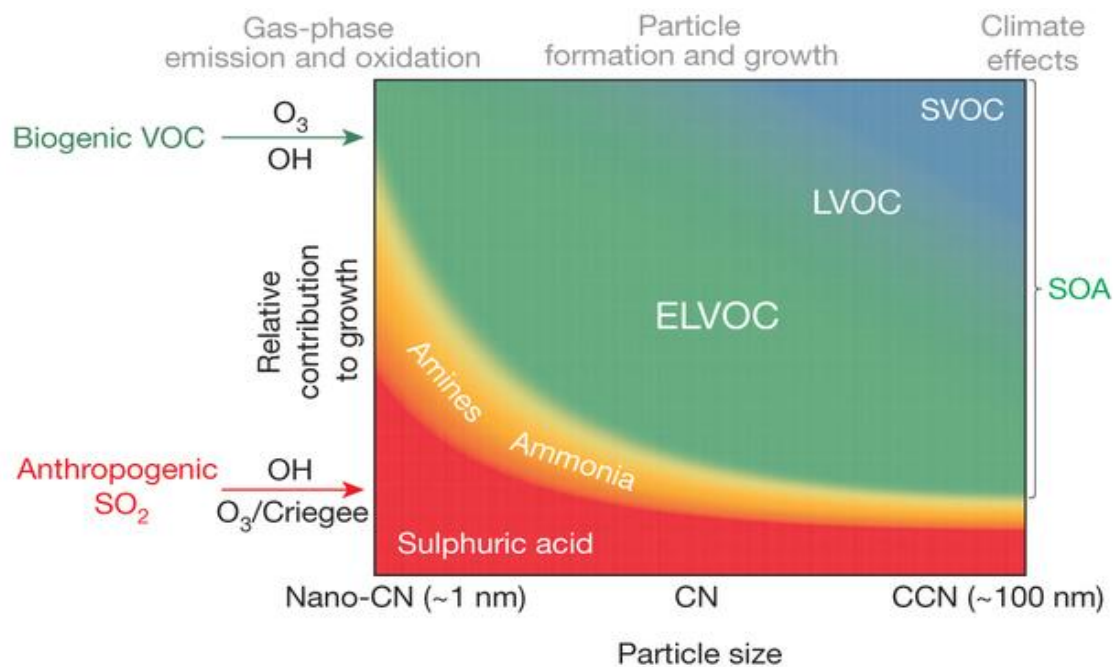
Figure A.23 The importance of precursor vapours for aerosol growth at different sizes (Ehn et al., 2014).
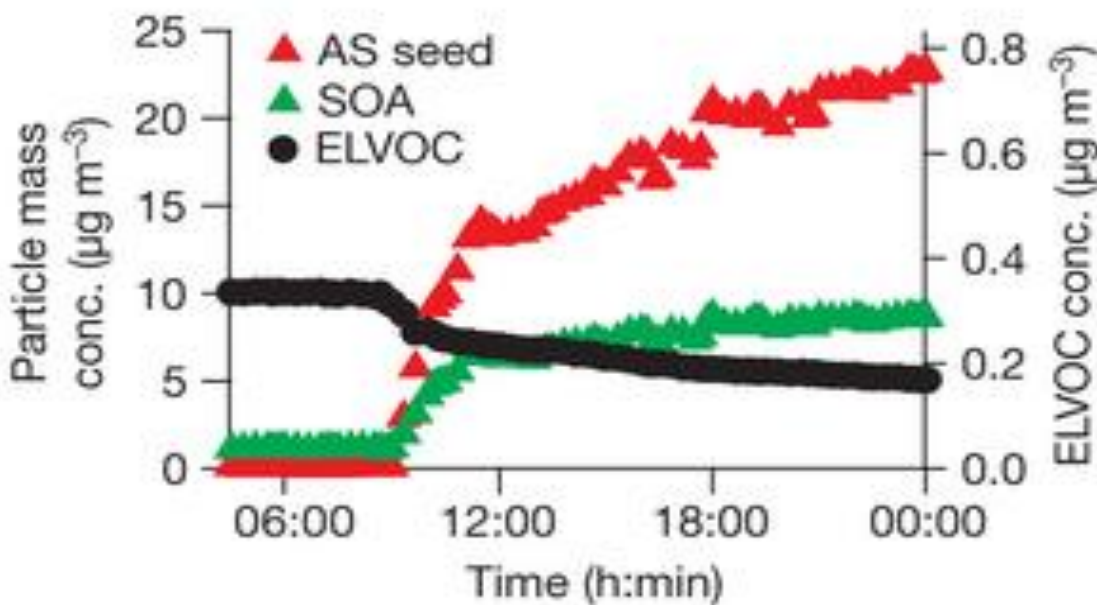
Figure A.24 Ammonium sulphate (AS) seed addition (red triangles, left axis) causes a decrease in ELVOCs (black dots, right axis) due to an increased particulate condensation sink, and a corresponding increase in SOA mass (green triangles, left axis) is detected Figure source : Ehn et al., 2014.

A-6. Revised Carbon Budget at Green Lakes 4, Niwot Ridge
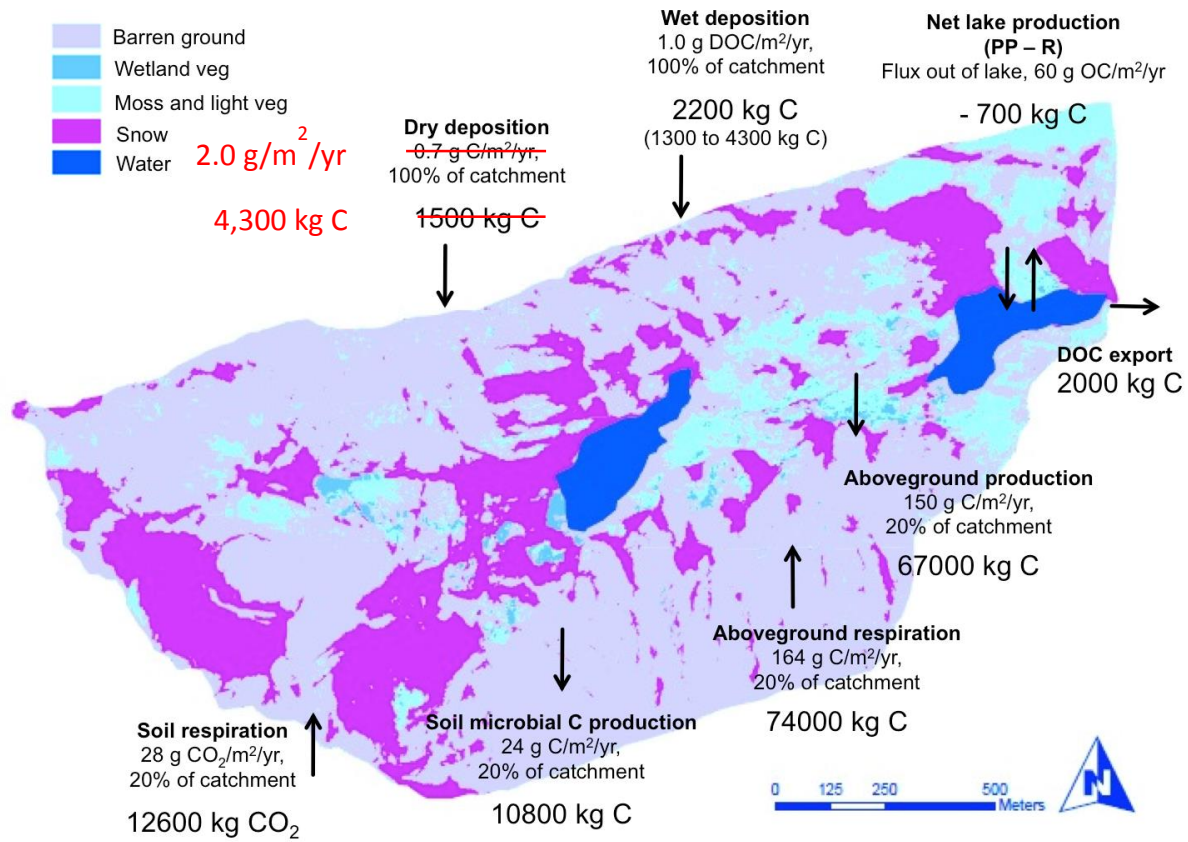
Figure A.25 Revised carbon budget from Mladenov et al., 2012 using wet deposition DOC and dry deposition (POC) values from this study.

Appendix B - Supplemental Information to Chapter 3. Organic Matter Characterization of Atmospheric Wet and Dry Deposition Found in Alpine Environments in the Colorado Rocky Mountains

B-1. Fluorescence Indices and UV-vis Absorbance Measurements of Wet and Dry Deposition

Table B.1 Fluorescence Indices and UV-vis Absorbance Measurements of Wet Deposition

Sample	FI	FrI	HIX	Peak A (R.U.)	Peak B (R.U.)	Peak T (R.U.)	Peak C (R.U.)	Peak M (R.U.)	SUVA (mg C^{-1} m^{-1})
F12MWNADP18	1.0547	0.5467	0.8122	18.2228	13.815	5.2653	0.2362	1.0313	1.0838
F12MWNADP19	0.9798	0.3632	1.7779	0.5920	0.6168	0.2483	0.0547	0.2013	1.0546
F12MWNADP20	0.9141	0.4070	1.7500	0.2262	0.1662	0.0817	0.0260	0.1045	0.6442
F12MWNADP21	1.3739	0.5208	1.4153	0.0773	0.0584	0.0280	0.0160	0.1747	0.3557
F12MWNADP23	1.4455	0.7254	0.9028	402.476	104.793	51.231	0.8864	24.6878	1.6147
F12MWNADP24	1.4172	0.5283	1.8825	4.1512	1.5797	0.8590	0.1921	1.3645	0.9323
F12MWNADP25	1.4706	0.6181	2.5652	5.3127	0.7680	0.5945	0.1029	5.3610	0.8396
F12MWNADP28	1.3324	0.5242	0.7965	0.0575	0.0712	0.0388	0.0121	0.1071	2.2212
F12MWNADP29	1.5435	0.5054	0.8670	0.0692	0.1053	0.0448	0.0191	0.0881	0.5404
F12MWNADP31	1.4089	0.5943	2.9654	1.6381	0.2152	0.1563	0.0453	3.4703	0.7780
F12MWNADP32	1.3548	0.5877	2.1369	1.3308	0.2754	0.1973	0.0483	3.2749	2.1444
F12MWNADP33	1.1556	0.5942	0.5912	0.0278	0.0486	0.0345	0.0069	0.0357	1.6087
F13MWNADP5	1.2893	0.6076	0.6345	0.0182	0.0262	0.0300	0.0044	0.0106	1.5130
F13MWNADP6	1.2756	0.4293	0.9117	0.0333	0.0597	0.0377	0.0087	0.0286	1.4081
F13MWNADP7	1.2534	0.5661	1.0920	0.0118	0.0119	0.0164	0.0040	0.0102	0.7315
F13MWNADP8	1.3233	0.6204	2.8954	0.1234	0.0481	0.0556	0.0358	0.0546	1.7018

116

Sample	FI	FrI	HIX	Peak A (R.U.)	Peak B (R.U.)	Peak T (R.U.)	Peak C (R.U.)	Peak M (R.U.)	SUVA (mg C⁻¹ m⁻¹)
F13MWNADP9	1.2137	0.5426	1.2292	0.0212	0.0231	0.0271	0.0067	0.0164	0.9366
F13MWNADP10	1.2442	0.5757	1.4416	0.1620	0.1076	0.1002	0.0324	0.1916	1.3066
F13MWNADP11	1.3651	0.6395	2.2375	0.1236	0.0613	0.0609	0.0409	0.0898	2.1631
F13MWNADP12	1.8776	0.7032	1.4889	0.7396	0.2463	0.2970	0.1059	1.7381	4.9371
F13MWNADP13	3.3980	1.3329	0.0680	469.086	1056.33	1290.536	38.7867	163.486	8.4488
F13MWNADP14	1.2625	0.6559	1.7247	0.1091	0.0686	0.0719	0.0239	0.0425	1.1445
F13MWNADP20	1.1760	0.7453	0.5357	0.3256	0.9995	0.9332	0.0513	0.1010	1.1576
F13MWNADP21	1.5012	0.6369	1.2752	1.3085	0.7560	0.7576	0.0855	1.1138	0.9989
F13MWNADP22	1.2247	0.4878	1.5254	0.0680	0.0518	0.0510	0.0176	0.0473	0.5873
F13MWNADP23	1.3639	0.6531	1.0919	0.0891	0.1076	0.1037	0.0218	0.0558	0.5354
F13MWNADP24	1.2887	0.3922	3.0555	0.4420	0.1493	0.1080	0.0660	0.1227	0.6907
F13MWNADP25	1.2863	0.5051	1.7647	0.1691	0.1058	0.0794	0.0354	0.1038	0.5255
F13MWNADP27	1.2923	0.5188	1.7076	0.1015	0.0715	0.0720	0.0283	0.0847	0.7920
F13MWNADP28	1.2459	0.4980	2.9907	0.0744	0.0201	0.0226	0.0248	0.0443	0.3210
F13MWNADP29	1.3591	0.4198	1.7173	0.1680	0.1035	0.1095	0.0372	0.0791	0.5385

Table B.2 Fluorescence Indices and UV-vis Absorbance Measurements of Dry Deposition

Sample	FI	FrI	HIX	Peak A (R.U.)	Peak B (R.U.)	Peak T (R.U.)	Peak C (R.U.)	Peak M (R.U.)	SUVA (mg C⁻¹ m⁻¹)
F12NMDD2	1.2731	0.9654	0.1887	0.2515	1.2416	0.5587	0.0695	0.1812	0.9187
F12NMDD3	1.3729	0.6477	0.4490	0.0544	0.1275	0.0726	0.0220	0.0476	0.7077
F12NMDD4	1.3092	0.6494	0.4247	0.1550	0.4423	0.2915	0.0456	0.0825	2.3567
F12NMDD9	1.4074	0.7908	0.5578	0.1716	0.2952	0.2373	0.0306	0.0685	1.1107
F12NMDD10	1.3487	0.8427	0.4713	0.1198	0.2554	0.2010	0.0292	0.0564	1.3582
F12NMDD11	1.4432	0.5575	0.3068	0.9657	2.8541	0.9477	0.0971	0.2094	1.2848
F12NMDD12	1.0117	0.6284	0.2328	0.9180	3.3995	1.1004	0.0563	0.1467	0.8866
F12NMDD13	1.0707	0.6814	0.2868	4.8895	15.9570	5.6182	0.1234	0.3829	2.0693
F12NMDD17	1.0017	0.7226	0.5095	0.1212	0.2217	0.1695	0.0193	0.0435	0.8650
F12NMDD19	1.3877	0.6861	0.5179	1.0660	1.8054	0.6154	0.0753	0.2926	1.0629
F12NMDD20	1.5526	0.6906	0.6812	0.2910	0.4677	0.2521	0.0597	0.1313	1.1272
F12NMDD21	1.4458	0.7347	0.3244	0.5209	1.3588	1.3731	0.0632	0.1815	2.3675

F12NMDD22	1.4016	0.6662	0.4977	0.1486	0.2728	0.3304	0.0272	0.0857	1.0646
F12NMDD23	1.4308	0.6282	0.3481	2.0999	7.9801	3.4253	0.1524	0.4766	3.8683
F12NMDD24	1.3981	0.5971	0.7429	0.1118	0.2024	0.1010	0.0262	0.0475	1.1034
F12NMDD31	1.3218	0.7361	0.4328	0.0260	0.0602	0.0434	0.0070	0.0148	1.7438
F13NMDD1	1.2284	0.7528	0.2546	0.0553	0.1373	0.1291	0.0101	0.0264	1.0456
F13NMDD2	1.3056	0.6860	0.7895	0.0291	0.0407	0.0332	0.0082	0.0153	1.0330
F13NMDD3	1.2932	0.6593	0.3986	0.1689	0.3212	0.2559	0.0268	0.0623	2.0948
F13NMDD4	1.5740	0.7269	0.8856	0.1170	0.1339	0.0961	0.0219	0.0467	1.3613
F13NMDD5	1.6402	0.7579	0.6578	0.1645	0.2514	0.1958	0.0342	0.0662	1.3437
F13NMDD6	1.4618	0.7985	0.3270	0.0863	0.1659	0.1602	0.0174	0.0339	1.3440
F13NMDD7	1.6237	0.8383	0.4736	0.2312	0.3169	0.4277	0.0480	0.1129	1.0629
F13NMDD8	1.4580	0.8086	0.6593	0.5222	0.7342	0.3231	0.0510	0.1163	1.7145
F13NMDD9	1.3665	0.6046	0.8029	0.2231	0.2208	0.1388	0.0342	0.1171	2.5071
F13NMDD10	1.4595	0.8631	0.1591	2.1948	23.4511	9.7823	0.1046	0.3462	3.3521
F13NMDD11	1.4663	0.6855	0.6296	0.6651	0.9808	0.5590	0.0596	0.1491	1.8969
F13NMDD17	1.4327	0.7994	0.2087	12.4715	59.3596	39.1134	0.6035	1.4041	4.3229
F13NMDD18	1.2630	0.7994	1.3877	0.3400	0.2828	0.3181	0.0878	0.1240	0.1762
F13NMDD19	1.6470	0.8462	0.8057	1.0770	1.3398	0.9741	0.1126	0.2734	0.6089
F13NMDD20	1.4161	0.6671	0.8063	0.1444	0.2234	0.1781	0.0336	0.0684	1.1687
F13NMDD24	1.2292	0.6452	0.7113	1.3402	1.1825	0.5764	0.1647	0.3993	2.3224
F13NMDD25	1.4430	0.6255	0.9388	0.0786	0.0522	0.0459	0.0194	0.0394	0.6424
F13NMDD27	1.5075	0.6988	0.6461	0.1180	0.2307	0.1038	0.0231	0.0460	1.4032
F13NMDD28	1.3755	0.6492	0.4519	0.1645	0.4365	0.1747	0.0186	0.0406	2.1733
F13NMDD30	1.3539	0.6583	0.4466	0.0477	0.1056	0.0616	0.0122	0.0238	0.8194
F13NMDD31	1.3894	0.5983	0.5284	0.0230	0.0638	0.0255	0.0087	0.0159	
F13NMDD33	1.3815	0.6361	0.2760	0.0374	0.1557	0.0456	0.0094	0.0232	2.1775